### Modelling and Simulation in Materials Engineering

N. Hort<sup>1</sup>, D. Höche<sup>1</sup>, H. Dieringa<sup>1</sup>, P. Maier<sup>2</sup>

<sup>1</sup> Magnesium Innovation Centre, Helmholtz-Zentrum Geesthacht, Geesthacht, DE
<sup>2</sup> University of Applied Sciences Stralsund, Stralsund, DE

**INTRODUCTION:** Modelling and simulation approaches are nowadays an integral part of materials engineering processes. Especially under Industry 4.0 they will gain an increasing influence. However, modelling does not necessarily mean that only theoretical approaches by computational calculations are applied. Definitions of models (incomplete list) are<sup>1</sup>:

- 1. "A three-dimensional representation of a person or thing or of a proposed structure, typically on a smaller scale than the original."
- 2. "A simplified description, especially a mathematical one, of a system or process, to assist calculations and predictions."

In both cases it is clear that models are not the reality itself. It is also clear that definition 1 describes a real object. However, let's discuss this in more detail by taking the simple tensile test as an example.

A MODEL – THE TENSILE TEST: For predicting the behaviour of a real structure during service it would be wise to have trustable parameters prior to build the structure. Therefore (amongst others) the tensile test was developed in the second half of the 19<sup>th</sup> century and optimized over decades. Nowadays it is an ISO standard<sup>2</sup> and the obtained values from this test are used for construction and to predict the load of failure.

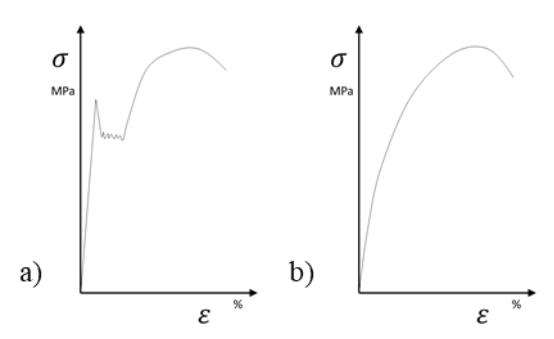


Figure 1: typical  $\sigma$ - $\varepsilon$  curves a) of a ferrous and b) a non-ferrous metal (schematic curves)<sup>3</sup>.

Figure 1a) shows a typical stress-strain ( $\sigma$ - $\epsilon$ ) curve of a mild steel. In the elastic area strain increases linearly with increasing stress. After a certain stress is exceeded the correlation is no longer linear and the behaviour becomes more complex; plastic deformation occurs. Due to definition 2, equation 1 is a model (Hooke's law) that describes the elastic behaviour of a metallic material under tension. Stress and strain correlate linearly and the Young's modulus E is a material dependent constant. However,

this strict linear relation is often not observed in the case of non-ferrous materials (figure 1b).

$$\sigma = E \times \varepsilon \tag{1}$$

It is also assumed that the load applied during tension to the material is uni-directional. The volume of the tensile specimen is constant regardless its deformation. As long as the loading is in the elastic range the origin shape will not be altered after stress release. However, as the specimen is elongated in z-direction the dimensions in x- and y-direction will shrink. At a certain stress necking will occur and in reality this means that the assumption of a uni-directional loading is not true. Furthermore the tensile sample geometry is standardized and has defined sample surface

**SUMMARY:** In today's world computational approaches become more and more popular due to an enormous increase in computational power. However, models are only reflections of the reality. Experiments also do not mirror the reality completely. They reflect a part of a real structure but they do it in a way that they can be used to predict a structure's behaviour. When definition 1 is altered slightly to

"A physical representation of a person or thing or of a proposed structure, typically on a different scale than the original."

it becomes obvious that all experiments are models and are used to simulate a certain property of a real structure in a real environment. And indeed a good experiment with real components is much closer to reality compared to most (all?) computational approaches to model and simulate materials behaviour. Moreover, experiments need to be performed anyway to validate predictions of computer models. Additionally nowadays it is also possible to test entire structures rather than their models. But of course the price of computational approaches is much less than the infrastructure for testing real components.

**REFERENCES:** <sup>1</sup> https://en.oxforddictionaries.com/definition/model. <sup>2</sup> ISO 6892:2016, Metallic materials – Tensile testing. <sup>3</sup> W. D. Callister (2007) 7<sup>th</sup> edition, Materials Science and Engineering, Wiley & Sons Inc.

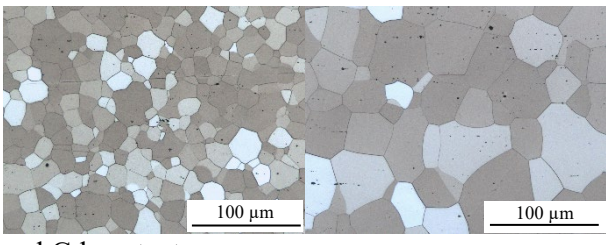
#### Suitability of as extruded Mg-Gd-0.5Mn for biomedical applications

J Harmuth, B Wiese, J Bohlen, T Ebel, R Willumeit-Römer Helmholtz-Centre Geesthacht (HZG), Germanv

**INTRODUCTION:** The application of an implant defines the requirements for a material, e.g. biocompatibility, homogeneous corrosion and mechanical properties. Both, Gd and Mn proofed to be suitable for biomedical applications and are investigated in this work.<sup>1,2</sup>

**METHODS:** Ternary Mg-Gd-0.5Mn alloys were prepared by permanent direct chill casting in a resistance furnace. Pure Mg and M2 master alloy (Mg + 2 wt.% Mn) were molten in the furnace at 710 °C, followed by the addition of pure Gd. Details of casting and extrusion processes as well as material characterization have been described in a previous study<sup>3</sup>. Different to that, for this work extrusion temperature was set to 450 °C with profile exit speed ranging from 0.75 to 1.50 and 3.00 m/min. In addition, grain orientations were characterized by texture measurements. Inverse pole figures in extrusion direction were measured by X-ray diffraction. Degradation behaviour was determined by weight loss after semi static immersion in Dulbecco's Modified Eagle Medium for 7 d. Sample size was 1.4 mm height and 9 mm diameter.

**RESULTS:** Microstructure evolution is exemplarily shown in Fig. 1. An increase in extrusion speed leads to an increase in grain size and a decrease in hardness. Grain sizes are ranging from 14 to 28 μm for all alloys. Degree of recrystallization is increased with increasing speed

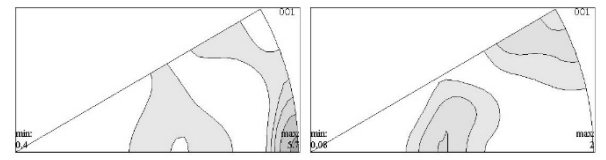


and Gd content.

Fig. 1: Left: 0.75 m/min, right: 3.00 m/min.

Different grain orientations after extrusion are caused by different extrusion speeds and Gd contents as exemplarily shown in Fig. 2. Low extrusion speeds cause higher intensities for <10-10> poles which vanish with increasing speeds and Gd content. Beneficial rare earth textures with basal planes titled out of extrusion directions are present<sup>4</sup>. Consequently, yield strengths for tension (TYS) and

compression (CYS) vary as seen in Fig. 3. Overall, Mg-10Gd-0.5Mn shows highest yield strengths with Mg-2Gd-0.5Mn and Mg-5Gd-0.5Mn possessing similar tensile properties. However, yield asymmetry is observed for all alloys. Furthermore, with increasing Gd content this asymmetry is gradually reversed as was reported before.<sup>5</sup> Corrosion measurements reveal slow and



homogeneous degradation of around 0.1 mm/year.

Fig. 2: Left: Mg-2Gd-0.5Mn @ 0.75m/min, right: Mg-10Gd-0.5Mn @ 3.00 m/min

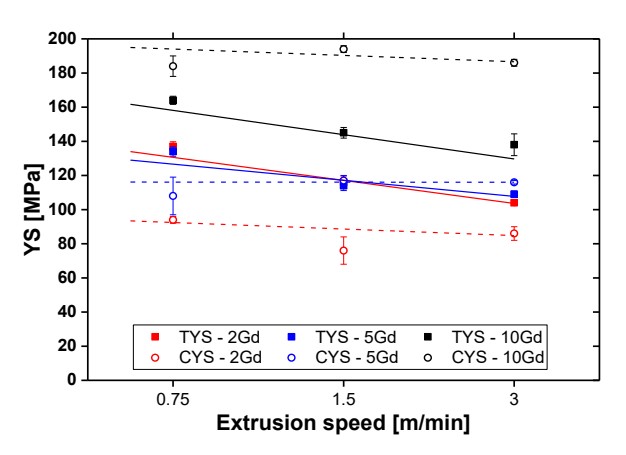


Fig. 3: Yield strengths showing a change in asymmetry with increasing Gd content (all alloys with addition of 0.5 wt.% Mn).

DISCUSSION & CONCLUSIONS: Ternary Mg-Gd-Mn alloys show high potential for biomedical application as sufficient mechanical and robust corrosion properties are present. Microstructures can be tailored by processing according to required properties of implant materials. Anisotropy in mechanical properties might be advantageous for different types of implant.

**REFERENCES:** <sup>1</sup>F. Feyerabend et al. (2010) Acta Biomaterialia, 6: 1834. <sup>2</sup>M. Silva Campos (2016) Dissertation. <sup>3</sup>J. Harmuth et al. (2017) Influence of extrusion parameters on Mg-10Gd, 9<sup>th</sup> Biometal, Bertinoro, Italy. <sup>4</sup>N. Stanford, M. R. Barnett (2008) Mat Science Eng A, 496: 399. <sup>5</sup>D. Nagarajan et al. (2016) Metall and Mat Trans A, 47: 5401.

#### Densification and microstructure of spark-plasma sintered WE43 powder

J. Soderlind<sup>1</sup>, R. Schäublin<sup>2</sup>, M Cihova<sup>2</sup>, S.H. Risbud<sup>1</sup>, T. Y. J. Han<sup>3</sup>, J. F. Löffler<sup>2</sup>

<sup>1</sup>Department of Materials Science, University of California Davis, Davis, CA, USA; <sup>2</sup> Laboratory of Metal Physics and Technology, Department of Materials, ETH Zurich, 8093 Zurich,

Switzerland; <sup>3</sup>Lawrence Livermore National Laboratory, Livermore, CA, USA

**INTRODUCTION:** Microstructural refinement of Mg alloys is known to be beneficial for both mechanical and corrosion properties. Processing by conventional methods (melt casting) does not result in a refined microstructure<sup>1</sup>. Spark plasma sintering (SPS) is an attractive alternative processing method which offers both densification and microstructure control<sup>2</sup>. We report here on the characterization of microstructural evolution in gas-atomized WE43 powder upon sintering with different SPS conditions.

METHODS: The WE43 powder (provided by Magnesium Elektron Ltd) has been gas atomized in Ar with a cooling rate on the order of 10<sup>6</sup> K/s. Powder had a wide size distribution (10-300μm), and a regular spherical shape. Samples were sintered at temperatures from 300-450°C for 10 minutes, and resulting microstructures were observed in scanning and transmission electron microscopy (S/TEM) chemical analysis using energy dispersive X-ray spectroscopy (EDS).

RESULTS: The atomized powder presents a dendritic microstructure with grain sizes ranging from 10-50 µm (Fig.1a). Samples sintered for 10 min at  $T_{\text{max}}$  of 300°C, 350°C, 400°C and 450°C have an average porosity of 24%, 20%, 3%, and ~0% respectively. Samples sintered from 300-350°C show no significant microstructure difference to the powder even as consolidation begins, and densification has not passed stage II sintering (Fig.1b). Segregation of alloying elements was observed between samples sintered at 350°C and 400°C, with Nd precipitatig within the Mg matrix and Y migrating to particle interfaces (Fig.1c) and sintering has reached stage III. The sample sintered at 450°C for 10 min (Fig.1d) shows well-pronounced elemental segregation with Ndrich intermetallics and thickened Y rich particle boundaries. Additionally, the Mg matrix shows some nanoscale precipitates of both an Nd and Y rich phase.

DISCUSSION & CONCLUSIONS: Results show that the densification depends strongly on the sintering temperature. We find that at low temperatures the powder begins to sinter, while the microstructure remains unaltered. At higher temperatures, however, densification is

accompanied by a drastic microstructural modification from an intermetallic network to isolated intermetallic precipitates.

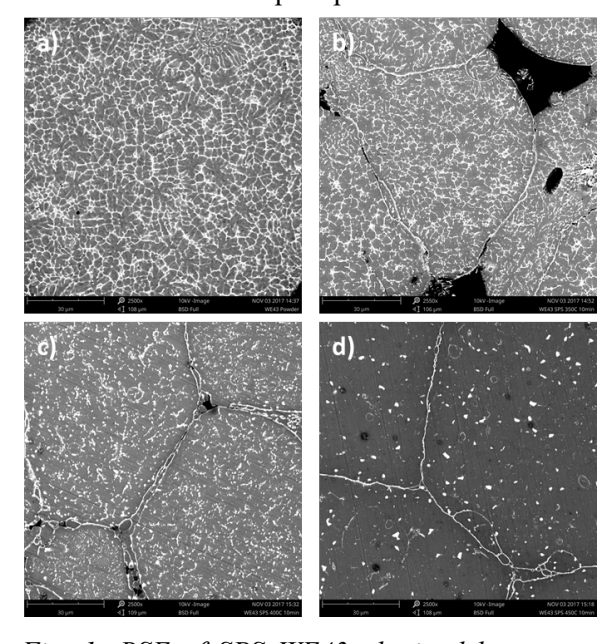


Fig. 1: BSE of SPS WE43 obtained by means of Scanning Electron Microscopy (SEM) showing (a) the WE43 powder and the densified microstructure after sintering at (b) 350 °C, (c) 400 °C, and (d) 450 °C.

The precipitates obtained by SPS are substantially smaller than those typically obtained by melt-casting of WE43<sup>1</sup>. SPS provides a method to obtain fully dense WE43 together with a highly refined microstructure. It further takes place at comparatively low temperature with rapid processing times of only a few minutes.

**REFERENCES:** <sup>1</sup> Y.H. Kang *et al* (2014) *Journal of Magnesium and Alloys*. 2:109-115 <sup>2</sup> Z. A. Munir *et al* (2006) *Journal of Materials Science* 41:763-777

**ACKNOWLEDGEMENTS:** The authors acknowledge support by the UC Laboratory Fees Research Program, UCOP, Grant LGF-17-476556, and thank the Scientific Centre for Optical and Electron Microscopy (ScopeM) at ETH Zürich for providing access and assistance.

## Strengthening of a biodegradable lean Mg–Zn–Ca alloy by Equal Channel Angular Pressing

J Horky<sup>1</sup>, K Bryła<sup>2</sup>, M Krystian<sup>1</sup>, B Mingler<sup>1</sup>, L Sajti<sup>1</sup>

<sup>1</sup> <u>AIT Austrian Institute of Technology GmbH</u>, Center for Health & Bioresources, Biomedical Systems, Wr. Neustadt, AT. <sup>2</sup> <u>Institute of Technology</u>, Pedagogical University of Cracow, Kraków, PL.

**INTRODUCTION:** Low alloyed Mg-Zn-Ca is a very promising material for biodegradable metallic implants due to its slow and homogenous degradation behaviour [1]. However, its strength is limited due to only very week solid solution and precipitation hardening. It was the aim of this study to explore the possibilities of strengthening this material by severe plastic deformation.

**METHODS:** The alloy Mg-0.6Zn-0.5Ca (ZX00) was received in extruded condition. The rods with 12 mm diameter were then processed by Equal Channel Angular Pressing (ECAP) using a special double-ECAP tool [2] with an equivalent strain per (double-)pass of 1.8. Different numbers of passes were performed at different temperatures to find the optimum process parameters to achieve samples with highest hardness but still good surface quality. Microstructure was investigated by means of light microscopy on polished and etched (with dilute nitric acid) samples. Mechanical behaviour was mainly characterized by hardness tests using a Vickers indenter. In addition, tensile tests were performed on the most promising conditions. The degradation behaviour was investigated immersion tests at 37°C where the evolving H<sub>2</sub> gas was collected [3] using simulated body fluid (SBF) with TRIS-HCl buffer.

**RESULTS:** The extruded ZX00 alloy exhibits a bimodal microstructure with large grains (tens of microns) elongated in the extrusion direction and areas of smaller grains with about 6 µm diameter. The hardness in the extruded condition is  $62 \pm 2$ HV0.1. ECAP-processing decreases the fraction and size of the larger grains as well as the diameter of the finer grains. Both depends on the ECAP temperature. As an example, the microstructure after one pass at 300°C and another pass at 280°C is depicted in fig. 1. Bands of fine grains divide the larger grains and the average diameter of the fine grains is less than 2 µm. This rises the hardness to  $76 \pm 2$  HV0.1 and leads to an increase of tensile strength of 13%. Lower processing temperatures (280°C+240°C) lead to an even higher hardness (85  $\pm$  3 HV0.1, see fig. 2c) and strength, however, at a reduced tensile ductility.

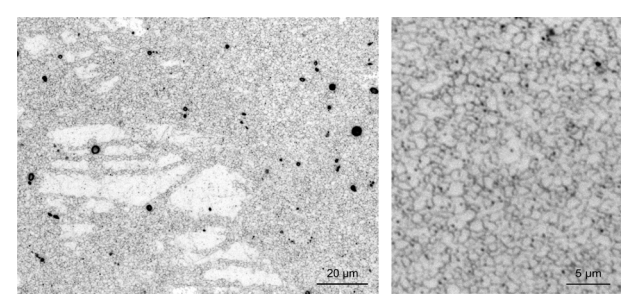


Fig. 1: Microstructure of ECAP-processed ZX00.

The immersion tests showed that ECAP and the corresponding grain refinement do not change the degradation rate in SBF.

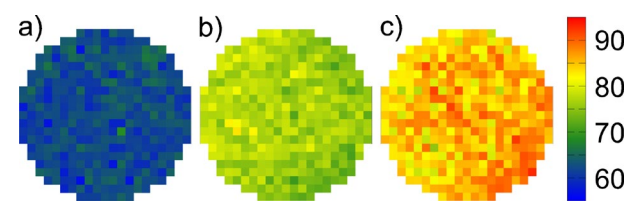


Fig. 2: Color-coded space resolved hardness values (HV0.1) of (a) as-extruded, (b-c) ECAP-processed ZX00. Two passes at the following processing temperatures were conducted: (b) 300°C+280°C, (c) 280°C+240°C.

**DISCUSSION & CONCLUSIONS:** The tensile strength of extruded low alloyed Mg-Zn-Ca can be increased through double-ECAP to ~350 MPa without forming surface cracks in the severely deformed samples. By varying the temperature of ECAP, it is possible to achieve different combinations of hardness/strength and ductility. Furthermore, the desirable low degradation rate is not altered by ECAP.

**REFERENCES:** <sup>1</sup> J. Hofstetter (2015) PhD thesis ETH Zürich. <sup>2</sup> M. Krystian, K. Bryła, J. Horky, and B. Mingler (2016) Eur Cell Mater 32 Suppl. 6:4. <sup>3</sup> G. Song, A. Atrens, and D. StJohn (2001) Magnesium Technology 2001, 255-262.

**ACKNOWLEDGEMENTS:** This work was supported by the government of Lower Austria and European Funds for Regional Development, contract No. WST3-F-5030665/001-2016

#### About the precipitates' structure in Mg–Zn–Ca-lean alloys

R. Schäublin<sup>1,2</sup>, M. Cihova<sup>1</sup>, S. A. Gerstl<sup>1,2</sup>, D. Deiana<sup>3</sup>, J. F. Löffler<sup>1</sup>

<sup>1</sup> Laboratory of Metal Physics and Technology, Department of Materials, ETHZ, 8093 Zurich, Switzerland; <sup>2</sup> Scientific Center for Optical and Electron Microscopy, ETHZ, 8093 Zurich, Switzerland; <sup>3</sup> Interdisciplinary Centre for Electron Microscopy, EPFL, 1015 Lausanne, Switzerland

**INTRODUCTION:** Biodegradable Mg-Zn-Ca (ZX)-lean alloys are promising implant materials due to their slow degradation rate, biologically safe composition, and appropriate mechanical properties [1]. The rate of degradation may depend on the type of secondary phases. In order to understand and better tailor the material to the desired properties, the microstructure of those precipitates must thus be properly assessed. In this study we have undertaken detailed investigations of the intermetallic precipitates that occur in this type of alloy using ZX20, which contains 1.5 wt.% Zn and 0.25 wt.% Ca, as a representative. The microstructure of the alloy was assessed by scanning / transmission electron microscopy ((S)TEM) in correlation with atom probe tomography (APT). The detailed crystallographic structure of the early fine precipitation and the evolving equilibrium Zn- and Ca-rich precipitates, commonly believed to be Ca<sub>2</sub>Mg<sub>6</sub>Zn<sub>3</sub>, was scrutinized.

METHODS: A lean Mg alloy containing 1.5 wt.% Zn and 0.25 wt.% Ca, named ZX20, was prepared by extrusion. Ultra-high purity Mg [2] was used to exclude the impact of impurity on the corrosion behavior. Extrusion was performed at 250°C from a diameter of 50 mm to 6 mm (extrusion ratio 1:69) with a ram speed of 0.3 mm·s<sup>-1</sup>. The extruded rods were heat treated at 500°C for 2 h in quartz tubes filled with Ar followed by quenching in water. Samples were then heated to 260°C and 350°C, which correspond to phase transitions observed in calorimetry.

The detailed microstructural characterization was performed at CIME EPFL on a TEM Osiris operated at 200 kV and on a S/TEM Themis equipped with a spherical-aberration corrector and operated at 80 kV. Both TEM's are equipped with a large-collection angle energy-dispersive X-ray spectrometer (EDS), allowing for fast chemical mapping. With the Themis chemical mapping at the atomic level was reached. APT was conducted with a LEAP 4000X HR at ScopeM ETHZ at a specimen temperature of 60 K in voltage pulsing mode.

**RESULTS:** Following heating to 260 and 350°C, ZX20 exhibits, respectively, a fine dispersion of

Guinier-Preston (G.P.) zones about 10 nm in diameter containing Zn and Ca with a ratio of 1, and Zn–Ca-rich particles. Fig. 1 shows a typical ultrahigh resolution STEM micrograph of the microstructure of a Zn–Ca-rich particle, which was matched by simulation to possible intermetallic compounds.

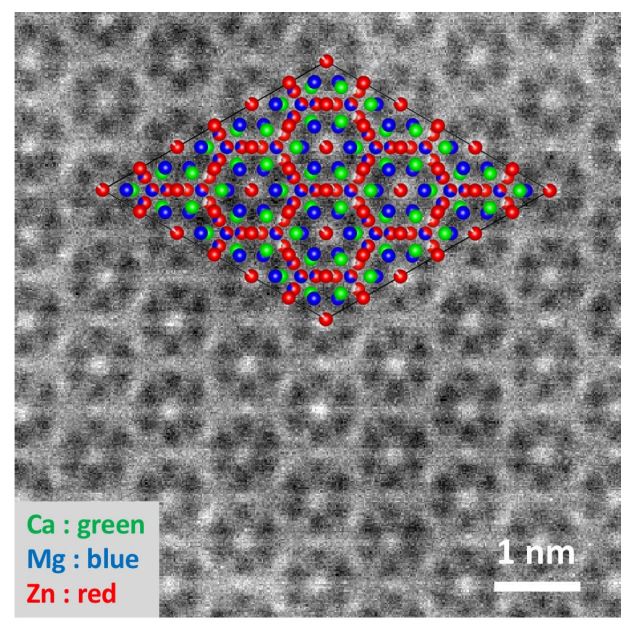


Fig. 1: STEM micrograph of a Zn–Ca-rich precipitate in ZX20 annealed at 350°C. The matching atomic structure is that of  $Ca_2Mg_5Zn_5$  [2].

**DISCUSSION & CONCLUSIONS:** The microstructural study performed, using correlative TEM and APT, allowed revealing the fine details of the precipitates' structure in Mg–Zn–Ca alloys. The G.P. zones are made of Zn and Ca, and it appears that the Zn–Ca-rich precipitates contained in ZX20 are, instead of Ca<sub>2</sub>Mg<sub>6</sub>Zn<sub>3</sub>, made of Ca<sub>2</sub>Mg<sub>5</sub>Zn<sub>5</sub>.

**REFERENCES:** <sup>1</sup>J. Hofstetter *et al.* (2015), *Acta Mater.*, 98:423-432. <sup>2</sup>J. D. Cao *et al.* (2016), *J. Mater. Res.*, 31:2147-2155. <sup>3</sup>J. F. Löffler *et al.* (2013), WO2013/1076442012

**ACKNOWLEDGEMENTS:** Support by the Swiss National Science Foundation (Grant No. 200021-157058) is acknowledged.

## On the degradation of binary Mg alloys with an ultra-low content of Ca and Zn under simulated physiological conditions

M Casas-Luna<sup>1</sup>, EB Montufar<sup>1</sup>, L Čelko<sup>1</sup>, M. Horynová<sup>1</sup>, L Klakurková<sup>1</sup>, N Hort<sup>2</sup>

<sup>1</sup>Central European Institute of Technology - Brno University of Technology, Brno, Czech Republic.

<sup>2</sup>Magnesium Innovation Centre - Helmholtz-Zentrum Geesthacht, Geesthacht, Germany.

**INTRODUCTION:** Biodegradable Mg alloys must possess appropriate corrosion rate and good mechanical properties during their service as orthopaedic implants. Mg containing Ca and Zn as alloying elements have been previously studied as finding biodegradable materials that concentrations of Ca and Zn lead to the precipitation of secondary phases which are detrimental for the corrosion resistance [1]. In the present work, a set of binary Mg alloys containing very low amount of Ca or Zn (to assure a single-phase allov) have been processed to assess the corrosion behaviour under simulated physiological conditions.

**METHODS:** Mg containing Ca or Zn as alloying element below their maximum solubility limit were processed by indirect chill casting [2] technique. Ca was mixed into Mg in amounts of 0.2, 0.4, 0.6 and 0.8 wt.%, while Zn was added into Mg in concentrations of 1, 2 and 3 wt.%. Annealing treatment was applied to get a homogeneous microstructure. The final ingots were extruded to obtain bars of 1 cm in diameter. Microstructural characterisation of the alloys was carried out by optical and scanning electron microscopy. 6-mm long discs were cut from the bars to determine the mass loss after immersion test at 7, 14 and 28 days. In addition, hydrogen evolution test was monitored for 2 weeks. Tests were performed in conventional simulated body fluid (SBF) at 37 °C.

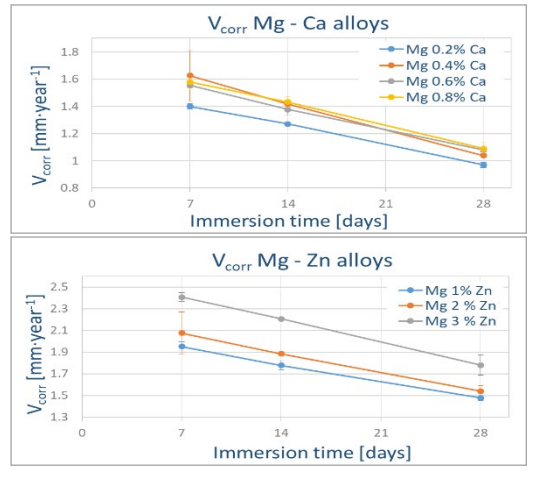


Fig. 1: Corrosion rate at 7, 14 and 28 days in SBF for Mg with an ultra-low content of Ca or Zn.

RESULTS: Fig. 1 shows the corrosion rates by mass loss of the Mg-Ca and Mg-Zn alloys. All the studied alloys tend to grow a corrosion protective layer that slows down the corrosion rate. For lower content of Ca and Zn, the degradation is slower. Corrosion rate increases with content of Zn, meanwhile the corrosion rate is similar for the alloys containing 0.4, 0.6 and 0.8 wt.% of Ca, suggesting that there is no effect of the composition in that range for the Mg-Ca alloys. Table 1 compares the corrosion rates obtained by mass loss and H<sub>2</sub> evolution tests, being slightly higher but not statistically different.

Table 1. Corrosion rate of processed Mg alloys after 2 weeks in SBF at 37 °C.

Alloy	V <sub>corr</sub> by mass	V <sub>corr</sub> by H <sub>2</sub>
composition	loss	evolution
[wt.%]	[mm·year-1]	[mm·year <sup>-1</sup> ]
Mg – 0.2%Ca	1.27	2.88
Mg - 0.4%Ca	1.42	3.02
Mg - 0.6%Ca	1.38	2.80
Mg - 0.8%Ca	1.43	2.80
Mg - 1%Zn	1.78	1.88
Mg - 2%Zn	1.89	3.25
Mg - 3%Zn	2.21	3.03

**DISCUSSION & CONCLUSIONS:** For the Mg alloys containing Ca or Zn in concentrations below the solubility limit, the corrosion rate is found to be decreased compared to the pure Mg under SBF at 37 °C [3]. In general, Mg alloys with low content of Ca exhibit better corrosion resistance. When the Ca content is 0.2 wt.%, the best resistance to the degradation was observed. Nevertheless, the H<sub>2</sub> production is higher during the first 24 h for the Mg-Ca alloys in comparison to the Mg-Zn. After 48 h, a passivation and consequently decrement in the H<sub>2</sub> production is achieved for the Mg-Ca alloys, reflected in a nearly constant corrosion rate for the followed monitored 14 days.

**REFERENCES:** <sup>1</sup> F. Witte, N. Hort, C. Vogt, et al (2008) *Curr. Opin. Solid St. M.* **12**:63-72. <sup>2</sup> F.R. Elsayed, N. Hort, M.A. Salgado-Ordorica, et al (2011), *Mater. Sci. Forum* **690**:65-68. <sup>3</sup> Y. Wang, M Wei, et al (2008) *Mater. Lett.* **62**:2181-84.

**ACKNOWLEDGEMENTS:** To CEITEC Nano RI, MEYS CR, 2016-2019. To project CEITEC 2020 (LQ1601); and MCL to Brno Ph. D. Talent scholarship.

# Microstructure and mechanical properties of Mg-RE biomaterials processed by rotary swaging

F D'Elia<sup>1</sup>, P Hiester<sup>1</sup>, A Kopp<sup>1</sup>, C Ptock<sup>1</sup>

<sup>1</sup> Meotec GmbH & Co. KG, Aachen, Germany.

INTRODUCTION: Magnesium-rare earth (Mg-RE) alloys show promise for use in biomedical applications. This is mainly attributed to their excellent mechanical properties, good corrosion resistance and biocompatibility. Nevertheless, advantages, improvements despite such mechanical properties and corrosion resistance are always desired when developing new alloys for biomedical implants. In turn, processing parameters and post-processing techniques are of critical importance. Rotary swaging (RS) is a hammer forging process for the reduction of cross section of rods, tubes and wires that can lead to substantial grain refinement and corresponding enhancement of mechanical properties. Moreover, such grain size reduction can further improve corrosion resistance hence making the alloys more suitable for biomedical applications.

**METHODS:** In this research, an investigation on microstructure and mechanical properties of WE43 Mg alloy and a recently developed Mg-RE WEZ221 alloy2 processed using RS was carried out. Magnesium alloy WE43 and WEZ221 billets were produced via a modified direct chill casting method. The alloys were prepared from high purity (99.97 %) Mg ingots with addition of 4 wt% pure (99.9%) Y, 3 wt% pure (99.9%) Nd and 0.5 wt% Zr (Mg-Zr master alloy) for WE43 and addition of both 2 wt% pure (99.9 %) Gd and pure Y, 0.7 wt% pure (99.99%) Zn and 0.2 wt% Zr for WEZ221. The billets were then machined and extruded at 450 °C and finally either aged or subjected to RS with varying deformation degrees. Extensive microscopy (optical and scanning electron) was carried out on samples after casting, extrusion and ageing, and RS. Finally, microhardness and degradation testing via

hydrogen evolution tests were carried out after each processing stage.

**RESULTS:** A significant increase in hardness was observed for both alloys after extrusion and ageing. This was attributed to a reduction in grain size and development of texture. Moreover, ageing was seen to promote a dense precipitation of very fine β phases in the WEZ221 matrix, which also contributed to the improved hardness for this alloy2. Rotary swaging was found to have a pronounced impact on the alloy microstructure and subsequent hardness of WE43 and WEZ221. Overall grain size reduction was more pronounced for samples processed by RS in comparison to those solely extruded. As a result, the overall hardness was also further improved after RS.

Finally, the rate of degradation was found to be consistent with grain size. Extruded samples with larger grains were seen to degrade faster than those processed by RS.

**DISCUSSION & CONCLUSIONS:** The results suggest that RS is a feasible method to reduce grain size and subsequently improve mechanical properties and corrosion resistance of Mg alloys. Hence, RS demonstrates potential for post-processing of Mg alloys intended for use in biomedical applications.

**REFERENCES:** 1 W.M. Gan et al. (2014) *Mater. Des.* **63**:83-88. 2 T. Homma, N. Kunito and S. Kamado (2009) *Scripta Mater* **61**:644-647.

**ACKNOWLEDGEMENTS:** The authors are grateful to Mr. G. Meister from MagIC at Helmholtz Zentrum Geesthacht for carrying out the casting experiments of WEZ221 and to Mr. I. Schestakow from Meotec for help with sample preparation.

### Biodegradable implants: Fe-Mn-Ag alloy for bone regeneration scaffolds

C Tonna<sup>1</sup>, B Mallia<sup>1</sup>, J Buhagiar<sup>1</sup>

<sup>1</sup> <u>Department of Metallurgy and Materials Engineering, University of Malta, Msida, MSD 2080, Malta</u>

INTRODUCTION: Biodegradable metals have recently gained particular focus for use as bone regeneration scaffolds, particularly in cases of trauma and genetic malformations [1]. Iron and its alloys were proposed as an alternative to the avidly studied Mg-alloys, with the aim of providing adequate strength and stiffness as well as a slower degradation rate in-vivo. The first and consequent studies however, showed that the corrosion rate for Fe was inadequately slow [2]. Thus, this work explores the possibility of creating macro-porous scaffolds from Fe-Mn-Ag using powder metallurgical techniques. This alloy is expected to be MRI-compatible while exhibiting enhanced strength compared to Fe and good densification through the flow of silver via a liquid-phase sintering mechanism. The alloy is also expected to trigger micro-galvanic corrosion to enhance the corrosion rate.

**METHODS:** The macro-porous scaffolds were fabricated using the replication technique. This involved the creation of a slurry using the metallic powder mixture, polyvinyl alcohol binder and ethanol. Reticulated polyurethane foam sponges were dipped into the slurry and then squeezed in order to remove excess slurry from the pores. The foam was then subjected to a heat treatment in order to burn-off all organic material and sinter the metallic powders at 1200°C for 4 hours.

The resulting scaffolds were investigated using Scanning Electron Microscopy (SEM). Phase analysis was also carried out by compacting the scaffolds into a disk shape under a pressure of 440 MPa for 5 minutes and carrying out X-ray Diffraction. Static immersion testing was conducted in 100 ml phosphate-buffered saline (PBS) solution. The samples were incubated in 5% (v/v) CO<sub>2</sub> at 37°C for 7 and 14 days. Mechanical performance was analysed via compression testing.

**RESULTS:** The resulting macro-porous scaffold may be seen in Figure 1. The SEM image confirms the presence of interconnected porosity. The analysed pore window size is approximately  $1118 \pm 218 \, \mu m$ . Figure 2 also shows the effective

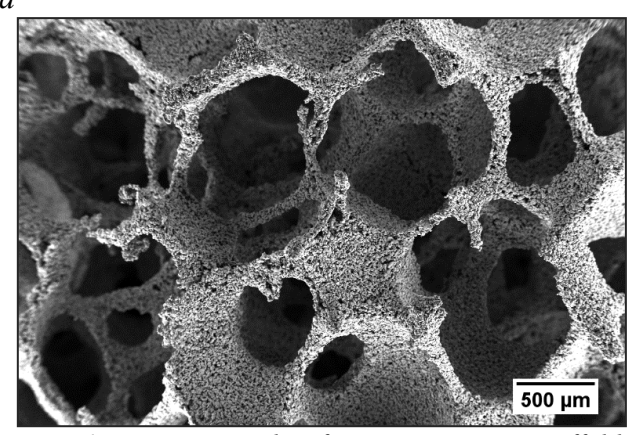


Fig. 1: Micrograph of macro-porous scaffold structure showing interconnected porosity

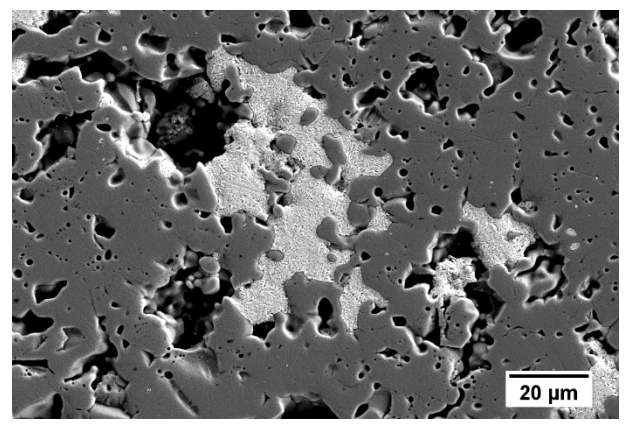


Fig. 2: Cross-section of scaffold strut showing densification through the flow of liquid silver.

densification of the struts through the flow of liquidphase silver.

DISCUSSION & CONCLUSIONS: The developed scaffolds both exhibited good densification, as shown in Figures 1 and 2. The interconnectivity of the pores is crucial for the application to allow for effective movement of growth factor, cells and waste transport, to support and regenerate viable bone. Silver provided effective densification in uniformly distributed localised areas within the Fe-based matrix.

**REFERENCES:** <sup>1</sup> Y. Fillingham, J. Jacobs (2016) *The bone and joint journal* **98-B**: 6-9. <sup>2</sup> M. Peuster, P. Wohlsein, M. Brgmann, M. Ehlerding, K. Seidler, C. Fink, H. Brauer, A. Fischer, and G. Hausdorf (2001) *Heart* **86**: 563–9.

### Ag-alloyed degradable twinning-induced plasticity steel for improving the corrosion behaviour

Sergio Loffredo<sup>1,2</sup>, Carlo Paternoster<sup>1</sup>, Nicolas Giguère<sup>3</sup>, Maurizio Vedani<sup>2</sup>, Diego Mantovani<sup>1</sup>

<sup>1</sup>Lab. Biomaterials and Bioengineering, CRC-I, Dept. Min-Met-Mat Engineering & CHU de Québec Research Center, Laval University, Quebec City, Canada <sup>2</sup>Dept. of Mechanical Engineering, Politecnico di Milano, Italy <sup>3</sup>Quebec Metallurgy Center, Trois-Rivières, Canada

**INTRODUCTION:** Mechanical properties of suitable materials for absorbable cardiovascular scaffolds have an influence on the final performance of the device: even if degradable Mg-based stents are already available on the market, the quest for materials with high mechanical properties is still open. For example, twinning-induced plasticity (TWIP) steels have mechanical properties comparable to those of Co-Cr alloys, while having a limited resistance to chloride attack [1]. In spite of the passivation tendency of certain alloying elements [2], galvanic coupling of iron with noble elements is a proposed solution to accelerate degradation without significantly affecting the mechanical performance [3].

METHODS: Two Fe-Mn-C(-Ag) alloys were produced by melting pure elements (≥ 99.7% wt.) in an induction furnace with a liquid argon protection system, in order to minimize fire losses. The cast billets were then solution treated at 1100°C for 12 hours in vacuum, followed by Ar-assisted high pressure quench. The billets were then rolled at different thickness reductions (10%, 25% and 50%) in order to have different levels of deformation. Annealing was performed for 1 batch of 25% cold rolled samples at 800°C for 15 minutes, followed by water quench. Optical microscopy, SEM and XRD were performed to assess the microstructure of both alloys. Tensile tests were carried out to evaluate the effect of Ag on mechanical properties.

Static immersion tests for 14 days in Hanks' modified salt solution in a 5% CO<sub>2</sub> atmosphere were used to study the degradation behaviour of both alloys in the annealed and deformed conditions. Degradation products were analysed by means of XRD and SEM. The amount of released ions was assessed by MP-AES.

**RESULTS:** XRD showed that only  $\gamma$ -Fe is present in the Ag-free alloy. On the other hand, for the Agbearing alloy, XRD revealed the formation of  $\varepsilon$ -martensite for high levels of deformation (rolling reduction  $\geq$  25%). The addition of Ag produced a slight, but significant, hardening effect. The ductility was decreased, but kept at acceptable levels (> 40%).

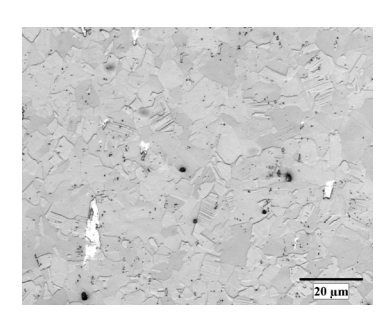


Fig. 1: Optical micrograph of the Ag-bearing alloy after 10% thickness reduction by cold rolling

While the degradation rate for the Ag-free alloy increased with increasing deformation level, no significant difference was observed in the case of the Ag-bearing alloy. Moreover, the degradation rate was significantly lower for the Ag-bearing alloy. Degradation product analysis revealed the presence of rhodochrosite (MnCO<sub>3</sub>) for both alloys, while goethite (FeO·OH) was detected only for the Ag-bearing alloy. On the other hand, the amount of Fe and Mn released in solution was similar for both alloys. No Ag was released in solution (< 1 ppm). A nearly compact degradation layer was observed for high deformation levels in the Ag-bearing alloy.

DISCUSSION & CONCLUSIONS: The addition of Ag in a TWIP steel resulted in modified microstructure and mechanical properties. However, degradation was prevented by the formation of a compact degradation layer. Further investigations must be carried out to fully elucidate the degradation mechanism.

**REFERENCES:** <sup>1</sup> Y. Zhang, X. Zhou (1999) *Corr Sci* **41**(9):1817-33. <sup>2</sup> T. Kraus, F. Moszner, S. Fischerauer, et al (2014) *Acta Biomater* **10**(7):3346-53. <sup>3</sup> M. Schinhammer, A. Hänzi, J. Löffler et al. (2010) *Acta Biomater* **6**(5):1705-13.

ACKNOWLEDGEMENTS: This work was funded by Natural Sciences and Engineering Research Council of Canada under the CU-I2I program. SL acknowledges funding from a Vanier Canada Graduate Scholarship.

### Micro-alloying of Mg-Zn based alloys – Influence on corrosion behaviour

YM Jin<sup>1</sup>, B Wiese<sup>1</sup>, F Feyerabend<sup>1</sup>, C Blawert<sup>2</sup>, J Bohlen<sup>2</sup>, R Willumeit-Römer<sup>1</sup>

<sup>1</sup> Institute of Metallic Biomaterials, Helmholtz-Zentrum Geesthacht, 21502, Germany

<sup>2</sup> Institute of Magnesium Innovation Center, Helmholtz-Zentrum Geesthacht, 21502, Germany

**INTRODUCTION:** Mg and its alloys have many outstanding properties comparing to other materials such as low density, high strength and non-toxicity, which make them perfect candidates for biomedical implants<sup>1</sup>. Zinc is one of the most abundant nutritionally essential elements in the human body, and can improve the corrosion resistance and mechanical properties of magnesium alloys2. Nowadays, much attention have been paid to microalloying system due to its limited release amount of alloying elements even with high corrosion rate. In this study, Mg-0.5Zn and Mg-0.5Zn-0.2X (X=Ca, Sr, Ag, In, Cu) were cast and then extruded. Different characterization techniques were applied to investigate the corrosion behaviour of these alloys.

**METHODS:** Pure alloying metals were melted at 720 °C and then cast into crucibles which were preheated to 680 °C. The cylindrical ingots were machined into billets and then extruded at 350 °C with extrusion speed of 0.6 mm/s, 2.2 mm/s and 4.4 mm/s. The compositions of all samples were determined by spark emission spectroscopy for Fe, Cu and Ni and by atomic absorption spectroscopy for Ca and Ag. In order to characterize the corrosion behaviour, Hydrogen (H<sub>2</sub>) evolution in 0.9 wt.% NaCl solution at room temperature was measured for one week.

**RESULTS:** By changing the extrusion speed, different alloys with similar grain size were obtained. The grain sizes of Mg-Zn and Mg-Zn-Cu with extrusion speed of 2.2 mm/s and Mg-Zn-Ca, Mg-Zn-Sr, Mg-Zn-In, Mg-Zn-Ag with extrusion speed of 4.4 mm/s are around 30  $\mu$ m.

Using Eq. 1 the corrosion rate was calculated as shown in Fig. 1, where  $V_H$  is the hydrogen evolution rate  $(ml/cm^2/d)$  and  $P_w$  is the corrosion rate (mm/year).<sup>3</sup>

$$P_w = 2.279 \, V_H \tag{1}$$

For the as-cast Mg-Zn-X alloys, by comparing to the as-cast Mg-Zn reference, the corrosion resistance becomes higher by the addition of Ca. For the as-extruded Mg-Zn-X alloys, the corrosion resistance of Mg-Zn-Ca, Mg-Zn-Sr and Mg-Zn-In are better than that for the reference material. The corrosion rate of Mg-Zn-Ca after one week immersion is  $0.12\pm0.03$  and  $0.05\pm0.01$  mm/year for as-cast and as-extruded condition, respectively.

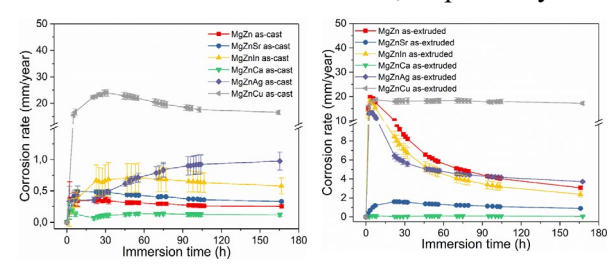


Fig. 1: Images of corrosion rate of as-cast and asextruded Mg-Zn and Mg-Zn-X alloys indicated by Hydrogen evolution test up to one week.

**DISCUSSION & CONCLUSIONS:** In order to exclude the effect of grain size on the corrosion behaviour of Mg-Zn-X systems, alloys with similar grain size (~30 µm) have been successfully obtained. Although adding only 0.2 wt.% of the alloying element, a big difference can still be seen among the alloys considering the corrosion rate. In the case of both as-cast and as-extruded condition, Mg-Zn-Ca behaves the best and Mg-Zn-Cu behaves the worst. In addition, Cl<sup>-</sup> is well known as detrimental to the corrosion behaviour due to its pitting effect. It is reasonable to assume that the corrosion performance of these alloys will be better when immersed into in vitro media such as simulated body fluid and cell culture medium. To elucidate the corrosion mechanism, Scanning Kelvin Probe Force Microscope will also be used to determine the electrochemical potential of the intermetallics and the matrix.

**REFERENCES:** <sup>1</sup> G.L. Song (2011) *Corrosion electrochemistry of magnesium (Mg) and its alloys*, Woodhead publishing. <sup>2</sup> S.X. Zhang, X.N. Zhang, C.L. Zhao, et al (2010) *Acta Biomaterialia* **6**: 626-640. <sup>3</sup> G.L. Song, A. Atrens, D. StJohn (2001) Magnes. Technol. 2001: 254-262.

**ACKNOWLEDGEMENTS:** Yiming Jin thanks China Scholarship Council for the award of fellowship and funding.

### In vitro degradation behaviour of biodegradable Mg alloy wires/Polylactic acid composite used for orthopedic implants

Hong Cai<sup>1,2</sup>, F Xue<sup>1,2</sup>, CL Chu<sup>1,2</sup>, J Meng<sup>1,2</sup>, Y Zhang<sup>1,2</sup>, J Bai<sup>1,2\*</sup>

<sup>1</sup> School of Materials Science and Engineering, Southeast University, Nanjing, China

<sup>2</sup> Jiangsu Key Laboratory for Advanced Metallic Materials, Jiangning, Nanjing, Jiangsu, China

**INTRODUCTION:** We prepared the Mg alloy wires/Polylactic acid composite for orthopedic implants to replace current polylactic acid (PLA), which has the shortness of low strength and long term acidic micro-environment with low pH value around the implant susceptible to induce local inflammation during degradation process [1][2]. The composite combines the advantages of PLA and magnesium alloy to achieve the adjustability of mechanical properties, pH value and degradation rate of implants.

**METHODS:** The Φ 0.3mm Mg alloy wires after micro-arc oxidation (MAO) treatment were covered with PLA/dichloride solution. After dried, the PLA lamina containing Mg alloy wires and blank PLA lamina were stacked according to the pre-calculated content. The composite rods with the sizes of 6 mm in diameter and 120 mm in length were fabricated by hot press (HP) at 165°C followed by cooling down to 80°C, and were sequentially hot drawn (HD) through molds of different sizes at 165°C each pass. To evaluate their in vitro degradation performance, the immersion experiments in Hanks solution with pH=7.2 were performed.

**RESULTS:** We got the degradation rates from the changes of bending strength and the number average molecular weight  $(M_n)$  with time (Fig. 1).

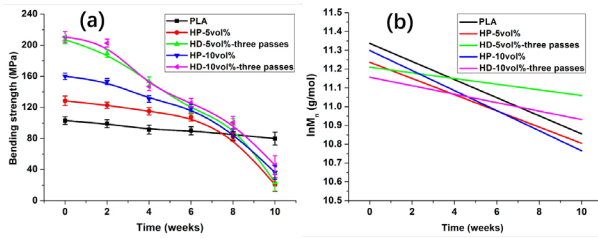


Fig.1: (a) The changes of bending strength with degradation time, (b) The relationship between  $lnM_n$  of PLA and degradation time in various groups of sample.

The sequences of bending strength changes is HD-5 vol%-three passes > HP-5 vol% > HD-10 vol%-three passes > HP-10 vol% > PLA. The sequences of degradation rate k value listed as HP-10 vol% >

PLA > HP-5 vol% > HD-10 vol%-three passes > HD-5 vol% three passes illustrates the degradation rate of PLA in each group. Firstly, the degradation rate of PLA in different pH medium is alkaline > acidic > neutral. Secondly, the amorphous regions in the HP composite made the water easily diffused into the interior of PLA molecular chains than the composite with higher crystallinity. Additionally, the amount of PLA molecular chains in the specimen with 10 vol% initial wires content is less than that with 5 vol% initial wires content. The main composition of the corrosion products with a flower-like structure (Fig. 2) on the surface of Mg alloy wires include CaO, Mg(OH)2 and MgCO3 according to the XPS results.

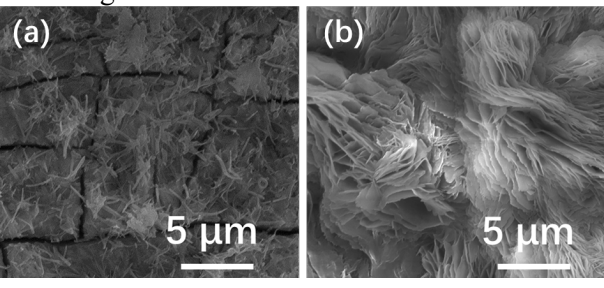


Fig.2: The morphologies of corrosion product on the surface of Mg alloy wires at different position in the composite (a) inner layer (b) outer layer.

**DISCUSSION** & **CONCLUSIONS**: The degradation rate of the composite is slow in the early stage and fast in the later period, which could meet the actual requirement and satisfy the doctor's expectation. The corrosion product is benefit to the formation of new bone tissue.

We can effectively control the mechanical properties and the degradation rates of the composite rods. So the novel composite rods show good potential for biomedical applications in the instruments of orthopedic inner fixation.

**REFERENCES:** <sup>1</sup>P. Mainil-Varlet, S. Gogolewski, P. Nieuwenhuis (1996) *J Mater Sci Mater Med* 7:713-21. <sup>2</sup> J.E. Bergsma, W.C. Bruijn, F.R. Rozema, et al (1995) *Biomaterials* 16:25-31.

### Development of novel chill cast Zn – based alloys for degradable paediatric stent applications

A. L. Ramírez-Ledesma<sup>1,2</sup>, D. Mantovani<sup>2</sup>, M. Vedani<sup>1</sup>

Department of Mechanical Engineering, Politecnico di Milano, Milan, Italy. Lab. for Biomaterials & Bioengineering (CRC-I), Dept. Min-Met-Materials Engineering & Research Center CHU de Québec, Laval University, Québec City, Canada.

**INTRODUCTION:** It is well known that one of the most important challenges to be overcome regarding bioabsorbable alloys is the selection of non - toxic elements [1]. The aforementioned becomes more critical when research lies on the fabrication of paediatric stents [2]. Zn - based biodegradable materials are an important promise due its standard corrosion potential (-0.76 V) which is between Fe (-0.44 V) and Mg (-2.37 V). Moreover, posses an inherent properties pro human health: is essential element in human nutrition and is crucial in cell proliferation and induces wellness to the immune and nervous system, etc [3]. During the 9th BIOMETAL symposium Prof. N. Hort et al [4] provide to all audience the relevance to perform in a properly way all the production process regarding biodegradable alloys. Among several parameters stand out: fusion, casting, solidification and protective atmospheres involved. In this work, it is exhibit microstructural features related to chill – cast Zn – based alloys and its corresponding extruded SEM micrographs. Extrusion experiments were carried out with specific intention to use these materials as paediatric stents.

METHODS: High purity Zn, Mg and Ag were used as starting materials for processing the experimental Zn - Mg and Zn - Ag - Mg alloys. All alloys were processed by vacuum induction melting under an argon (Ar) atmosphere. In order to avoid melt contamination alumina crucibles were used for alloy casting [5]. A master alloy was melt which consist in Ag - 10.2 wt. % Mg, with the main purpose to decrease the melting point of Ag and dilute it into Zn. The ternary alloy was poured at ~ 750 °C (1023.15 K) in a copper mold with a cooling system where water is recirculating all the time during melting and in the casting process, in consequence, the cooper mold maintain its temperature similar or below the room temperature. A solution treatment at 370 °C (643.15 K)  $\pm$  2 °C for 5 hours followed by water quenching was applied to all alloy systems to induce a stress relaxation due high cooling rates, dissolve soluble phases formed during

solidification and homogenize the alloying elements. To produce stents precursors extrusion experiments were perform at 250 °C (523.15 K) with a ratio of 25:1.

**RESULTS:** Fig. 1(a – c) exhibit optical micrographs of the microstructural evolution steps described in the last section from the as – cast, solution treatment and extrude conditions, respectively. Fig. 1(d) shows microstructural details by SEM of the extrude condition related to a Zn – Ag-Mg biodegradable alloy.

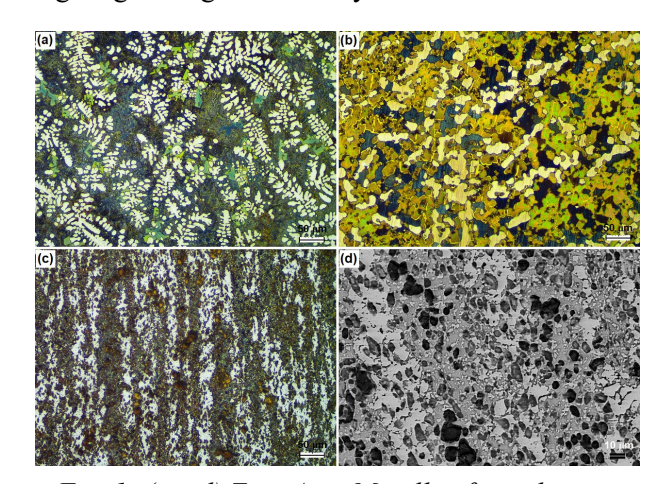


Fig. 1: (a - d) Zn - Ag - Mg alloy from the as – cast to extrude condition.

**DISCUSSION & CONCLUSIONS:** In this work it is exhibit principally a novel chill – cast Zn – Ag – Mg alloy to be use as biodegradable material and subsequently produce stent precursors to treat congenic paediatric diseases.

**REFERENCES:** <sup>1</sup> H. Hermawan et al (2010) *Acta Biomater*. **6**:1693-97. 2 D. Schranz et al (2006) *Catheter. Cardiovasc. Interv.* **67**:671-73. P. Zartner et al (2007) *Catheter. Cardiovasc. Interv.* **69**:443-46. <sup>3</sup> E. Mostaed et al (2018) Acta Biomater. In press. <sup>4</sup> N. Hort et al (2017) 9<sup>th</sup> BIOMETAL Met – 1. <sup>5</sup> A. L. Ramirez-Ledesma et al (2016) *Acta Mater.* **111**:138-47.

**ACKNOWLEDGEMENTS:** Consejo Nacional de Ciencia y Tecnología (CONACYT).

### Fabricating bio-scaffolds by coating hydroxyapatite on metallic 3D woven lattices

Ju Xue<sup>1</sup>, James Guest<sup>2</sup>, Warren Grayson<sup>3</sup>, Shoji Hall<sup>1</sup> and Timothy P. Weihs<sup>1</sup>

1 Department of Materials Science and Engineering, Johns Hopkins University

2 Department of Civil Engineering, Johns Hopkins University

3 Department of Biomedical Engineering, Johns Hopkins University

**INTRODUCTION:** There is a strong need for the next generation of bio-scaffolds that combine biologically activated coatings with porous and biodegradable substrates. Here we present studies of 3D woven metallic lattices that are designed using optimization enhance topology to permeability and mechanical stiffness and are coated uniformly with hydroxyapatite (HAp) to improve bioactivity and osteointegration. The ultimate goal is to weave and coat Mg alloy wires. Here we present initial results describing successful coating of HAp on 304 stainless steel weaves and a study of in vitro corrosion of Mg alloy wires of various chemistries and diameters.

**METHODS:** 304 stainless steel wires with diameters of 152 μm (Z direction) and 202 μm (Warp and Fill direction) were woven into parts with dimensions of 3.6mm x 36mm x 500mm using a 3D weaving machine (Fig. 1(A)). The weave was then cut into smaller samples, ultrasonically cleaned and electrochemically coated with HAp using an aqueous solution containing  $Ca(NO_3)_2$ ,  $NH_4H_2PO_4$  and  $NaNO_3$ . Various coating parameters were explored to offer a systematic understanding of the deposition process.

Immersion testing was carried out according to ASTM-G31-72 standard practice<sup>2</sup> on a range of Mg alloy wires using a modified-simulated body fluid (m-SBF)<sup>3</sup> at 36.5°C. Weight losses and pH changes were monitored and the chemistry and microstructure of the resulting corrosion products were characterized.

**RESULTS:** The HAp coatings are uniformly distributed throughout the weaves and consist of "nano flakes" or crystals (Fig. 1(B)). X-ray diffraction (XRD), energy dispersive spectroscopy (EDS), and Raman spectroscopy data confirm that the coating is HAp under the optimized deposition conditions.

Weight loss and pH changes are reported as a function of time for multiple chemistries and wire diameters. The corrosion products are relatively uniform along the lengths and diameters of the wires, and they are depleted in Mg as expected. Sites of more intense corrosion appear to correlate with the as-drawn microstructures and cracking

within the corrosion product is attributed to the development of tensile stresses within the product. **DISCUSSION & CONCLUSIONS:** By using an electrolyte containing calcium and phosphate ions, coatings of HAp with a nearly ideal atomic ratio were deposited onto stainless steel 3D weaves. The coatings are distributed relatively uniformly across the multiple layers of the weave, suggesting that ion flux is high during deposition and local depletion zones within the 3D weaves are avoided. The effects of deposition parameters, such as potential, are reported. Plans for applying the deposition method to bio-degradable 3D Mg alloy weaves will be described. The Mg alloy wires to be used for the 3D weaving will be chosen based on the corrosion results. The initial in vitro results suggest that corrosion rates are high and need to be minimized through judicious choices of Mg alloys and wire drawing and annealing parameters.

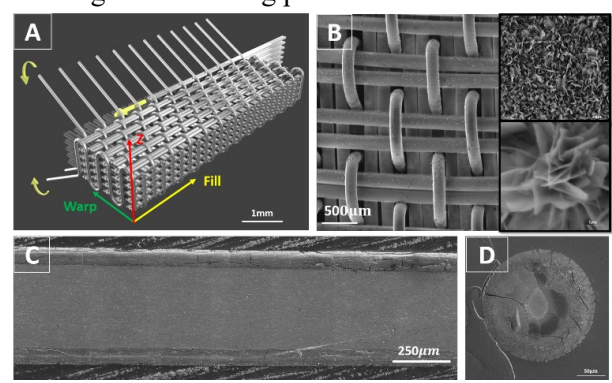


Figure 1: (A) schematic of 3D weave; (B) a top view image of HAp on stainless steel weave; (C) longitudinal cross-section of Mg wire after 22 hr corrosion; (D) normal cross-section image of Mg wire after 193hr.

**REFERENCES:** 1. Zhao, L. *et al.* Permeability measurements and modeling of topology-optimized metallic 3-D woven lattices. *Acta Mater.* **81,** 326–336 (2014). 2. Cor, E. Standard Practice for Laboratory Immersion Corrosion Testing of Metals 1. *Corrosion* **72,** 1–8 (2004). 3. Oyane, A. *et al.* Formation and growth of clusters in conventional and new kinds of simulated body fluids. *J. Biomed. Mater. Res. A* **64,** 339–348 (2003).

**ACKNOWLEDGEMENTS:** the authors acknowledge partial financial support from NSF as well as meaningful discussions with Yunfei Wang, Dr. Xiaolong Ma and Ashley Farris.

### Microstructural and biocorrosion characterization of Mg-Nd alloys

Yaping Zhang, Yuanding Huang, Carsten Blawert, Frank Feyerabend, Weimin Gan, Yuling Xu, Karl Ulrich Kainer, Norbert Hort

Institute of Materials Research, Helmholtz-Zentrum Geesthacht, Max-Planck-Strasse 1, 21502 Geesthacht, Germany

**INTRODUCTION:** Intermetallics in magnesium alloys can improve their mechanical properties by precipitate or load transfer strengthening <sup>1</sup>. Unfortunately, for degradable magnesium alloys, in most case the existence of these intermetallics deteriorates the corrosion resistance of magnesium alloys due to the galvanic corrosion <sup>2</sup>. How to balance corrosion resistance and mechanical strength plays an important role in the future development of degradable magnesium alloys with intermetallics. The present investigation focuses on the influence of intermetallics on the degradability of Mg-Nd alloys.

**METHODS:** Mg-Nd alloys with different contents of Nd (0.2, 0.5, 1, 2, 5 wt. %) were prepared by permanent mold direct chill casting, homogenized by an electromagnetic induction furnace at 440 °C. Indirect extrusion was carried out to produce circular bars with a diameter of 12 mm. Since the solubility of Nd in Mg matrix is close to zero, these alloys have different amounts of Mg-Nd intermetallics. Microstructures were investigated using optical, scanning and transmission electron microscopy, and synchrotron radiation diffraction techniques. The amount of intermetallics in Mg-Nd alloys were also calculated by thermodynamic software Pandat. The morphology, distribution and amount of intermetallics on the degradation behavior of Mg-Nd alloys were evaluated by immersion and electrochemical tests.

**RESULTS & DISCUSSION:** The amount of intermetallics is shown in  $Fig.\ 1$  for Mg-Nd alloys with different Nd contents. With increasing addition of Nd, the amount of intermetallics increases. Especially, when the content of Nd is more than 2 wt.%, it sharply increases. The Nyquist plots are shown in  $Fig.\ 2$ . It compares the respective corrosion response of binary Mg-Nd alloys in SBF solution at  $37.0 \pm 0.5$  °C up to 72 h. At early stages (< 6 h) the behaviour is similar for all five alloys with double-loop pattern in Nyquist plots. For immersion periods > 6 h, the behaviour is keeping and the resistance is continuously increasing up to 72 h. Mg5Nd behaves different and shows one inductive

loop. For Mg this inductive loop is normally associated with the breakdown of corrosion film or formation of pitting corrosion <sup>3</sup>.

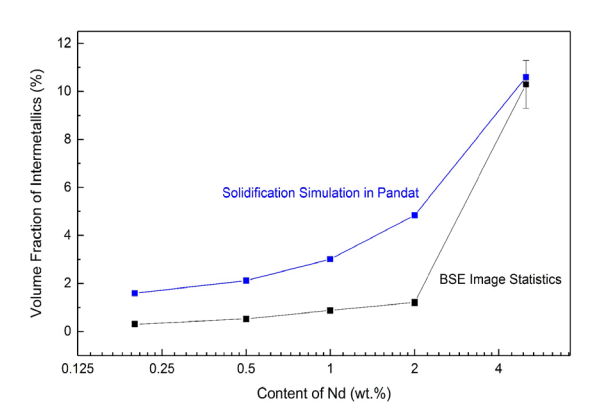


Fig. 1: Amount of intermetallics in the as-extruded Mg-Nd alloys

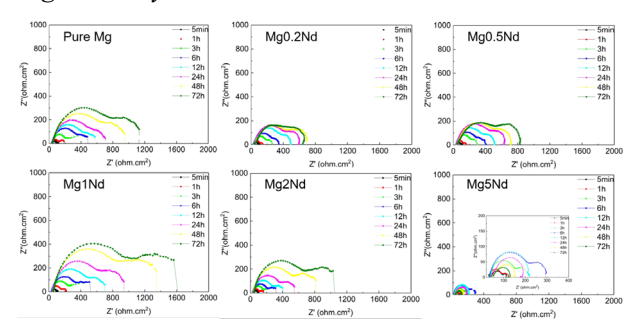


Fig. 2: Nyquist plots for the extruded Mg-Nd alloys after different immersion durations

**CONCLUSIONS:** Regarding the as-extruded Mg0.2Nd, Mg0.5Nd and Mg1Nd alloys with almost the same grain size, their corrosion rates decrease with increasing the amount of intermetallics after a longer immersion duration.

**REFERENCES:** <sup>1</sup> G. Song (2007) Corros Sci **49**: 1696-1701. <sup>2</sup> F. Witte (2010) Acta Biomater **6**: 1680-1692. <sup>3</sup> F. Cao, et al (2013) Corros Sci **75**: 78-99.

**ACKNOWLEDGEMENTS:** Yaping Zhang would like to thank the China Scholarship Council (CSC) for the financial support.

#### Development of novel biodegradable surgical Zn-Ag-Mg staple

A. L. Ramírez-Ledesma<sup>1,2</sup>, D. Mantovani<sup>2</sup>, M. Vedani<sup>1</sup>

<sup>1</sup> <u>Department of Mechanical Engineering</u>, Politecnico di Milano, Milan, Italy. <sup>2</sup> <u>Lab. for</u> <u>Biomaterials & Bioengineering (CRC-I)</u>, Dept. Min-Met-Materials Engineering & Research Center CHU de Québec, Laval University, Québec City, Canada.

INTRODUCTION: Nowadays several authors have reported the use of bioabsorbable Zn – based alloys for vascular applications [1]. Moreover, the main route of fabrication related with these materials is extrusion [1]. Thus, a wide research field is open for Zn - based alloys involving new applications and fabrication routes. permanent biomedical alloys are used as staples or clips to treat gastrointestinal anastomosis [2, 3]. In this respect, biodegradable alloys could be used to replace the aforementioned materials [1]. The advantages are obvious since they can be absorbed inside the human body and no retention of materials will remain which could promote pain and damages to patients. In this work, it is presented a biodegradable Zn - Ag - Mg alloy to produce staples or clips using warm - rolled as fabrication route.

METHODS: High purity Zn, Mg and Ag were used as starting materials for processing the experimental Zn - Ag - Mg alloy. The alloy was processed by vacuum induction melting under an argon (Ar) atmosphere. In order to avoid melt contamination alumina crucibles were used for alloy casting. A master alloy was melt which consist in Ag - 10.2 wt. % Mg, with the main purpose to decrease the melting point of Ag and dilute it into Zn. The ternary alloy was poured at  $\sim 750$  °C (1023.15 K) in a copper mold with a cooling system where water is recirculating all the time during melting and in the casting process, in consequence, the cooper mold maintain its temperature similar or below the room temperature. Thus, plates with 10 cm length, 5 cm with and 7 mm thickness were produced to be rolled at 200 °C (473.15 K) and, in this way, obtain plates with 700 micros thickness as a final product.

**RESULTS:** Fig. 1(a, b) exhibit microstructural features related to Zn - Ag - Mg plates in the as – cast condition were two principal phases were identified: dendrites conformed by solid solution of Zn - Ag and eutectic constituent of Zn - Ag - Mg. Also, Mg – enriched intermetallic compounds are present in low amount. Fig. 1(c, d) shows a unique microstructure related to Zn - Ag - Mg alloy rolled at 200 °C were recrystallization could be

appreciated which is responsible of fine grain formation. Table 1 contain mechanical properties corresponding to the aforementioned alloy.

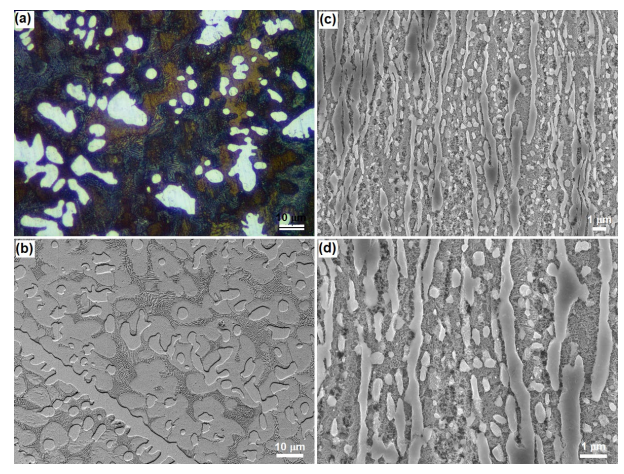


Fig. 1: (a, b) OM and SEM as – cast Zn – Ag – Mg micrographs, respectively. (c, d) SEM of rolled Zn – Ag – Mg alloy micrographs at different magnifications.

Table 1. Mechanical properties of Zn - Ag - Mg alloy and preliminary prototype of staple or clip.

Material	Yield strength (MPa)	Ultimate tensile strength (MPa)	Elongation (%)	
Rolled	341	383	25	1 cm

**DISCUSSION & CONCLUSIONS:** In the present work new alternatives of fabrication and application of Zn – based biodegradable alloys were exposed.

**REFERENCES:** <sup>1</sup> E. Mostaed et al (2018) Acta Biomater. In press. <sup>2</sup> H. Wu (2016) Bioactive Mat. **1**:122-26. <sup>3</sup> N. Ikeo et al (2016) Acta Biomater. **29**:468-76.

**ACKNOWLEDGEMENTS:** Consejo Nacional de Ciencia y Tecnología (CONACYT).

## Antibacterial Hydrogel Coating Enhances Antibacterial and Anti-Corrosive Properties of Magnesium

Cong Dai<sup>1</sup>, Yixin<sup>2</sup>, Jiapeng He<sup>2</sup> Lei Zhou<sup>2</sup>, Chengyun Ning<sup>2</sup>, Guoxin Tan<sup>\*1</sup>

<sup>1</sup> College of Chemical Engineering and Light Industry, Guangdong University of Technology, Guangzhou 510006, China. <sup>2</sup> College of Materials Science and Technology, South China University of Technology, Guangzhou 510641, China. \*e-mail: tanguoxin@126.com

**INTRODUCTION:** Degradable magnesium alloys are ideal bone implant materials, but the bacterial adhesion may cause implantation failure. Therefore, Mg implants are often surface-modified to increase their antibacterial properties and degradation behavior can be reduced and controlled. Here, the antibacterial hydrogel coating was grafted on the Mg surface to endow it excellent antibacterial properties, while the polymer coating enhanced the corrosion resistance of Mg.

**METHODS:** Gelatin methylacrylic (GelMA) monomers were prepared according to a previously reported method<sup>2</sup>, and the Mg sheets were modified 3-(Trimethoxysilyl) propyl-methacrylate (TMSPMA). In the dark, histidine and acryloyl chloride react under alkaline conditions for 1 hour, and then adjust the pH to 3.0 to obtain N-acrylic acid-L-His. The GelMA-His-Zn(II) hydrogels was constructed on the the modified Mg sheet, according the ultraviolet light with GelMA monomer and N-Acry-L-His, forming a hydrogel coating, which was immersed in zinc sulfate solution. The antibacterial activities of the modification Mg against both E. coli and S. aureus were evaluated using surface antibacterial activity tests.

**RESULTS:** Comparing the 1H NMR spectra of histidine and N-Acry-L-Hist, Fig. 1a shows new signals, which can be observed at 6.21, 6.11 and 5.71, corresponding to the two protons of acrylamide double bond. Fig.1b shows that the average pore sizes of the GelMA-His-Zn(II) hydrogel on modified Mg were 10 µm, which possess 3D porous structure and was useful in tissue engineering. From Figure 1c and 1d, the GelMA-His-Zn(II) coatings possess better antibacterial properties than GelMA hydrogels coatings on modified Mg, and the antibacterial activity of the GelMA-His-Zn(II) coating is better than that of the GelMA coatings, up to 100% of *S. aureus* and *E.* coli were killed by the GelMA-His-Zn(II) hydrogels.

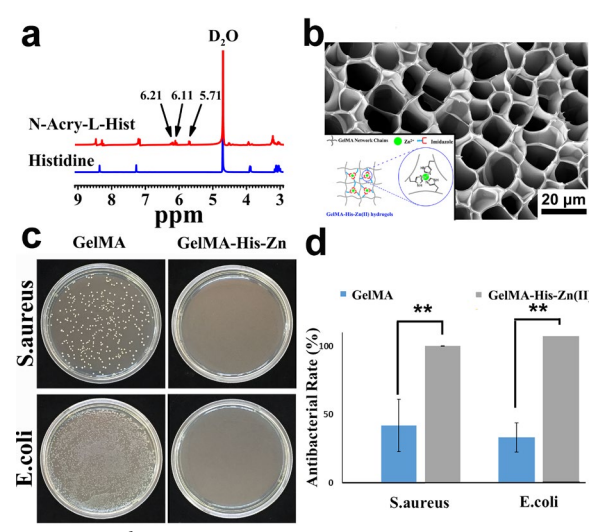


Fig. 1 a) <sup>1</sup>H NMR spectra of N-Acryloyl-L-histidine and histidine; b) Schematic and SEM images of GelMA-His-Zn(II) hydrogel, with a dual network of metal coordination and covalent bonds.

; c) Bacterial colonies and d) AR of S. aureus and E. coli after co-culture with GelMA, GelMA-His-Zn(II) hydrogel coatings, respectively n=4, \*\*p<0.01.

#### **DISCUSSION & CONCLUSIONS:**

The novel antibacterial GelMA-His-Zn(II) hydrogel coating was constructed on the surface of the Mg implants by TMSPMA. Antibacterial results shown that the new hydrogel coating has excellent antibacterial activities. At the same time, the coating can also prevent magnesium from directly contacting the physiological environment, thereby improving the corrosion resistance of the implant.

#### REFERENCES:

<sup>1</sup> Y.F. Zheng, X.N. Gu, F. Witte, *Materials Science* and Engineering R (2014) 77: 1–34. <sup>2</sup> J.W. Nichol, S.T. Koshy, H. Bae, C.M. Hwang, S. Yamanlar, A. Khademhosseini, (2010) *Biomaterials* 31: 5536-44.

**ACKNOWLEDGEMENTS:** The authors gratefully acknowledge the National Natural Science Foundation of China (Grant Nos. 31771080)

## Study on the in vitro properties of Mg-alloy stent using AZ31 and WE43 wire for benign biliary stricture

Bong Seok Jang<sup>1,2</sup>, Dongsu Im<sup>2</sup>, Won Ho Park<sup>1</sup>

<sup>1</sup> Department of Advance Organic Materials and Textile System Engineering, Chungnam National University, Daejeon 34134, Republic of Korea

<sup>2</sup> R&D Institute of Intervention, M. I. Tech Co., Ltd., Pyeongtaek 17711, Republic of Korea

**INTRODUCTION:** Benign biliary strictures are common results from cholecystectomy. In general, two therapies, including surgical and endoscopic, were adopted to cure the strictures. Endoscopic stenting provides options for those who cannot tolerate surgery procedure. So far, polymer stents, either permanent or degradable, were reported to perform displacement and lack of strength. Biodegradable Mg and its alloys have attracted increasing attention implantable stents [1,2]. Especially, Mg and its alloys may be the new kind of biodegradable materials for bile duct stent. In this study, Mg-alloy stents using AZ31 and WE43 wire for benign biliary stricture were studied their properties in vitro environment.

METHODS: Commercial AZ31 and WE43 wire were purchased from ADVANCED METAL Co., Ltd (Korea). The range of Outer Diameter of each wire is from 200 to 400 um. The stents were manufactured by hand-made using specific weaving Jig. After weaving stent type, the stent had specific heat treatment under 300°C due to their shape setting and removal of stress concentration. The stent of radial force was measured when the diameter of stent is half of diameter. The stent was observed the in vitro degradation behavior with time point under 1X PBS solution (Sigma-aldrich, Korea). The degradation behaviour was performed with dry weight change and SEM & EDS analysis onto the surface.

**RESULTS:** The radial force of Mg-alloy stent showed increasing value according to thicker diameter of stent with same size & shape type. Especially, WE43 stent was significantly higher radial force than AZ31 stent with same diameter (Fig. 1.b).

At the graph of Fig. 2, in vitro degradation behaviour under 1X PBS solution,  $37^{\circ}$ C, 100rpm was showed different result between WE43 & AZ31 stent. WE43 stent was faster degradation than AZ31 stent for 70 days.

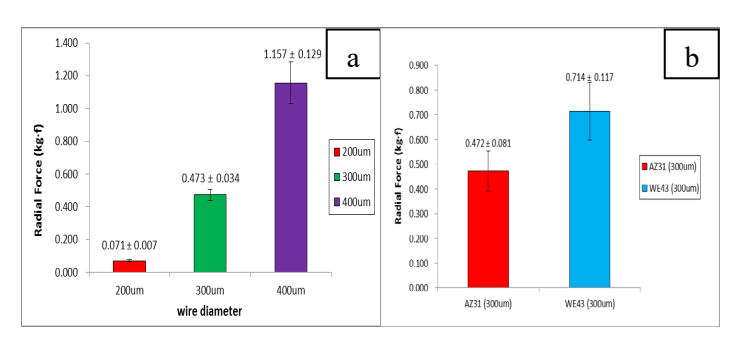


Fig. 1: Graph of Radial Force of stent with different Mg-alloy wire size (a) & composition (b)

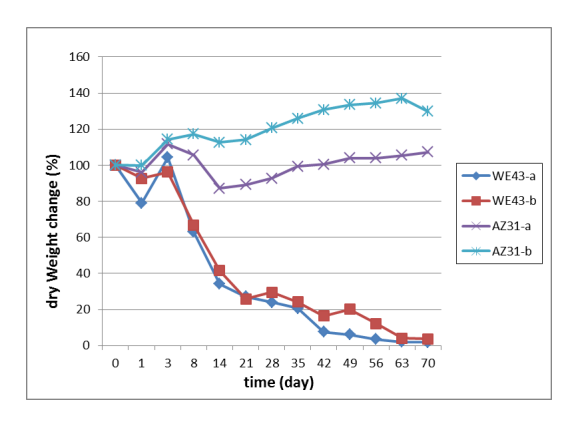


Fig. 2: Dry weight change (%) with time point under the 1X PBS solution according to different Mg-alloy stent

**DISCUSSION & CONCLUSIONS:** The Mg-alloy stents with different composition is called WE43 & AZ31 were compared mechanical and degradable properties under in vitro condition. Further study may be needed appropriate biodegradable polymer coating onto the stent surface for keeping structure as biliary stent during longer period.

**REFERENCES:** <sup>1</sup> F.Witte, N.Hort, C.Vogt, S.Cohen, K.U.Kainer, R.Willumeit, et al (2008) *Curr. Opin. Solid State Mater Sci.* **12**:63-72. <sup>2</sup> Y.F.Zheng, X.N.Gu, F.Witte (2014) *Mat. Sci. Eng. R.* **77**:1-34

**ACKNOWLEDGEMENTS:** This template was modified with kind permission from eCM Journal.

### **Progress in Absorbable Wire Technology**

AJ Griebel<sup>1</sup>, JE Schaffer<sup>1</sup>

<sup>1</sup> Fort Wayne Metals, Fort Wayne, IN, USA.

**INTRODUCTION:** This year, as our field gathers for the 10<sup>th</sup> time, it is fitting to review progress in a key material form over the past decade: wire.

WIRE IN **MEDICINE:** Wire has been indispensable to civilization for centuries<sup>1</sup>. The medical field is also heavily reliant on wire products for surgical intervention. Minimally invasive access devices like guidewires, catheters, and endoscopy assemblies are all heavily reliant on high-quality wire, primarily composed of 304V stainless steel. Permanent implantable devices like pacemakers employ highly conductive, highly fatigue-resistant cables made from a composite of cobalt-chrome and silver. While these applications will not be replaced by absorbable metals wire, there are myriad other uses for such material.

Orthopedic applications for absorbable wire include fracture fixation with k-wires and nails. Femoral cerclage and sternal repair are also prime indications. Soft tissue fixation, including stapling, hernia tacking, and ligation, and wire based stents may also be well-served by an absorbable material.

Absorbable wires in medicine are not a recent concept. Iron wires were used in surgery as early as the 18<sup>th</sup> century<sup>2</sup>, and magnesium wires were first reported to be used in ligation in 1878<sup>3</sup>. This presentation will review much of the progress in absorbable wire over the last decade.

**IRON:** As noted above, ferrous wires have a long history, even in medical applications. More recent work to develop iron-based wires suitable for medical devices was published in 2012, with a target application of self-expanding braided stents<sup>4,5</sup>. This work investigated 0.127 mm wires of pure Fe, Fe35Mn, and wire composites with Mg cores. While high strength and good cytocompatibility were achieved, the problem of early localized corrosion was found to be a key barrier. Ongoing work aims to reduce this early fracture.

**ZINC:** Zinc wire also has many industrial uses, but was not considered as an absorbable implant until publication by Bowen et al<sup>6</sup>. With a corrosion rate between that of Fe and Mg, it may be ideally suited for stents. However, the strength of pure Zn is insufficient, and higher-strength alloys are under investigation. Zn-Mg alloys are unstable as wires<sup>7</sup> but other Zn-based alloys hold promise<sup>8</sup>. A key

consideration with all Zn alloys is strain-rate sensitivity, which may make the materials prone to creep.

MAGNESIUM: Magnesium is simultaneously the most widely applicable and the most challenging to produce of the three alloy classes. Though made challenging by the HCP structure of Mg, work by this group and others has shown the potential for the wire-drawing process to refine microstructure and improve mechanical properties of the Mg alloys while maintaining good corrosion properties <sup>9-12</sup>. Dozens of alloys have been investigated as wire, and many are currently being pursued in device-specific functions. A key area of current development is a scaled, repeatable, and microstructurally clean supply.

**CONCLUSION:** Absorbable wire has made considerable progress over the past decade, and is primed for enabling new absorbable devices.

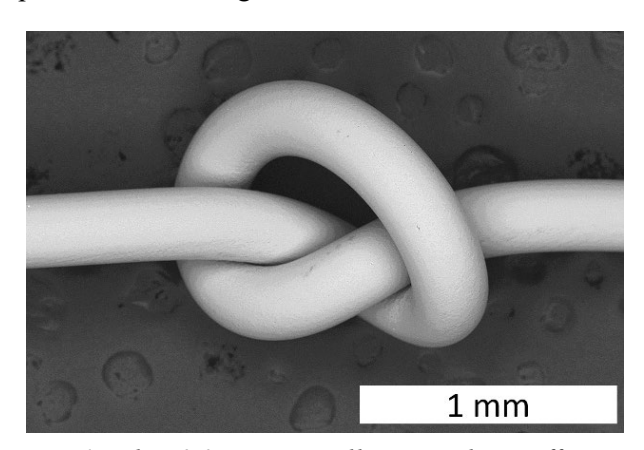


Fig. 1: This 0.3 mm Mg alloy wire has sufficient ductility to be knotted.

REFERENCES: <sup>1</sup>Theophilus (1979) *On Divers Arts*, Dover Publications. <sup>2</sup>P. Laing (1979) ASTM Standard STP684. <sup>3</sup>E. Huse (1878) *Chicago Medical J. Exam.* <sup>4</sup>J. E. Schaffer et al (2013) *Metal and Mater Trans B*. <sup>5</sup>J. E. Schaffer et al (2012) *Acta Biomaterialia*. <sup>6</sup>Bowen et al (2013) *Advanced Materials*. <sup>7</sup>Jin et al (2017) *Mat Sci Eng C*. <sup>8</sup>Mostaed et al (2018) *Acta Biomaterialia*. <sup>9</sup>Griebel et al (2017) *J Biomed Mater Res Part B*. <sup>10</sup>Maier et al (2015) *ECM Vol 30 Suppl 3*. <sup>11</sup>Bai et al (2014) *Prog Nat Sci: Mat Int*. <sup>12</sup>Seitz et al (2011) *Adv Eng Materials*.

#### Design and testing of zinc stent fabricated by photo-chemical etching

V Shanov<sup>1,2</sup>, B S P K Kandala <sup>2</sup>, G Zhang<sup>2</sup>, S Pixley<sup>3</sup>, Z Dong<sup>4</sup>

<sup>4</sup> Department of Internal Medicine, University of Cincinnati, OH

INTRODUCTION: Zinc is a promising material for medical implants due to its biocompatibility and the ability to resorb in the body [1]. However, this metal is less studied, especially for stent application, compared to magnesium [2-4]. Manufacturing stents by laser cutting has become an industrial standard. Nevertheless, this approach reveals some issues, such as thermal stress, dross sticking, surface oxidation, need of expensive tubing and post-treatment. All this motivated us to employ photochemical etching for fabricating different designs of Zn stents and to test them in vitro and in vivo.

**METHODS:** The starting material was a rectangular sheet of zinc with thickness of 250 microns and purity of 99.95%, purchased from Goodfellow. The photo-chemical etching method transfers a pattern of the stent onto the sheet, followed by chemical etching [5]. Finally, etched sheets with the desired dimensions are rolled into cylinders and laser welded along the side seam. This inexpensive process does not generate residual stress in the material during processing and no posttreatment of the stent after manufacturing is required. For fabricating helical stents, twodimensional Zn ribbons with selected dimensions were photo-chemically etched with a desired pattern. The spiral shape was formed by simple winding on a guiding rod which determined the stent diameter. No welding is required for the helical design and the dimensions of the device can be varied. In some cases, conformal parylene coating was applied by vapor deposition to enhance the corrosion resistance of the Zn stents.

RESULTS: Figure 1 displays images of photochemically etched Zn stents fabricated in 2 designs: helical and cylindrical, which have been optimized through simulation using ANSYS. The corrosion of uncoated and parylene coated stents have been studied in vitro using cell culture media (DMEM) + 10% fetal bovine serum with antimycotics and antibiotics (AAA) [6]. Balloon expanded helical and cylindrical stents coated with parylene were observed under AEM and optical microscopes and no substantial delamination was detected. Mechanical tests under load showed that the radial force and recoil of the cylindrical Zn stent with U

design were comparable with the same design stents made of the Mg alloy AZ31. Preliminary in vivo tests of Zn disks have been conducted using a mouse model in a subcutaneous environment.

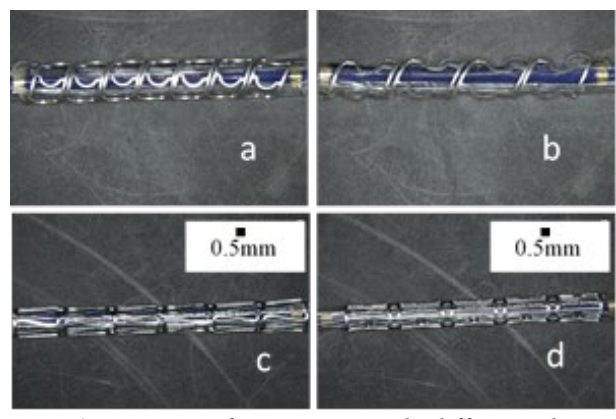


Fig. 1: Images of Zn stents with different design fabricated by photo-chemical etching. (a) Helical stent 4\*25mm made of 3mm wide ribbon; (b) Helical stent 4\*25mm made of 5mm wide ribbon; (c) Cylindrical stent with  $\Omega$  design-crimped; (d) Cylindrical stent with U design-crimped.

DISCUSSION & CONCLUSIONS: Photochemical etching is a robust and inexpensive approach for fabrication of Zn biodegradable stents. The Zn helical stent reveals a different mode of balloon expansion compared to the cylindrical stent. It allows for expansion to 2 times its initial diameter. Cylindrical Zn stents expand smoothly and uniformly which was observed in both uncoated and parylene-coated devices. The in vitro and in vivo experiments confirmed that Zn is a promising material for biodegradable stent applications.

**REFERENCES:** <sup>1</sup> P. Bowen, J. Drelich, *et al* (2013) *Advanced Materials* **25**:18, 2577-2582. <sup>2</sup> J. Wang, V. Shanov, et al (2014) *Acta Biomaterialia* **10**:5213-23. <sup>3</sup> X. Gu, V. Shanov, et al (2016) *Colloids and Surfaces B: Biointerfaces*, **140**:170-179. <sup>4</sup> Y. Koo, V. Shanov, et al (2017) Scientific Reports, 7:1-10. <sup>5</sup> V. Shanov, P. Roy-Chaudhury, et al (2017) *US Patent* 9,655,752. <sup>6</sup> K. Ojo, V. Shanov, et al (2016) *Electroanalysis*, **28**:3000–3008.

**ACKNOWLEDGEMENTS:** NSF ERC for Revolutionizing Biomaterials, EEC-EEC-0812348.

<sup>&</sup>lt;sup>1</sup> <u>Department of Chemical and Environmental Engineering</u>, University of Cincinnati, OH.

<sup>&</sup>lt;sup>2</sup> Department of Mechanical and Materials Engineering, University of Cincinnati, OH.

<sup>&</sup>lt;sup>3</sup> <u>Department of Pharmacology and Systems Physiology,</u> University of Cincinnati, OH.

### Heat treatment of Mg<sub>1-x</sub>Ag<sub>x</sub> thin films to achieve supersaturated alloys

LK Jessen<sup>1</sup>, C Zamponi<sup>1</sup>, E Quandt<sup>1</sup>

<sup>1</sup>Chair for Inorganic Functional Materials, Institute for Materials Science, Faculty of Engineering, University of Kiel, Germany

**INTRODUCTION:** Magnesium alloys are of great interest for the application as temporary implant. Other elements are added to pure Mg to tailor the material properties with respect to mechanical and corrosion properties as well as therapeutic behavior. Within the scope of the GRK 2154 – "Materials for Brain", the fabrication and characterization of Mg<sub>1</sub>xAgx thin films is one of the topics. In the case of Mg<sub>1-x</sub>Ag<sub>x</sub> alloys the biodegradable properties of Mg are combined with the antibacterial properties of Ag [1]. This could be used as a coating for medical application. As sputtered Mg<sub>1-x</sub>Ag<sub>x</sub> materials show an increase of the corrosion rate compared to pure Mg as result of formation of precipitates (Fig. 1) which leads to different potentials. A T4 heat treatment generates a single phase material due to solution heat treatment. In low concentration silver is soluble in magnesium. Materials with different concentrations of 2 and 6 wt% of silver were fabricated and investigated.

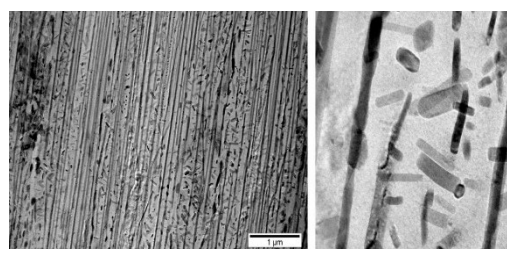


Fig. 1: STEM cross section of  $Mg_{90}Ag_{10}$  sample show precipitates in the as deposited state [2].

**METHODS:** Magnetron sputtering was used to fabricate thin films which are either free standing or on a substrate with a thickness up to  $20\mu m$ . To achieve a variation of the microstructure a T4 heat treatment was done (Fig. 2). The microstructure was investigated using X-ray diffraction, scanning electron microscopy, transmissions microscopy and energy dispersive X-ray spectroscopy.

**RESULTS:** With magnetron sputtering free standing thin films can be achieved. X-ray

diffraction showed a preferential growth in the <0001> direction and precipitates in the as sputtered films. Due to the T4 heat treatment a change of the microstructure is visible.

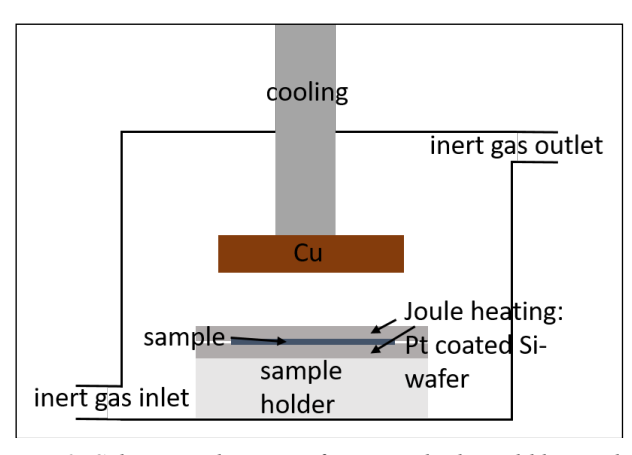


Fig. 2: Schematic drawing of a oven which could be used for the T4 heat treatment to achieve single phase material.

**DISCUSSION & CONCLUSIONS:** It was shown that it is possible to fabricate free standing thin films via magnetron sputtering. The microstructure can be tailored due to a T4 heat treatment.

**REFERENCES:** <sup>1</sup> Lansdown, A.B.G. (2002) Silver I: Its antibacterial properties and mechanism of action, Journal of wound care, vol 11, no. 4. <sup>2</sup> D. Haffner (2015) Magnetron sputtered biodegradable Mg-Ag thin films, Proceedings of Magnesium Alloys and Application, 11-16 October, pp 366-372, Jeju, South Korea.

**ACKNOWLEDGEMENTS:** Funding via the GRK2154 is gratefully acknowledged.

### Microstructure of WE43 fabricated by Laser-Powder Bed Fusion in comparison to conventional processing routes

L Berger<sup>1</sup>, F Bär<sup>1</sup>, L Jauer<sup>2</sup>, R Schäublin<sup>1</sup>, J H Schleifenbaum<sup>2,3</sup>, J F Löffler<sup>1</sup>

<sup>1</sup> Laboratory of Metal Physics and Technology, Department of Materials, ETH Zurich, 8093 Zurich, Switzerland; <sup>2</sup> Fraunhofer Institute for Laser Technology ILT, Aachen, Germany; <sup>3</sup> Digital Additive Production, RWTH Aachen, Germany

**INTRODUCTION:** Laser-Powder Bed Fusion (L-PBF) is a promising method to fabricate magnesium-based, biodegradable structures for bone support. Of special interest is the high-strength and corrosion resistant Mg-Y-RE-Zr alloy WE43. Parts are typically fabricated by powder extrusion (PE), but for more complex geometries L-PBF appears to be a promising alternative. However, the influence of process parameters and the extremely high cooling rates on microstructure are not yet fully understood.

METHODS: Samples of WE43 were prepared by casting, PE, and L-PBF (single-mode ytterbium fiber laser with 230 W maximum output power). A layer thickness of 30 μm and a hatch spacing of 40 μm were chosen [1]. Microstructure was investigated using optical light microscopy and a 200 kV transmission electron microscope with energy-dispersive X-ray spectroscopy mapping.

**RESULTS:** Cast WE43 exhibited the largest average grain size ( $10.2\pm2.1~\mu m$ ), while powder extruded ( $1.8\pm0.2~\mu m$ ) and L-PBF ( $2.4\pm0.7~\mu m$ ) samples showed significantly smaller grains.

Whereas Y was found to be uniformly distributed in cast WE43, it was found mostly incorporated as Y<sub>2</sub>O<sub>3</sub>-particles scattered throughout the bulk material in the case of PE and L-PBF (Fig. 1).

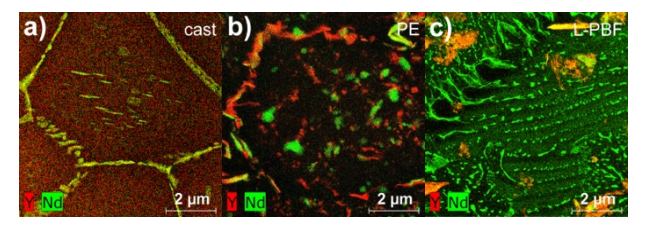


Fig. 1: Microstructural EDX chemical mapping of WE43 (a) cast, (b) powder extruded and (c) additively manufactured by L-PBF.

Rare-earth (RE)-rich platelet-shaped precipitates (size approximately  $500 \times 500 \times 50 \text{ nm}^3$ ) were detected in the cast material, but not in the PE material. Similar precipitates were found in L-PBF material, but of significantly smaller dimensions (max. size  $100 \times 100 \times 10 \text{ nm}^3$ ) (Fig. 2). They were identified as  $Mg_{41}RE_5$  and appear to be ordered along the Mg-matrix's prismatic planes, and in the

case of L-PBF they form planes of regular distance (visible as lines in TEM images; see Fig. 1c)

Additionally, potato-shaped Mg<sub>3</sub>RE-precipitates were discovered in the L-PBF produced and in the cast material (Fig. 2). Those agglomerate preferentially at grain boundaries.

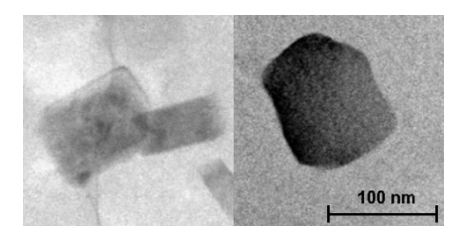


Fig. 2: Platelet-shaped  $(Mg_{41}RE_5)$  and potatoshaped  $(Mg_3RE)$  precipitates found in the L-PBF-microstructure. Same scale for both images.

**DISCUSSION & CONCLUSIONS:** While the low cooling rates in cast material lead to large grains, rapid solidification of L-PBF causes a fine microstructure and precipitates ordered in planes. The latter can be explained by a dendritic growth of the crystals.

Yttrium, originally used in WE43 to form a protective oxide layer on the material's surface, was found to be bound in  $Y_2O_3$ -particles for PE and L-PBF processed samples. Those particles are assumed to be shells from the original powder, which were scattered during the materials synthesis process. This is expected to generate a reduced corrosion resistance.

Adaptation of the alloying system to the unique processing parameters of PE and L-PBF is therefore recommended. With regard to its deployment as biomaterial a reduction of the controversially discussed Y might also be beneficial.

**REFERENCES:** <sup>1</sup> Jauer, L. et al. Selective Laser Melting of magnesium alloys. *European cells & materials*. 30, pp. 1, (2015).

**ACKNOWLEDGEMENTS:** We acknowledge ScopeM from ETH Zurich for providing the electron microscope facility and assistance.

#### Combining the best of both worlds: partly degradable permanent implants

T Ebel<sup>1</sup>, S Bußacker<sup>1</sup>, J Schaper<sup>2</sup>, V Haramus<sup>1</sup>

<sup>1</sup> <u>Helmholtz-Zentrum Geesthacht</u>, Centre for Materials and Coastal Research, Metallic Biomaterials, Geesthacht, DE, <sup>2</sup> <u>Element 22 GmbH</u>, Kiel, DE

INTRODUCTION: Enhancing functionality and durability of permanent implants is still an important issue of current research and development in medicine. The idea of this study is to functionalize a titanium bone implant by combining it with a magnesium layer or part. After implantation magnesium degrades, enhances bone formation and – if desired – releases a drug. Powder metallurgical fabrication of such a composite provides great flexibility in geometry, density and surface morphology of both titanium and magnesium part. To show the basic feasibility first Mg-0.9Ca / Ti parts were produced and their interface strength was tested in this study.

**METHODS:** Metal Injection Moulding (MIM) [1-2] was applied to fabricate the Mg-0.9Ca / Ti composite. First, the titanium part of the composite was manufactured from gas atomized Ti Grade 1 powder with a size smaller 45  $\mu$ m. The powder was mixed with a polymeric binder, injection moulded, debinded and sintered. Then, the magnesium part was injection moulded onto the finished Ti-part and the joined structure was debinded and sintered. Mg-0.9Ca powder < 45  $\mu$ m was used for the second feedstock.

In order to test the interface strength the used mould formed a standard dog bone shape tensile specimen. The interface between Mg-0.9Ca and Ti was located in the middle of the sample. Two different morphologies of the interface were fabricated: a 'smooth' one and a 'rough' one with undercuts on the titanium side. The rough surface was produced using NaCl spaceholders during injection which were removed before debinding in a water bath. Figure 1 shows a schematic and an optical microscopy image of the interface region.

Tensile tests were performed on the as-sintered samples using a universal testing machine (RM100, Schenck Trebel, Germany). The interface was investigated by optical and electron microscopy including EDS.

**RESULTS:** The composite tensile samples could be successfully produced by the chosen method. The main result is the high strength of the interface, especially in the case of the rough surface: in this case all samples broke inside the Mg-alloy part and

not in the interface (Fig. 2) and showed a tensile behaviour similar to that of a pure Mg-0.9Ca specimens.



Fig. 1: Schematic setup and optical image of the interface between Mg-allov part and Ti-part.

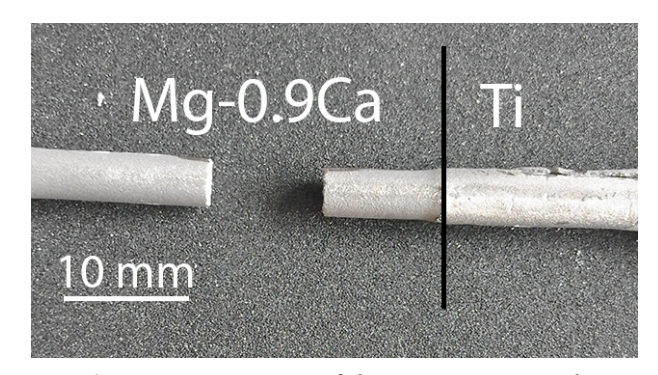


Fig. 2: Fracture region of the composite tensile specimens.

**DISCUSSION & CONCLUSIONS:** Considering that Mg and Ti are almost not miscible, the high strength of the interface is surprising. In the case of the rough surface some interlocking effect enhances the connection; however, even the smooth surface provides reasonable strength. Additional EDS measurements showed an increase of Ca at the interface which might effect the bonding between Ti and Mg. These first results show that, together with powder metallurgical approach manufacturing this basic setup of a composite of degradable and permanent material enables the production of sophisticated and functionally optimized implants, even being capable for drug delivery.

**REFERENCES:** <sup>1</sup> M. Wolff, T. Ebel, M. Dahms, (2010), *Adv. Eng. Mater.* **12**: 829-836. <sup>2</sup> M. Wolff, J.G. Schaper, M.R. Suckert, M. Dahms, F. Feyerabend, T. Ebel, R. Willumeit-Römer, T. Klassen (2016) *Metals* **6**: 118.

#### Study on degradable magnesium alloys for bone screws

Zhentao Yu, Chang Wang

Northwest Institute for Nonferrous Metal Research, Shaanxi Key Laboratory of biomedical metal materials, Xi'an, China

INTRODUCTION: Magnesium is an essential nutrient for the human body, and most of it (about 50% to 60%) is present in bone tissue [1]. Magnesium and its alloys have a density close to that of human bone. The modulus of elasticity is closer to that of human bone than other bone implant materials, and can effectively reduce stress shielding effects. As a bone nail material in the human body can be degraded without secondary removal, and the degradation of magnesium ions is conducive to bone marrow stem cell-derived osteoblasts adhesion, growth and proliferation of osteogenic differentiation [2, 3].

**METHODS:** Mg-2Zn and Mg-2Zn-0.5Zr alloys were smelted and pure magnesium was used as a comparison. Φ6mm rods were made from optimized extrusion process and their mechanical properties and corrosion resistance were evaluated. Mg-2Zn-0.5Zr alloy rods were then machined into bone screws according to China Pharmaceutical Industry Standard. The corrosion performance of screws were tested according to ASTM-G31-72.

**RESULTS:**  $\Phi$ 6 mm extruded Mg-2Zn-0.5Zr alloy rods have the highest mechanical properties and low corrosion rate with fine grain size about 11  $\mu$ m which were shown in Fig. 1 and Fig. 2. After 18 days of vitro immersion test in SBF, its bone screws exhibits a uniform corrosion morphology, and the degradation products contained with Mg, Zn, Ca and P elements (as shown in Fig. 3).

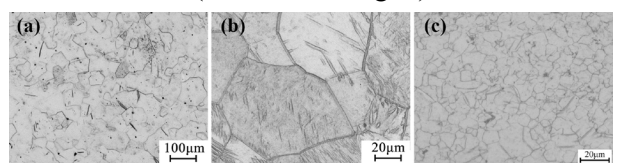


Fig. 1: Microstructure of extruded rods: (a) Pure Mg; (b) Mg-2Zn; (c) Mg-2Zn-0.5Zr.

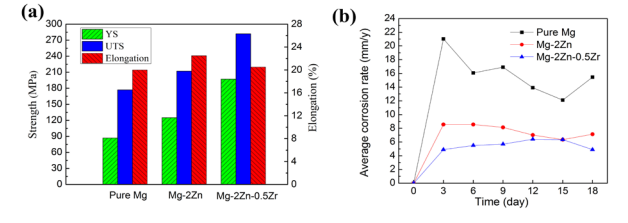


Fig. 2: Performance of extruded rods: (a) mechanical properties; (b) corrosion rate.

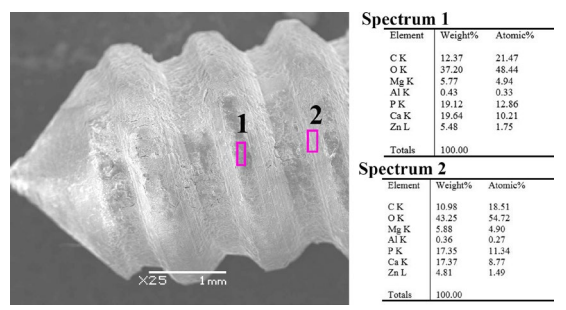


Fig. 3: Morphology and composition of Mg-2Zn-0.5Zr alloy bone screw after 18 days of immersion in SBF.

DISCUSSION & CONCLUSIONS: Mg-Zn alloy with Zr addition has a highly increase of mechanical properties compared with Mg-2Zn and pure Mg after extruded. Which is due to the microstructure refinement and solid solution strengthening. The corrosion rate of Mg-2Zn-0.5Zr alloy rods is low with uniform corrosion morphology for the comparable homogeneous microstructure. The Ca and P elements in the degradation layer of its bone screws could promote the nucleation of osteoconductive minerals [4] and benefit for new bone growing.

**REFERENCES:** <sup>1</sup> Y. Ishimi. (2010) *Clinical Calcium* **20(5)**: 762-767. <sup>2</sup> R.W. Li, N.T. Kirkland, J. Truong, et al (2014) *J Biomed Mater Res A* **102(12)**: 4346-4357. <sup>3</sup> Y.H. Yun, Z. Dong, D. Yang, et al (2009) Mater Sci Eng C, **29(6)**: 1814-1821. <sup>4</sup> X. Zhang, X.W. Li, J.G. Li, et al (2014) acs appl mater interfaces **6(1)**:513-525.

**ACKNOWLEDGEMENTS:** This work was supported by Shaanxi Provincial Science and Technology Research Project (2016GY-210).

## Tailored degradation and improved biocompatibility of magnesium alloys for resorbable bone fixation products

<u>J Acheson</u><sup>1</sup>, N Fullen<sup>1</sup>, S McKillop<sup>1</sup>, P Lemoine<sup>1</sup>, A Boyd<sup>1</sup>, B Meenan<sup>1</sup>

<sup>1</sup>Nanotechnology & Integrated Bioengineering Centre (NIBEC), School of Engineering, Ulster University, UK

INTRODUCTION: The use of bio-resorbable bone fixation products offers the opportunity to eliminate the need for secondary removal operations and negate the associated complications such as infection and pain. Magnesium alloys display great potential as biodegradable metal implants; however, the corrosion rate of magnesium can be difficult to control, in vivo thereby limiting its use.<sup>[1]</sup> In this study, sputter deposited hydroxyapatite (HA) coatings acting as a barrier layer, to tailor the degradation of magnesium alloys have been investigated.

**METHODS:** Magnesium alloy (AZ31, Goodfellow, UK) coupons (10 x 10 x 1 mm) were coated with HA from CAPTAL R (Plasma Biotal, UK) via RF magnetron sputtering, a wellestablished methodology. A design of experiments approach was used to create a response surface plot that allows for a tailored degradation rate to be chosen based on the required in vivo response.

HA coated, and uncoated control coupons were exposed to simulated body fluid (SBF) for up to 14 days. Samples were characterised via microcomputed tomography (microCT), X-ray photoelectron spectroscopy (XPS), optimal microscopy, scanning electron microscopy (SEM), atomic absorption spectroscopy (AAS), time of flight secondary ion mass spectroscopy (ToF-SIMS) and gravimetric analysis.

**RESULTS:** The presence of a  $700 \pm 350$  nm HA coating, determined from ToF-SIMS depth profiling, significantly reduced magnesium alloy corrosion, with a corrosion rate of  $61.66 \pm 4.24$  mpy for HA coated coupons and  $68.56 \pm 2.92$  mpy for uncoated controls (Figure 1c). The nature and scale of the corrosion that occurred was clearly different with much less pitting observed in the presence of the HA coating (Figure 1a and 1c). The extent of damage to the surface of the magnesium alloy can be seen (Figure 1d).

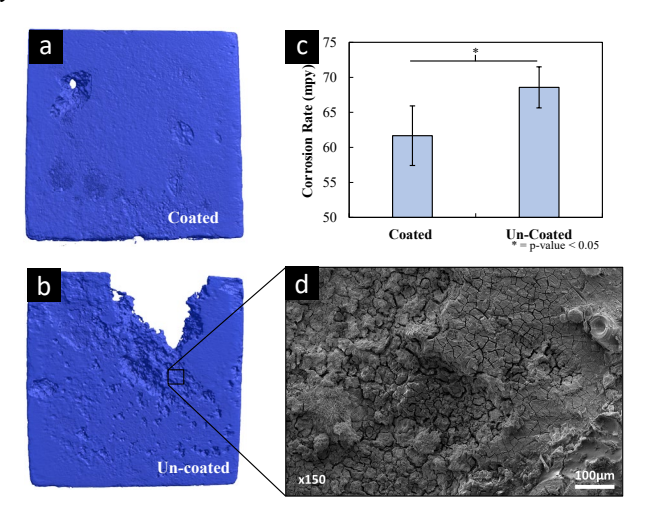


Fig. 1: Reconstructions of AZ31 alloys after degradation in SBF for 14 days a) coated with HA b) un-coated. c) difference in corrosion rates of coated and un-coated AZ31 alloys. d) SEM image of surface damage on un-coated AZ31 alloy.

DISCUSSION & CONCLUSIONS: HA coatings offer potential as a barrier layer to tailor the corrosion rate of magnesium alloys in SBF by controlling the diffusion of ionic solution to the underlying metal. Variation of the coating thickness, through a design of experiments approach allowed for tailored degradation rates to be achieved. The presence of the HA in the biological environment associated with magnesium alloy breakdown offers the additional advantage of enhanced bone cell response.

#### **REFERENCES:**

[1] Brooks E. et al., J. Funct. Biomater. 8, 38 (2017); [2] Boyd A. et al., Surf & Coatings Technol. 233, 131-139 (2013).

**ACKNOWLEDGEMENTS:** Funding from the Department for the Economy for Northern Ireland under the US-Ireland R&D Partnership Centre-to Centre Award scheme (Grant No. USI 111) is gratefully acknowledged.

#### **Process Chain for Additive Manufacturing of Magnesium Implants**

L Jauer<sup>1</sup>, M Kimm<sup>2</sup>, N Labude<sup>3</sup>, M Bienert<sup>3</sup>, S Neuß<sup>3,4</sup>, B Lethaus<sup>5</sup>, F D'Elia<sup>6</sup>, M Müther<sup>6</sup>, A Kopp<sup>6</sup>, C Ptock<sup>6</sup>, JH Schleifenbaum<sup>1,2</sup>

<sup>1</sup> Fraunhofer Institute for Laser Technology ILT, Aachen, Germany <sup>2</sup> Chair for Digital Additive Production, RWTH Aachen University, Germany <sup>3</sup> Institute of Pathology, RWTH Aachen University, Germany <sup>4</sup> Helmholtz Institute for Biomedical Engineering - Biointerface Group, RWTH Aachen University, Germany <sup>5</sup> Department of Cranio-Maxillofacial Surgery, RWTH Aachen University, Germany <sup>6</sup> Meotec, Germany

INTRODUCTION: Additive Manufacturing (AM) enables the economic manufacture of individualized and highly complex parts such as implants with interconnected pore structures. Not only allow such pore structures tailoring mechanical properties, but they enable also a significant reduction of bulk material, full vascularization of the implant and the ingrowth of newly formed bone which is particularly advantageous for biodegradable implants.

**METHODS:** For producing complex, individualized magnesium implants with interconnected porosity the AM technology laser powder bed fusion (LPBF) is chosen using a laboratory machine based on AconityMINI (Aconity3D, Germany) system technology and MAP+43® powder material (Magnesium Elektron Powders, USA) with WE43 chemistry and a particle size between 20 – 63 µm. To reduce LPBF induced surface roughness and counteract increased initial corrosion due to the design induced large total surface area post processing of LPBF implants features an electrochemical etching process and a subsequent surface conversion by electrolytic oxidation (PEO).

**RESULTS:** Fig. 1 shows SEM images of scaffolds at different stages of the AM process chain.

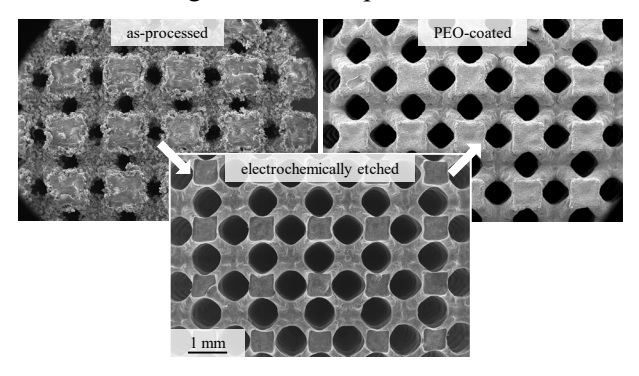


Fig. 1: SEM images showing scaffolds at different stages of the AM process chain

To demonstrate that this process chain is not only feasible for scaffolds with regular periodic pore structures fig. 2 shows several individualized implants made with LPBF out of WE43 and subsequent PEO: A supraorbital implant with surface adapted pore structure and integrated bores for fixation, a fixations plate and a mandible implant with gradient pore structure.



Fig. 2: demonstrator showing various patient specific implants made from biodegradable WE43 magnesium alloy after PEO

DISCUSSION & CONCLUSIONS: The presented AM process chain is highly flexible and capable of producing various biodegradable implants. Main disadvantage of the powder bed based LPBF such as high surface roughness and sintered particles are countered by electrochemical surface smoothening. A subsequent PEO of the surface prevents increased initial corrosion even for a large total surface area which is desired for implants with pore structures to promote bone ingrowth.

**ACKNOWLEDGEMENTS:** This work was funded by the European Regional Development Fund (ERDF).

#### Biodegradable Zn metal implants manufactured by laser powder bed fusion

Yu Qin<sup>1</sup>, Peng Wen<sup>1</sup>, Yanzhe Chen<sup>1</sup> Lucas Jauer<sup>2</sup>, Maximilian Voshage<sup>3</sup>, Reinhart Poprawe<sup>2</sup>, Johannes Henrich Schleifenbaum<sup>2, 3</sup>

<sup>1</sup> Department of Mechanical Engineering, Tsinghua University, Beijing, China. <sup>2</sup>Fraunhofer Institute for Laser Technology (ILT), Aachen, Germany <sup>3</sup>Digital Additive Production (DAP), RWTH Aachen University, Aachen, Germany

**INTRODUCTION:** Appropriate degradation rate and good biocompatibility of Zn allow it to attract increasing attention as the next generation biodegradable metal. Additive manufacturing (AM) of biodegradable implants shows many advantages like customized structure and degradation. Pure Zn cubes with high density were obtained by laser powder bed fusion (L-PBF)<sup>1</sup>. In this work, microstructure and mechanical performance of pure Zn parts by L-PBF were clarified. Bone structures with curved surface and porous interior were demonstrated.

METHODS: A compact machine (ACONITY) was used to perform laser melting on pure Zn powder bed (average diameter 28.2μm). The laser spot diameter was 75μm at wavelength of 1070nm. A specially designed gas circulation system was used with two main purposes: to keep the process from oxidation, and to eliminate the negative effect of Zn evaporation products on processing stability. The obtained samples were characterised by scanning electron microscope (SEM), electron back-scattered diffraction (EBSD) and X-ray diffraction (XRD). The tensile properties were measured.

RESULTS: A part of greater trochanter was printed by L-PBF with curved geometry obtained by the CT data of a patient. The interior was made up of lattice structure, which was expected to adjust the weight, strength and biodegradation time. The designed strut diameter was 500µm. After sandblasting, the macro formation quality was acceptable, but there were still some solidified particles attached to the surface of struts.

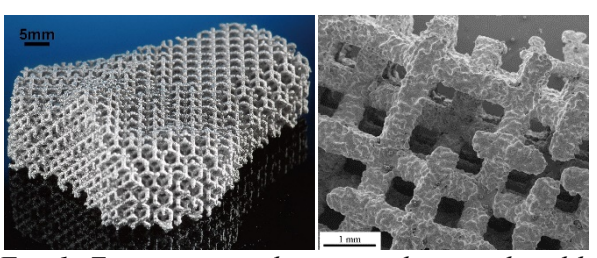


Fig. 1: Zn greater trochanter implant produced by L-PBF (left), and its local SEM image (right).

The XRD profiles in Fig. 2 did not show any secondary peaks of zincite, which meant no oxidation appeared during L-PBF processing. The chemical composition measurement showed the

average oxygen content was 0.98% in the powders and 1.14% in the L-PBF parts.

The EBSD images in Fig. 3 showed refined grains with average  $2.5\mu m$  in width. The elongated direction corresponded to building direction of powders, in which the temperature gradient was the biggest. Fig.4 shows the mechanical properties of L-PBF samples. They were superior to most manufacture methods due to the high densification and fine grains.

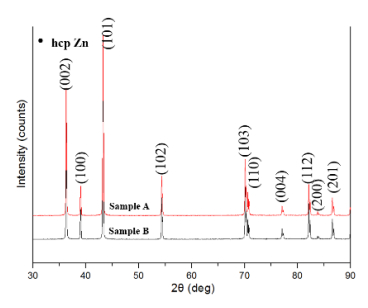


Fig. 2: XRD patterns of L-PBF samples.

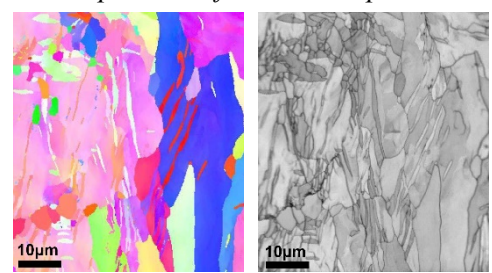


Fig. 3: EBSD images of L-PBF samples.

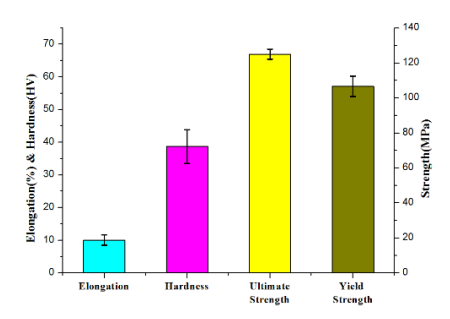


Fig. 4: Mechanical properties of L-PBF samples

**CONCLUSIONS:** The present results indicated the promising prospect of the application of L-PBF manufacturing biodegradable Zn metal implants.

**REFERENCES:** <sup>1</sup> A.G. Demir, et al. Additive Manufacturing, 2017(15): 20-28.

#### On the Fe-Mn-C alloys: processing and characterization

C. Paternoster<sup>1</sup>, C.Loy <sup>1</sup>, B. Occhionero<sup>1</sup>, <u>J.Fiocchi</u><sup>2</sup>, C. A. Biffi<sup>2</sup>, A.Tuissi<sup>2</sup>, D. Mantovani<sup>1</sup>

Laboratory for Biomaterials and Bioengineering, Dept. of Min., Met. and Mater. Eng. CHU de

Quebec Research Centre, Laval University, Québec City, Canada

<sup>2</sup>National Research Council – Institute of Condensed Matter Chemistry and Technologies for

Energy, CNR ICMATE Lecco, Italy.

Three Fe-Mn-C alloys, whose nominal composition is Fe-12Mn-1.2C, Fe-16Mn-0.9C and Fe-20Mn-0.6C, were investigated from a structural and mechanical point of view, to understand their suitability for biological applications. Moreover, degradation tests were carried out.

After casting, the alloys were hot and cold worked by flat rolling and finally heat treated. The material structure was investigated by means of optical (OM) and electronic (SEM) microscopy and x-ray diffraction (XRD) to assess the present phases. Mechanical properties were characterized by microhardness and tensile tests. Corrosion behaviour of the alloys was studied by 14 days static immersion test. The degraded samples were evaluated by scanning electron microscopy (SEM), energy dispersive X-ray spectroscopy (EDS), Fourier infrared transform spectroscopy (FTIR) and X-ray diffraction (XRD), both on the degraded sample surfaces and on the degradation products. Mn content was found to heavily affect both mechanical behaviour (by lowering strength and increasing ductility) and corrosion behaviour: a stable (Mn,Fe)CO<sub>3</sub> layer was formed on the surface, thus slightly reducing the corrosion rate.

## Microstructural evolution of open-porous, sintered magnesium (WZM211) short fibres scaffolds and its fatigue behaviour

G. Szakács<sup>1</sup>, D. Tolnai<sup>2</sup>, N. Hort<sup>2</sup>, F. Witte<sup>1</sup>

<sup>1</sup> Julius Wolff Institut, Charité-Universitätsmedizin Berlin , Germany <sup>2</sup>Magnesium Innovation Centre, Helmholtz Zentrum Geesthacht, Germany

INTRODUCTION: Open porous magnesium scaffolds were investigated for load-bearing application. This type of materials have unique potential for orthopedic and dental application [1]. They could be used to replace and regenerate the damaged bones or to provide structural support for healing bone defects. These types of implants are exposed mainly to continuous and cyclic comprehensive stresses in biological environment. The aim of the study is to determine the evolution of the mechanical property profile of the Mg scaffold, and how the structural behavior is related with the process resulted microstructure. These open-porous structure was manufactured by using the crucible melt extraction (CME) process and sintering of the produced magnesium fibers [2]. This method allows to adjust the porosity level from 55% up to 75 %, which is the normal porosity of the cancellous bone.

#### **METHODS:**

Microstructural investigation was carried out both on the CME processed fibers and on the sintered structure. The samples were embedded in a multicomponent plastic resin (Demotec 30). The open porous structural material had to be embedded in a high pressure chamber in order to let the embedding material penetrate and fully fill the sample. The embedded samples were ground with SiC-grinding papers by a Struers polishing machine. The samples were polished manually and automatically with an OP-Chem polishing cloth in combination with water free colloidal silica solution (OP-S) and 1 um diamond paste. The polishing step took 16-20h depending on the specimen. The fatigue test was carried out with an electromagnetic driven BOSE system.

**RESULTS:** After the CME step the fibers microstructure shows a dendritic structure with segregated areas filed with secondary phases.

microstructure evolved through pronounced directional solidification from the sides of the fibers. However generally these dendrites are progressing only from one-half side of the fibers and the other half either getting more equal axial or some cases there is a bit missing part of the fibers like a u-shaped crater from the other side. The sintered structure material has a significantly coarser grain structure with an obvious LPSO phase formation/growing compare to the as-cast structure. This material is based on the WZ21 and tend to form LPSO phases [3], however the applied heat treatment during promoted the phase formation.

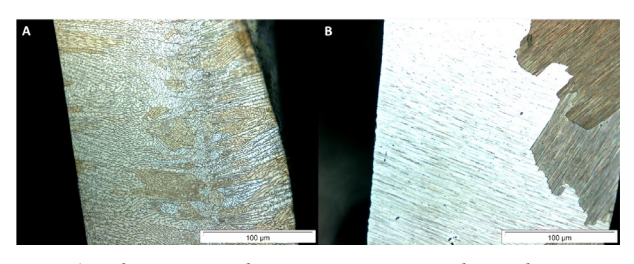


Fig. 1: The image shows an overview how the grain structure evolves during the sintering heat-treatment. On the left side (A) the "as-cast" structure while the right side (B) is the final microstructure of the sintered fibres.

**DISCUSSION & CONCLUSIONS:** The applied processes are significantly modifying the typical microstructure of the base material which can enhance the property profile in a desirable way.

**REFERENCES:** <sup>1</sup> Mostafa Yazdimamaghani et al (2017) *Materials Science and Engineering C*:1253-1266. <sup>2</sup>K. Bobe et al (2013) *Acta Biomaterialia 9*: 8611–8623. <sup>3</sup> E. Onorbe et al (2012) *J. Mater Sci.* 47:1085–1093

**ACKNOWLEDGEMENTS:** The project was founded by BMBF Syngomag (FKZ13GW0176B) and AIF MgStütz (FZ4122205AK6).

### Microstructure, mechanical property and in vitro biocorrosion behaviors of Mg-(1,3)Zn-0.4Zr-1Sc allovs

DN Shen, D Bian, YF Zheng

Department of Materials Science and Engineering, College of Engineering, Peking University, Beijing 100871, China

INTRODUCTION: Mg-Zn-Zr alloys are commercially used due to their excellent mechanical properties, and have been studied as biodegradable materials recently. The corrosion resistance of Mg-Zn-Zr alloy is significantly destroyed when Zn content exceeds a certain amount due to large amounts of second-phase. Therefore, Zn content is controlled under 3 wt.%, and as an compensation for decrease in mechanical performance as a result of decrease of Zn content, Sc is added to Mg-Zn-Zr alloy.

**METHODS:** As-extruded Mg-(1,3)Zn-0.4Zr-1Sc alloys are characterized. The microstructure is revealed via optical, scanning electron microscope and X-ray diffractometer. Tensile test was carried out on a universal material testing machine. Biocorrosion behaviour is studied via immersion and electrochemical tests.

**RESULTS:** Fig. 1 illustrated the microstructure of the alloys. Grain curling around the elongation axis and low degree of recrystallization was observed. Small particles of secondary phases mainly containing Mg-Zn were loosely distributed in the matrix. Sc<sub>3</sub>Zn<sub>17</sub> and ZrH<sub>2</sub> phases were also detected the hydrogen may come from decomposition of H<sub>2</sub>O during melting [1]. The UTS of Mg-(1,3)Zn-0.4Zr-1Sc alloys were 323 MPa and 362 MPa, and the YS were 287 MPa and 309 MPa respectively, as shown in Fig.2, displaying significant improvement in comparison to pure Mg, ZK10 and ZK30 [2-3]. The excellent strength of Mg-Zn-Zr-Sc alloys might be attributed to the deformed but unrecrystallized grains with high dislocation densities, which could hinder the movement of dislocations. In vitro corrosion parameters are listed in Table 1. It showed that the addition of alloy elements increased the corrosion potential of pure Mg, and higher content of Zinc caused a further increase. The investigated alloys, especially Mg-1Zn-0.4Zr-1Sc alloy exhibited good corrosion resistance comparable to pure Mg.

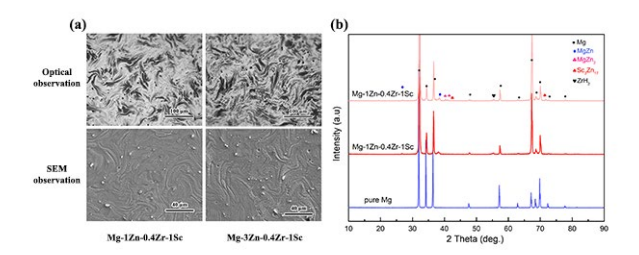


Fig. 1: (a)Microstructures of as-extruded pure Mg and Mg-(1,3)Zn-0.4Zr-1Sc alloys, (b)XRD results of alloys investigated.

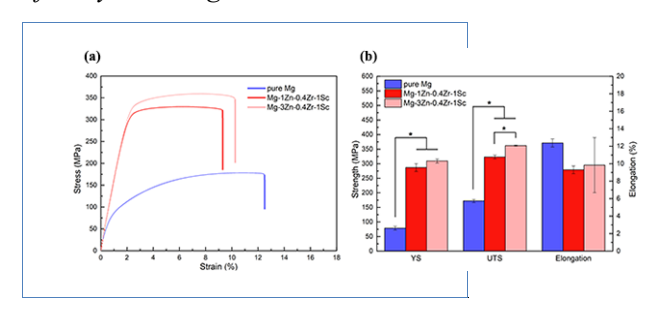


Fig.2:(a) Tensile stress-strain curves, (b)mechanical parameters.

Table 1. Corrosion parameters of Mg-Zn-Zr-Sc.

	P <sub>W</sub> (mm/y)	E <sub>corr</sub> (V)	j <sub>corr</sub> (μA/cm²)	V <sub>corr</sub> (mm/y)
Pure Mg	0.06	-1.687	2.01	0.05
Mg-1Zn- 0.4Zr-1Sc	0.10	-1.615*	3.38	0.08
Mg-3Zn- 0.4Zr-1Sc	0.17*	-1.523*	3.52	0.08

 $P_{W}$ : corrosion rate calculated from weight loss;  $E_{corr}$ : corrosion potential;  $j_{corr}$ : corrosion current density;  $v_{corr}$ : corrosion rate calculated from polarization plots using Tafel region extrapolation.

**DISCUSSION & CONCLUSIONS:** As-extruded Mg-(1,3)Zn-0.4Zr-1Sc alloys show excellent mechanical strength, superior to exsiting pure Mg, ZK10 and ZK30 alloys. These alloys also exhibit great corrosion resistance comparable to pure Mg.

**REFERENCES:** <sup>1</sup>P.H Fu, et al (2007), *Mater. Sci. Forum.* **546–549**: 97–100. <sup>2</sup> Z.G Huan, et al (2010) *J. Mater. Sci. Mater. Med.* **21**:2623-35. <sup>3</sup> Y Wan, et al (2017) *Mater. Manuf. Process.* **32**: 1360-62.

## Iron-based biodegradable stents: Impact of surface roughness on mechanical properties

M Croonenborghs<sup>1</sup>, PJ Jacques<sup>1</sup>

<sup>1</sup> Université catholique de Louvain, Institute of Mechanics, Materials and Civil Engineering, IMAP, Louvain-la-Neuve, Belgium

INTRODUCTION: Nowadays, permanent stents are used to open clogged artery. However, after 6 to 12 months the artery recovered its mechanical properties and the stent becomes useless. Moreover, risks of late complications, such as thrombosis or restenosis, are increased by the presence of permanent stent. Biodegradable stents aim at decreasing these risks. Such application requires good mechanical properties to support the expansion process, but also during the healing period (about 1 year) and an adapted degradation rate [1]. Transformation Induced Plasticity (TRIP) materials are investigated since they show good mechanical properties. However, their degradation rates are too slow for biodegradable stents. Therefore, a potential solution would be to increase the interface area by surface patterning. The present research aims at evaluating the impact of surface roughness on the mechanical properties of Fe-based biodegradable stents.

**METHODS:** Different alloys exhibiting a TRIP effect were investigated. These iron-based alloys also contained manganese, silicon, aluminium and nickel. The amount of the different elements is varying according to *Table 1*.

Table 1. Different chemical composition investigated for TRIP materials.

	Fe	Mn	Si	Al	Ni
Weight %	Bal.	15 - 30	0 - 3	1 - 3	0 - 3

These specific TRIP steels present after processing the face centred austenite and the body centred ferrite or martensite. Selective etching of the minority phase was then conducted in order to increase the roughness at the sub-micrometer scale. Several amplitudes of the surface roughness were generated owing to the control of the etching parameters. It was characterised and quantified owing to atomic force microscopy (AFM) and x-ray computed tomography (XCT).

The influence of this roughness on the mechanical properties was then observed in the case of uniaxial tensile tests. Different samples with different roughness and different surface over volume ratios were analysed.

EBSD and XRD were used to quantify the volume fraction of the 2 phases at different strain levels.

**RESULTS:** Chemical etching combined with prior dedicated thermomechanical treatments brought very fine controlled roughness.

The tested steel grades presented a uniform elongation of at least 0.3 prior to chemical etching resulting from the TRIP effect. The transformation of austenite to martensite during deformation has been observed using XRD.

When the surface roughness was increased, mostly the fracture strain decreased.

**DISCUSSION & CONCLUSIONS:** The results showed that TRIP effect is beneficial for the mechanical properties of the investigated steel grades. The loss of mechanical properties with an increase of the surface roughness is small also as a result of the TRIP effect. As a consequence, good mechanical properties are kept. Based on these results, the etching process has been validated and mechanical tests on miniaturised samples are considered.

**REFERENCES:** <sup>1</sup> Nasution, A. K., & Hermawan, H. (2016). Degradable biomaterials for temporary medical implants. In *Biomaterials and Medical Devices* (pp. 127-160). Springer, Cham.

**ACKNOWLEDGEMENTS:** The authors thank the ARC for the funding of this research.

#### Effects of laser shock processing on bioabsorbable Mg-1Zn and AZ31 alloys

M Lieblich<sup>1</sup>, JL González-Carrasco<sup>1,2</sup>, JC Galván<sup>1</sup>, FR García-Galván<sup>1</sup>, C Fernández-López<sup>1</sup>, JA Porro<sup>3</sup>, M Díaz<sup>3</sup>, F Cordovilla<sup>3</sup>, I Angulo<sup>3</sup>, JL Ocaña<sup>3</sup>

<sup>1</sup> <u>CENIM-CSIC</u>, Spain, <sup>2</sup> <u>CIBER-BBN</u>, Spain, <sup>3</sup> <u>Centro Láser UPM</u>, Spain

INTRODUCTION: One of the main effects sought in laser shock processing (LSP) [1] is the generation of relatively deep compression residual stresses fields into metallic components to improve their mechanical behavior, and more specifically, to enhance their fatigue life. In addition, in Mg-based bioabsorbable implants, LSP may also improve corrosion resistance [2,3]. This paper shows preliminary results of an ongoing investigation about the effects of LSP on mechanical and corrosion properties of two Mg alloys as a function of LSP parameters.

**METHODS:** The LSP experiments were performed on 6 mm thick disks cut away and sand polished from extruded Mg-1Zn and AZ31 alloy bars. The LSP set up is described in [4]. Equivalent overlapping distances (EOD) of 278 and 400 pulses/cm<sup>2</sup> were applied in an equally X-Y spaced overlapping scheme. Two specimens were treated for each LSP condition and the corresponding measured residual stress values, measured by the hole drilling strain gage method, were averaged. Parameters characterized were topography, mass variation. residual stresses. microhardness. microstructure and in vitro corrosion behavior.

**RESULTS:** Table I presents tensile yield stress and mass loss of both alloys. Due to the high intensity laser interaction in presence of water, characteristic of LSP, material ablation and local oxidation occur, as indicated by higher EDX oxygen signals at certain points of the surface. It is interesting to note that mass loss is smaller for the binary Mg-Zn than for the AZ31 alloy. It is also evident that the highest EOD promotes the largest mass loss per unit of processed area.

Table 1. As-received 0.2% yield stress, mass loss per unit area for LSP at 278 and 400 pulses/cm<sup>2</sup>.

Material	σ <sub>0.2</sub> , MPa	EOD pulses/cm <sup>2</sup>	Areal mass loss 10 <sup>-5</sup> g/mm <sup>2</sup>
Mg-1Zn	203 ± 5	278 400	$-7.6 \pm 0.7$ $-10.7 \pm 0.2$
AZ31	$285\pm3$	278 400	$-22.4 \pm 2.8$ $-27.1 \pm 0.2$

Figure 1 shows the minimum principal residual stresses induced in AZ31 as a function of depth. Both EOD levels are able to induce compressive stresses fields up to about 1 mm in depth. The minimum stress occurs in both cases at a distance between 0.1 and 0.2 mm from the treated surface. In the case of EOD of 400 pulses/cm², this stress is as high as 165 MPa, which represents 60% of AZ31 yield stress.

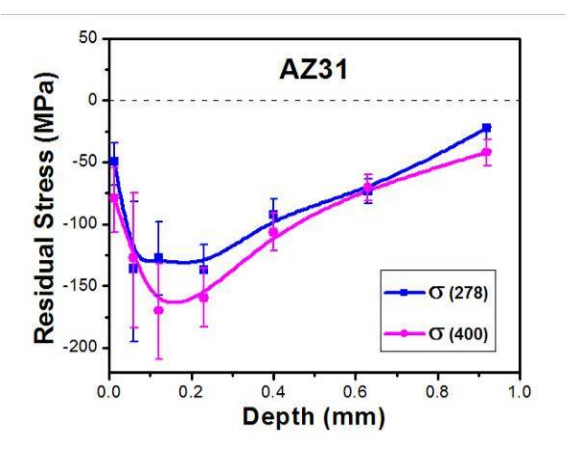


Fig. 1: Subsurface residual stress profile in AZ31 disks as a function of distance to the treated surface for two EOD.

**DISCUSSION & CONCLUSIONS:** The results presented above indicate that LSP was able to produce subsurface compression residual stresses, which should help to improve fatigue life of these Mg alloys. The subsurface grain refinement associated to the plastic deformation process is expected to enhance local mechanical properties and also to have beneficial effects on their *in vitro* corrosion behavior.

**REFERENCES:** <sup>1</sup>J.L. Ocana et al. (2014) in *Comprehensive Materials Processing;* Yilbas, Elsevier, pp 47–74. <sup>2</sup>R.A. Antunes et al. (2015) in *Surface Modification of Magnesium and its Alloys for Biomedical Applications, Elsevier*, pp 284-309. <sup>3</sup>T.C. Wu et al (2017) *Lasers Med Sci* **32**: 797–803. <sup>4</sup>J.L. Ocaña et al. (2017) *Mater Sci Forum* **879**:1408-1413.

**ACKNOWLEDGEMENTS:** MINECO, Spain: MAT2015-63974-C4, PCIN-2017-036; CM, Spain MULTIMAT Challenge: S2013/MIT-2862.

## Microstructure-biocorrosion correlation of Mg-Zn-Ca-lean alloys with varying Zn content

M. Cihova<sup>1</sup>, E. Martinelli<sup>2</sup>, R. Schäublin<sup>1,3</sup>, A. M. Weinberg<sup>2</sup>, P. Schmutz<sup>4</sup>, P. J. Uggowitzer<sup>1</sup>, J. F. Löffler<sup>1</sup>

<sup>1</sup>Laboratory of Metal Physics and Technology, Department of Materials, ETH Zurich, 8093 Zurich, Switzerland; <sup>2</sup>Department of Orthopaedics, Medical University Graz, 8036 Graz, Austria, <sup>3</sup>Scientific Center for Optical and Electron Microscopy, ETH Zurich, 8093 Zurich, Switzerland, <sup>4</sup>Laboratory of Joining Technologies and Corrosion, EMPA, 8600 Dübendorf, Switzerland.

INTRODUCTION: Fine-grained, wrought Mg-Zn-Ca (ZX)-lean alloys attract much attention due to their slow degradation rate, biologically safe composition, and appropriate mechanical properties [1, 2]. In order to ensure a safe, controllable and potentially tailorable biodegradation for such alloys, the influence of microstructural features on their biocorrosion needs to be understood. In particular, their role in the initiation of localized corrosion needs to be described. The low alloyingelement content, the sub-micrometer size, and the low volume fraction of intermetallic phase (IMP) particles in these lean alloys require methods of high spatial resolution (HR). For this purpose, a correlative approach, combining transmission electron microscopy (TEM) and electrochemistry, was applied. With such insights, the in vivo biocorrosion behavior can be evaluated and described in more detail.

METHODS: ZX-lean alloys with varying Zn content of 1.0 wt.% (ZX10) and 1.5 wt.% (ZX20), respectively, were prepared by extrusion. For all experiments, ultra-high purity (XHP) Mg [3] was used to exclude the impact of impurity-induced cathodic spots on the corrosion behavior. A detailed microstructural characterization as well as the corrosion-layer analysis were performed by TEM (FEI Talos®, ScopeM) equipped with an energydispersive X-ray spectrometer (EDS). Correlative electrochemical analysis was performed understand the evolution of in vitro corrosion behavior upon immersion. Pins fabricated by lathing were implanted transcortically in the femur of Sprague-Dawley rats. Implant degradation was followed via micro-computer tomography (µCT) over an implantation time of 12 months. Histological analysis and HR-µCT were performed post mortem to evaluate the tissue response, new bone formation and the homogeneity of the corrosion attack at the implant-bone interface.

**RESULTS:** Microstructural analysis confirms that the variation in Zn content results in different types of IMPs for the two alloys, with the binary phase Mg<sub>2</sub>Ca being the predominant phase in ZX10 and

ternary IM1 phase with composition  $Ca_3Mg_xZn_{15-x}$  (4.6 \le x \le 12, in at.\%) being the predominant phase in ZX20. Electrochemical studies reveal that ZX20 has not only a greater corrosion rate than ZX10, but also an increased cathodic activity, which increases with immersion time. Correlative microscopy reveals a cathodic protection of the IMPs in ZX20, in contrast to a rapid dissolution of the IMPs in ZX10. This difference in the in vitro corrosion behavior is confirmed in vivo, with ZX20 showing a higher degradation rate than ZX10. Histological analysis reveals that neither of the alloys caused adverse reactions.

DISCUSSION & CONCLUSIONS: Zn, which has a significantly higher electrochemical potential than Mg and Ca, appears to play the key role in governing the biocorrosion behavior. While the type of IMP determines the primary biocorrosion events, it is the matrix Zn content that generates a steady increase of the cathodic activity with progressing immersion time. Based on the obtained results we established a model for the active biocorrosion mechanisms in ZX-lean alloys, which decouples the impact of Zn content from the impact of the type of IMP on the active biocorrosion mechanisms.

**REFERENCES:** <sup>1</sup> J. Hofstetter *et al.* (2014), *JOM*, 66:566-572. <sup>2</sup> J. Hofstetter *et al.* (2015), *Acta Mater.*, 98:423-432. <sup>3</sup> J. F. Löffler *et al.* (2013), WO2013/1076442012.

ACKNOWLEDGEMENTS: The authors acknowledge support by the Swiss National Science Foundation (SNF Grant No. 200021-157058), by the Laura Bassi Center of Expertise BRIC (Bioresorbable Implants for Children), FFG, Austria, and by the Scientific Centre for Optical and Electron Microscopy (ScopeM) at ETH Zürich.

### Dual-functional biomimetic surface nanocoating strategy for biodegradable magnesium vascular stents

J Pei<sup>1</sup>, F Yuan<sup>1</sup>, JY Tan<sup>2</sup>, YJ Shi<sup>1</sup>, GY Yuan<sup>1</sup>

<sup>1</sup> National Engineering Research Center of Light Alloys Net Forming and State Key Laboratory of Metal Matrix Composite, Shanghai Jiao Tong University, Shanghai 200240, China; <sup>2</sup> Department of Vascular Surgery, Huashan Hospital of Fudan University, Shanghai 200040

INTRODUCTION: Biodegradable magnesium alloys show great promise as next-generation vascular stents for treating cardiovascular artery disease. Nevertheless, the major limitations lie in the excessive corrosion nature of Mg matrix<sup>1-2</sup>, and consequently rapid structural loss, biocompatibility issues and biological performance post implantation. Surface modification/functional coatings with rational design may provide a promising avenue. Herein, we propose a new strategy of engineering a bilayered polymeric nanoscale coating with dual functions of enhanced corrosion-resistance and biocompatibility and cell selectivity, involving the use of biomimetic chiral hydrolgel (Fig. 1(a)).

METHODS: JDBM (Mg-Nd-Zn-Zr) disks and stents were fabricated and pretreated following our previous protocol<sup>3</sup>. The bilayered coating was prepared with chemical solution deposition followed by solution casting of a REDV-grafted chiral hydrolgel layer. In vitro corrosion was studied by electrochemical measurements and long-term immersion tests. *In vitro* cytotoxicity and direct cell adhesion and activity assays were evaluated with endothelial cells (ECs) and smooth muscle cells (SMCs). Hemolysis and platelet adhesion and activation was analyzed. Rabbit aorta model was employed to assess the *in vivo* biosafety, degradation and biological performance of coated JDBM stents for up to 4 months.

RESULTS: The designed bi-layered coating structure and the physicochemical properties were confirmed with XPS, contact angle, CD and SEM measurements. ASTM "Tape Test" of coating adhesion strength was examined as 5B level of excellent adhesion. Electrochemical measurements and immersion tests demonstrated a considerable decrease of magnesium corrosion by ~89% with the optimized polymer coating structure (Fig. 1(b)). The systematic investigation of cellular response demonstrated the coating induced no cytotoxicity but rather promoted ECs adhesion and proliferation over SMCs (Fig. 1(c)). In vitro hemocompatibility was also greatly improved with the bilayered coating, showing hemolysis rate of <1% as well as few platelet adhesion. In vivo implantation confirmed the biosafety of the coated JDBM stents, and moreover, significantly decreased degradation rate accompanied with accelarated endothelialization process as compared to uncoated JDBM and NiTi control groups.

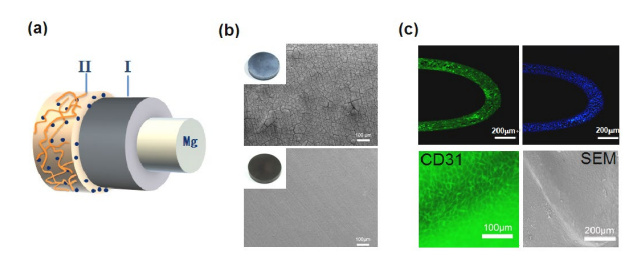


Fig. 1: (a) Schematic illustration of the bilayered nanocoating design on Mg; (b) SEM showing ameliorated magnesium corrosion with the coating(down) as compared to the uncoated(up); and (c) endothelial cell adhesion on the coated JDBM stent, in vitro(up) and in vivo (down).

DISCUSSION & CONCLUSIONS: To control magneiusm degradation while at the same time to improve biocompatibility and bioactivity is of significant importance in promoting clinic application of magnesium-based vascular stents. To address these challenges simultaneously, a bilayered biomimetic polymeric nanoscale coating was developed on JDBM alloy, demonstrating desirable dual functions, both *in vitro* and *in vivo*. The corrosion protection was investigated to be mainly due to the ability to govern anion (especially Cl<sup>-</sup>) permeability, and the improvement of biocompatibility and cell selectivity could be attributable to the selectivity of protein adsorption with the chiral structure of the hydrogel.

**REFERENCES:** <sup>1</sup> R. Zeng, et al. (2008) *Adv Eng Mater.* **10**: B13-B14. <sup>2</sup> N. Li N, et al. (2013) *J Mater Sci Technol.* **29**: 489-502. <sup>3</sup> L. Mao, et al. (2013) *Nanoscale.* **20**: 9517-9522.

ACKNOWLEDGEMENTS: This work was financially supported by the grants from the National Natural Science Foundation of China (No. 51501115 & 51701041), the Science and Technology Commission of Shanghai Municipality (No. 17DZ2200200) and the 111 Project (No. B16032).

#### Corrosion fatigue behaviour of additively manufactured porous magnesium

Y Li<sup>1</sup>, J Zhou<sup>1</sup>, MA Leeflang<sup>1</sup>, H Jahr<sup>2, 3</sup>, AA Zadpoor<sup>1</sup>

<sup>1</sup> Department of Biomechanical Engineering, Delft University of Technology, Delft, The Netherlands. <sup>2</sup> Department of Orthopaedics, University Hospital RWTH Aachen, Aachen, Germany. <sup>3</sup> Department of Orthopaedic Surgery, Maastricht UMC+, Maastricht, The Netherlands

**INTRODUCTION:** Recently, additive manufacturing (AM) has been successfully applied to develop biodegradable magnesium scaffolds [1]. To employ AM biodegradable scaffolds as loadbearing orthopaedic implants, their corrosion fatigue behaviour in simulated in vivo conditions must be well understood. We hypothesized that the corrosion of the AM magnesium scaffolds would be accelerated under cyclic loading, leading to earlier mechanical failure. However, the extent of the effect of the simultaneous action of cyclic loading and corrosion on the fatigue properties was unknown. Here we thus investigated the corrosion fatigue behaviour of the AM magnesium scaffolds.

**METHODS:** Cylindrical WE43 magnesium alloy scaffolds (10\*11.2 mm) with a diamond lattice unit cell were additively manufactured using a laboratory-scale selective laser melting (SLM) machine. They were then chemically polished in a solution composed of 5% (by volume) HCl, 5% HNO<sub>3</sub>, and 90%  $C_2H_5OH$  for 2 min.

Compression-compression fatigue tests were performed at a minimum to maximum load ratio of 0.1 at 15 Hz using a dynamic testing machine (Instron E10000 ElectroPlus with a 10 kN load cell). Fatigue tests were stopped when specimen failure occurred. unless failure did until 10<sup>6</sup> cycles of loading. Corrosion fatigue tests were performed by using the same machine equipped with a self-designed double-wall specimen chamber (Fig. 1). Scaffold specimens were immersed in SBF inside the chamber. The temperature of SBF was maintained at 37 °C and purging CO<sub>2</sub> at 5%.

**RESULTS:** It was found that the AM magnesium scaffolds possessed lower fatigue strength in SBF than in air, especially at a large cyclic number. However, unlike the extruded WE43 bulk material whose fatigue strength decreased by 0.25  $\sigma$  (yield strength) from 0.6  $\sigma$  in air to 0.35  $\sigma$  in SBF at 106 cycles [2], the fatigue strength of the AM WE43 scaffolds only decreased by 0.1  $\sigma$  from 0.4  $\sigma$  in air to 0.3  $\sigma$  in SBF. In addition, it was of interest to

observe that fatigue specimens tested in air and in SBF failed in a similar mode, as the primary fracture plane was all oriented at approximately 36 ° to the loading direction.

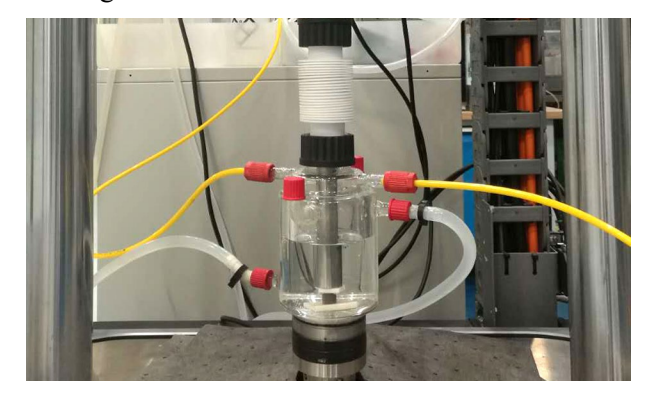


Fig. 1: Corrosion fatigue testing set-up.

**DISCUSSION & CONCLUSIONS:** Indeed, biodegradation deteriorated the fatigue resistance of the AM magnesium scaffolds. With increasing number of cycles, struts became thinner and would have to bear higher compressive stresses. Meanwhile, stress corrosion contributed to the acceleration of biodegradation. Under cyclic loading, stress concentrations may have occurred at corrosion pits where cracks initiated. However, moderate fatigue strength decreases until 106 cycles, indicating that the corrosion fatigue behaviour of the AM magnesium scaffolds was less sensitive to SBF than the bulk counterparts. Scaffold geometry may have played a profound role in determining the corrosion fatigue behaviour. Further research will be carried out to reveal the mechanisms of the fatigue failure of the AM magnesium scaffolds.

**REFERENCES:** <sup>1</sup> Y. Li, J. Zhou et al (2018) *Acta Biomater.* **67**:378-392. <sup>2</sup> X.N. Gu, W.R. Zhou et al (2010) *Acta Biomater.* **6**:4605-4613

ACKNOWLEDGEMENTS: The research was financially supported by the Prosperos project, funded by the Interreg VA Flanders – The Netherlands program, CCI Grant No. 2014TC16RFCB04.

## The effect of extrusion conditions on the corrosion and mechanical properties of biodegradable Mg alloys for orthopaedic applications

R.N. Wilkes<sup>1</sup>, M. P. Staiger<sup>1</sup>, B. Nowak<sup>1</sup>, G. J. Dias<sup>2</sup>

<sup>1</sup>Department of Mechanical Engineering, University of Canterbury, Private Bag 4800, 8140 Christchurch, New Zealand.

<sup>2</sup>Department of Anatomy School of Medical Sciences & Centre for Bioengineering and Nanomedicine, University of Otago, PO Box 913, Dunedin, New Zealand.

**INTRODUCTION:** The unique properties of Mg and its alloys have prompted significant research into their potential as biodegradable implants for orthopaedic applications. The biocompatibility, tailorable corrosion rate and mechanical properties exhibited by these materials have been studied extensively in recent years. However, there is still a need for a more detailed understanding of how thermomechanical processing affects the mechanical and corrosion properties.

The crystallographic texture that evolves during the thermomechanical processing of Mg alloys is known to influence the corrosion and mechanical properties of Mg.<sup>3,4</sup> However, the effect of texture on the corrosion behaviour of Mg alloys is not widely reported, although it could be a potentially useful method for controlling the biodegradation of Mg alloys *in vivo*.

METHODS: In the present work, the effect of variable extrusion temperature and Ca additions on the microstructure, corrosion behaviour and mechanical properties of a binary Mg alloy are examined. A Potentiostat (Bio-Logic VSP) was used to examine the electrochemical characteristics of the Mg alloy immersed in Earle's balanced salt solution (EBSS) buffered by a 5% CO<sub>2</sub> atmosphere. Both potentiodynamic polarisation (PDP) and electrical impedance spectroscopy (EIS) tests were carried out alongside immersion tests to better understand the degradation characteristics of the material. The microstructure and texture of the extruded alloys was analyzed via electron backscatter diffraction (EBSD).

**RESULTS AND DISCUSSION:** Electrochemical tests showed that texture plays a role in determining the corrosion resistance of the alloy. Surfaces made up of primarily basal (0001) texture displayed superior corrosion resistance compared to those with prismatic ( $10\overline{1}0$ ) and ( $\overline{1}2\overline{1}0$ ) planes. Samples that were extruded at higher temperatures experienced larger grain sizes, lower strength,

improved ductility and more random basal texture. Lower extrusion temperatures produced the most favourable strength and corrosion properties due to the fine microstructure.

**CONCLUSIONS:** This systematic study provides useful data for the development of biodegradable Mg-Zn-Ca alloys for orthopedic applications, as the extruded alloys showed improved strength and corrosion resistance. Furthermore, this study highlights the importance of considering extrusion texture when designing biodegradable Mg based implants due to the anisotropic properties of the material following thermomechanical processing.

**REFERENCES:** <sup>1</sup> A. H. M. Sanchez, B. J. C. Luthringer, F. Feyerabend and R. Willumeit, Acta Biomaterialia **13**, 16-31 (2015). <sup>2</sup> Y. Xin, T. Hu and P. K. Chu, Acta Biomaterialia **7** (4), 1452-1459 (2011). <sup>3</sup> R. Xin, Y. Luo, A. Zuo, J. Gao and Q. Liu, Materials Letters **72**, 1-4 (2012). <sup>4</sup> G. L. Song, JOM **64** (6), 671-679 (2012).

**ACKNOWLEDGEMENTS:** The authors acknowledge the New Zealand Health Research Council (HRC) for providing the funding for this research.

### Porosity and degradation behaviour of Mg-0.6Ca alloy under physiological conditions

E.P.S. Nidadavolu<sup>1</sup>, T. Ebel<sup>1</sup>, F. Feyerabend<sup>1</sup>, R. Willumeit-Römer<sup>1</sup>, M. Dahms<sup>2</sup>

<sup>1</sup> Institute of Materials Research, Helmholtz-Zentrum Geesthacht, 21502 Geesthacht, Germany <sup>2</sup> Materials Technology, Hochschule Flensburg, Kanzleistraße 91–93, Flensburg 24943, Germany

**INTRODUCTION:** Powder metallurgy (PM) is one of the fast emerging production techniques for magnesium alloys. In case of uni axially pressing, alloy specimens have an inherent porosity after final sintering stage. In view of magnesium implant applications, the porosity change can alter the exposed surface area of the alloy to the body fluid thereby affecting its degradation characteristics. Understanding the porosity influence is of importance in assessing the alloy's robustness in degrading environments. Hence, in this study, PM processed Mg-0.6Ca alloy with varying degrees of porosity were produced and it's degradation behaviour was evaluated over 16 days immersion under near physiological conditions.

METHODS: Sintering of Mg-0.6Ca alloy was carried out at temperatures indicated in Table 1 under Argon 6.0 atmosphere at 1000 mbar<sup>1</sup>. The test samples were subjected to spark emission spectroscopy (Fe, Cu, Ni contents) and atomic absorption spectroscopy (Ca content) prior to degradation test. Cleaning and sterilization was performed in an ultrasonic bath for 20 min using cyclohexane and ethanol, respectively. 'Mean degradation depth, h (µm)' of the samples was evaluated under semi static immersion test conditions with DMEM Glutamax with 10% fetal bovine serum (FBS) as cell culture medium<sup>2</sup>. Incubation was carried out in 37 °C, 20% O<sub>2</sub>, 5% CO<sub>2</sub>, 95% rH cell culture environment. Removal of degradation layer was carried out using chromic acid (180g/L in distilled water) treatment.

**RESULTS:** The h ( $\mu$ m) values of the samples were calculated from the equation:

$$h = \Delta m / A \rho \tag{1}$$

where,  $\Delta m$  (g) represents the mass change of the sample before and after immersion test,  $\rho$  (g/cm<sup>3</sup>) is the alloy density, A (cm<sup>2</sup>) is the exposed surface area of the alloy to medium. The straight lines in Figure 1 represent the linear regression of the form

h ( $\mu m$ )=Degradation rate ( $\mu m/d$ ) \* time (d)+ Intercept ( $\mu m$ )

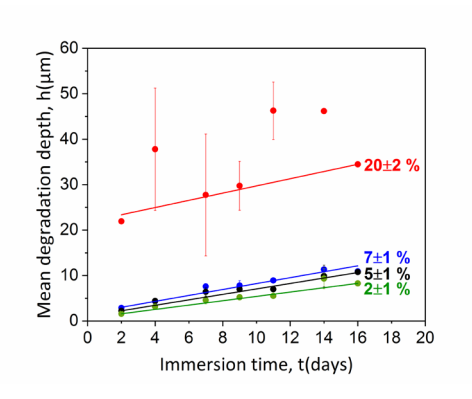


Fig. 1 MDD, h ( $\mu m$ ) vs time (d) plot for Mg-0.6Ca alloy with varying porosities.

Table 1. The linear regression fit parameters for Mg-0.6Ca alloy specimens sintered at varying temperatures.

Sintering temperature, °C	Degradation rate, µm/d	Intercept, μm
560-red line	0.79±0.36	21.79±5.86
590-blue line	$0.65\pm0.03$	1.71±0.32
620-black line	0.60±0.03	1.05±0.16
635-green line	0.48±0.01	0.64±0.08

**DISCUSSION & CONCLUSIONS:** The intercept value in Table 1 shows an increase in initial degradation with porosity during initial immersion times. Nevertheless, Figure 1 shows a controlled linear degradation for low porosity samples. This, in combination with low degradation rates ascertains the possibility of robustness in the alloy. Contrary to the general viewpoint of negative influence of porosity on degradation, these results demonstrated a minimal effect provided the porosity values are low. The porosity value till which the degradation behaviour is reproducible needs further experimentation.

**REFERENCES:** <sup>1</sup>M. Wolff, T. Ebel, M. Dahms (2010) *Sintering of Magnesium*. Adv. Eng. Mater, 12, 829–836. <sup>2</sup>E.P.S. Nidadavolu, M. Dahms et al (2016) *On the determination of Magnesium degradation rates under physiological conditions*, Materials, 9(8), 627.

**ACKNOWLEDGEMENTS:** Funding received from the Helmholtz Virtual Institute no VH-VI-523.

### Biocorrosion behaviour of the magnesium alloy WE43: influence of immersion conditions and surface modifications

Michael Höhlinger<sup>1</sup>, Svenja Heise<sup>2</sup>, AR Boccaccini<sup>2</sup>, S Virtanen<sup>1</sup>,

<sup>1</sup> Chair for Surface Science and Corrosion, Friedrich-Alexander Universität Erlangen-Nürnberg 
<sup>2</sup> Institute of Biomaterials, Friedrich-Alexander Universität Erlangen-Nürnberg

INTRODUCTION: Magnesium and its alloys have been in the focus of research for years as possible biomaterials candidates<sup>1</sup>. One of the reasons is that the corrosion products of magnesium may even have positive effects on bone regeneration<sup>2</sup>. Still certain problems remain to be resolved, such as the strong hydrogen evolution<sup>3</sup> when used as a biodegradable implant. In order to make progress in tailoring the corrosion rate and to understand the corrosion of the Mg-alloy better, different coating types have been studied with different types of corrosion tests. In the following abstract a brief overview of our ongoing research will be given.

METHODS: Samples were cut from a WE43 rod (~1 cm diameter) and ground with Microcut paper (Buehler, Lake Bluff, Illinois, USA) corresponding to a grit size of 1200. One set of samples was immersed into 100 ml of DMEM (Dulbecco's Modified Eagle's Medium, Biochrom AG) at room temperature for pre-treatment. After immersion for 24h the samples were dried with nitrogen. In addition, some samples were coated with a chitosan/bioactive glass coating prepared by electrophoretic deposition<sup>4</sup>.

Surface characterization before and after corrosion experiments was done with a scanning electron microscope (FE-SEM S4800, Hitachi). Electrochemical experiments were carried out using a three electrode set up. An electrochemical workstation "IM6eX" and a potentiostat "XPot" with the "Thales"-Software (Zahner-Elektrik GmbH & Co. KG., Kronach, Germany) were used for the measurements. The WE43 samples (bare or with the corresponding pretreatments) served as working electrodes. A platinum sheet was used as counter electrode and an Ag/AgCl electrode with 3M KCl as reference electrode. Polarization curves were recorded from a potential -300 mV relative to the respective OCP with a scan rate of 1 mV/s in the anodic direction in different electrolytes, including DMEM pH 7.4, as well as DMEM with pH value adjusted to 5, simulating inflammatory conditions.

**RESULTS:** Bare and modified Mg-alloy surfaces were tested in different immersion conditions and electrolytes. A drastically different corrosion

behaviour depending on various factors, such as pH value of the electrolyte and surface-treatments was observed. Moreover, presence of proteins (bovine serum albumin addition) in the electrolyte was found to strongly influence the degradation rate during immersion experiments; however the effect of proteins was very different for samples with different type of surface treatments; both acceleration and inhibition of corrosion could be observed. The observed corrosion morphology is being investigated by SEM and the nature of the corrosion product layers is characterized by a variety of surface analytical techniques (e.g., XPS and FTIR). In addition to immersion testing, electrochemical measurements provide insights on the corrosion processes and mechanisms.

CONCLUSIONS: The time-dependent corrosion process of bare and surface-modified Mg alloy WE43 is highly complex. A combination of different experimental approaches to study corrosion behaviour is required to understand this behaviour, for instance immersion testing, electrochemical measurements, hydrogen collection, combined with detailed surface analysis.

**REFERENCES:** <sup>1</sup> H. Hornberger, S. Virtanen, A.R. Boccaccini (2012) *Acta Biomater.* **8** 2442–2455. <sup>2</sup> C. Janning, E. Willbold, C. Vogt et al. (2010) *Acta Biomaterialia* **6** 1861–1868. <sup>3</sup> F. Witte, J. Fischer, J.Nellesen, et al. (2010) *Acta Biomater.* **6** 1792–1799. <sup>4</sup> S. Heise, M. Höhlinger, Y.T. Hernández et al. (2017) *Electrochim. Acta.* **232** 456-464.

ACKNOWLEDGEMENTS: The DFG is gratefully acknowledged for funding [grant number VI 350/12-1 and BO/12-1]. In addition partial support from the cluster of excellence EAM (bridge fund), project EXC 315 is acknowledged. This template was modified with kind permission from eCM Journal.

### Adsorption of proteins on degrading magnesium surface

R.Q. Hou<sup>1</sup>, F. Feyerabend<sup>1</sup>, R. Willumeit-Römer<sup>1</sup>

<sup>1</sup> <u>Metallic Biomaterials</u>, Helmholtz-Zentrum Geesthacht, Max-Planck-Str. 1, 21502 Geesthacht, Germany

**INTRODUCTION:** Contacting with proteins, one of the most abundant factors *in vivo*, are inevitable for biomaterials after implantation, and can affect the performance of materials. Their effect on Mg degradation is tightly related to the adsorption of proteins on Mg surface. However, due to the complex labile circumstance (pH, ionic strength, surface conditions) during Mg degradation [1, 2], few investigations focusing on the adsorption of proteins on Mg surface have been conducted. Hence, the objectives of this study are to investigate the adsorption of proteins on Mg surface and to analyse the factors affecting protein adsorption during immersion.

**METHODS:** 15 μg/mL fluorescent labelled bovine serum albumin (BSA) or fibrinogen (Fib) in HBSS and DMEM were prepared as immersion media. Ascast pure Mg samples (99.94%, 10 mm × 10 mm × 4 mm) were immersed in media at a ratio of 0.2 g/L (sample/medium) for 1 day under cell culture conditions. Afterwards, samples were cleaned with distilled water and dried at 50 °C in air. Finally, the samples were analyzed by using fluorescent microscopy with Texas Red filter for BSA (Ex./Em.: 590/622 nm) and FITC filter for Fib (Ex./Em.: 496/524 nm) to examine the adsorption of proteins on Mg surface. Additionally, the possible influencing factors for protein adsorption, such as surface hydrophilicity, surface composition and surface charge, were considered to understand the adsorption of proteins on degrading Mg surface.

**RESULTS:** As shown in Fig. 1, both BSA and Fib adsorbed on Mg surface. Moreover, it showed stronger and more uniform adsorption on Mg surface in HBSS than in DMEM. Only some spots showed an obvious adsorption for BSA and Fib in DMEM. As shown in Table 1, the surface roughness in DMEM remained stable during 24 h of immersion, while in HBSS it largely increased from nanoscale to microscale, which might provide larger surface areas for protein adsorption.

**DISCUSSION & CONCLUSIONS:** Based on the analysis of the possible influencing factors, surface conditions show a determined effect on the adsorption of protein on Mg surface. Larger roughness and lower compactness provide more

sites for protein adsorption. Moreover, different degradation products on Mg surface formed in HBSS and DMEM present different surface charge, thereby affecting protein adsorption on degrading Mg surface via electrostatic interaction.

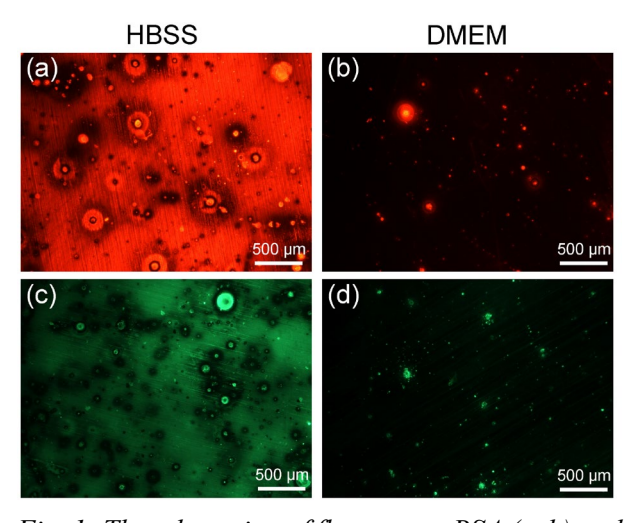


Fig. 1: The adsorption of fluorescent BSA (a, b) and Fib (c, d) after 1 day of immersion in HBSS and DMEM (exposure time: 1.5 s). Higher brightness indicates higher adsorption intensity of proteins.

Table 1. Surface roughness of Mg after different immersion time in HBSS and DMEM.

Immersion	Surface roughness [nm]	
time [h]	HBSS	DMEM
0	$240 \pm 28$	
1	$283 \pm 5$	$233 \pm 8$
6	$708 \pm 38$	$392\pm29$
24	$7344 \pm 1035$	$334 \pm 36$

**REFERENCES:** <sup>1</sup> F. Feyerabend, H. Drucker, D. Laipple, et al (2012) *J Mater Sci Mater Med* 23: 9-24. <sup>2</sup> R.-Q. Hou, N. Scharnagl, F. Feyerabend, et al (2018) *Corros Sci* 132: 35-45.

ACKNOWLEDGEMENTS: The first author thanks for the financial support from China Scholarship Council (CSC). This work was supported by the Helmholtz Virtual Institute "In vivo studies of biodegradable magnesium based implant materials (MetBioMat)" (grant number: VH-VI-523).

### Effect of severe plastic deformation on microstructure and corrosion behaviour of Mg alloy

Jiao Meng, Jing Bai, Feng Xue\*, Yue Zhang, Hong Cai, Chenglin Chu

<sup>1</sup> School of Materials Science and Engineering, Southeast University, Jiangning, Nanjing 211189, Jiangsu, China

**INTRODUCTION:** Magnesium and its alloys have attracted more and more attentions in the field of biomaterials. Mg alloy thin wire, which can be made to prepare biodegradable sutures, staple, woven stent/net, and as reinforcement in polymer based composite, etc., shows a very wider range of application potential. The aim of the present work is to investigate the effect of severe plastic deformation, namely cold drawing, on the microstructures and corrosion behavior of Mg alloy wire.

**METHODS:** Mg-2%Zn alloy wires with  $\Phi$  3.0 mm in diameter were first prepared through hot extrusion, subsequently constant strain multi-pass drawing was performed step by step at room temperature. The microstructures and texture of the wires with different strain were analyzed using scanning electronic microscopy (SEM) based electron back scattered diffraction (EBSD) technique. The hydrogen evolution and immersion testing were conducted at 25 °C in 5% NaCl solution, and corrosion rate measurement and morphological observations also were performed.

**RESULTS:** The EBSD results (Fig.1) shows that the crystallographic orientation of most grains in asextruded and 7%-strain samples are relatively uniformly dispersed with slightly more  $\{0002\}$  plane in both central and marginal areas. However, in 3%-strain sample, there are more  $\{10\bar{1}0\}$  and  $\{11\bar{2}0\}$  prism planes in marginal areas. The inverse pole figures (IPF) show that the surface normal lies perpendicular to prismatic planes  $\{11\bar{2}0\}$  in marginal areas instead of basal planes in central areas, indicating that there is an obvious crystallographic orientation gradient in 3%-strain specimen.

Compared with the as-extruded samples, the 3%-strain ones had poorer corrosion resistance with more H2 releasing and seriously non-uniform corrosion morphology with large amounts of pits, as shown in Fig. 2. When the strain increased to 7%, the corrosion resistance improved again to the same

level as the as-extruded ones with a relatively homogeneous corrosion morphology in their longitudinal section.

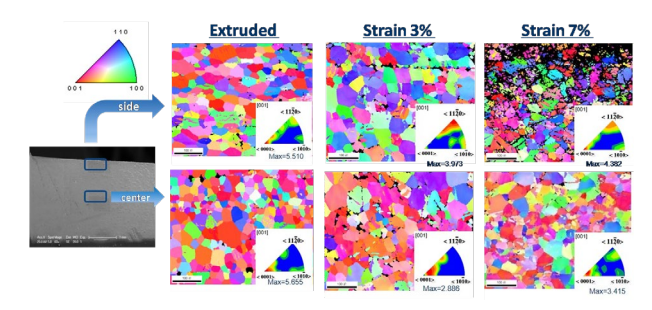


Fig. 1: EBSD analysis of the longitudinal surface in different area.

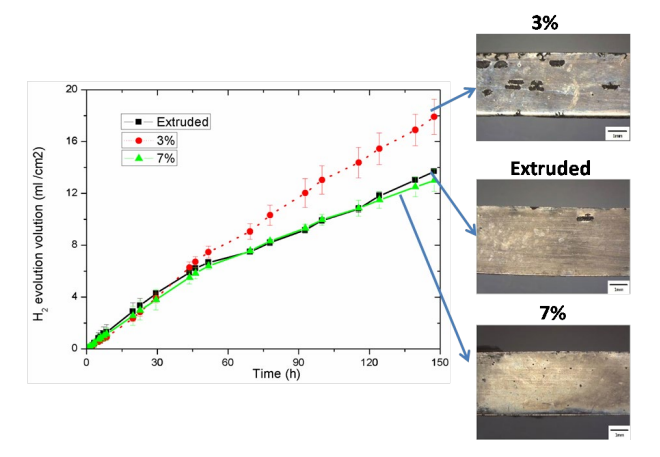


Fig. 2: Hydrogen evolution curves and morphological observations after immersion.

**DISCUSSION** & **CONCLUSIONS:** Theoretically, corrosion rates of  $\{10\overline{1}0\}$  and  $\{11\overline{2}0\}$  plans are about 18 - 20 times higher than those of  $\{0002\}$  planes. It is estimated that the crystallographic orientation gradient will cause potential difference, thus resulting galvanic corrosion. Therefore, in 3%-strain sample, there is potential difference between the marginal area and the central area and is finally severely corroded.

**REFERENCES:** <sup>1</sup> S. Pawar, T.J.A.Slater, T.L.Burnett, et al (2017) *Acta Mater* **133**: 90-99. <sup>2</sup> Liuxia Sun, Jing Bai, et al (2017) *Mater Design* **135**:267-274

## Evolution of local pH and dissolved oxygen concentration during *in vitro* degradation of pure Zn and Zn-Mg alloys

SV Lamaka, ML Zheludkevich

Magnesium Innovation Center, Helmholtz Zentrum Geesthacht, Germany

**INTRODUCTION:** The degradation rate of Zn and its alloys is slower than that of Mg and faster than Fe, making Zn an attractive material for prospective biodegradable implant applications [1-3]. However, the degradation mechanisms of Zn and its alloys, in biological environments, are not fully understood and are likely differ from that known for atmospheric corrosion of Zn-rich, sacrificial, metallic coatings [4].

METHODS: Pure Zn and Zn-rich alloys, Zn-1Mg, Zn-2Mg and Zn-4Mg were machined into rods of 1.5-3 mm diameter and embedded in an epoxy mount. Fixed in a sample holder they constituted part of a home-made flow-through cell (8mL). Either 0.14M NaCl or SBF (without any synthetic pH buffer) was constantly pumped through the cell at a rate of 1.0 mL·min<sup>-1</sup>. Under these conditions, the bulk pH in the cell remained constant: 6.7 for NaCl and 7.4 for SBF. The level of dissolved oxygen (DO) in bulk electrolyte was 8.0±0.3 ppm.

Local pH, dissolved oxygen and current density measurements were performed with commercial SVET-SIET equipment (Applicable Electronics) controlled by LV4 (ScienceWares). The Pyro Science micro-optode was integrated into the **SVET-SIET** equipment for simultaneous measurements of current density and concentration of DO. A glass-capillary micro-electrode (tip orifice diameter of 1.8±0.2μm) for local pH measurements was placed 50±10µm from the surface of the degrading metal sample. A vibrating Pt-Ir probe of SVET and fiber optic oxygen sensor (50 µm tip) were positioned 100±5µm from the sample surface and 100µm far from each other.

#### **RESULTS, DISCUSSION & CONCLUSIONS:**

Pitting like anodic dissolution was characteristic for pure Zn and Zn-Mg alloys, Fig.1. Several pits typically appeared during the first hour of immersion in NaCl or within 2-6 hours if exposed to SBF. Slight local acidification (compared to bulk pH) was observed in all the pits that passivated within several hours, followed by the activation of new active sites. Wider areas of cathodic oxygen reduction reaction (eq.1) were accompanied by local alkalinisation and local oxygen consumption,

decreasing its concentration to < 1ppm. This might be highly detrimental to the cells' viability.

$$\begin{array}{c} O_2 + 2H_2O + 4e^- \rightarrow 4OH^- \\ Zn_{(aq)}^{2+} + nH_2O \rightarrow [Zn(OH)_n]_{(aq)}^{(2-n)+} + nH_{(aq)}^+ \text{ pK}_{\text{hyd}} = 7.96 \ \ (2) \end{array}$$

In NaCl electrolyte, local pH varied between 5.7 in anodic areas to 9.5 in cathodic sites. In contrast, local pH in SBF varied in much narrower range of 5.9 to 8.4 for all the samples. Observed local acidification is caused by the hydrolysis of dissolved Zn<sup>2+</sup> [5], (eq.2). The pattern of precipitated corrosion products was changing during the immersion that was in line with cyclic activation and passivation of individual pits. Degradation products precipitated where the fronts of alkaline and acidified electrolytes met.

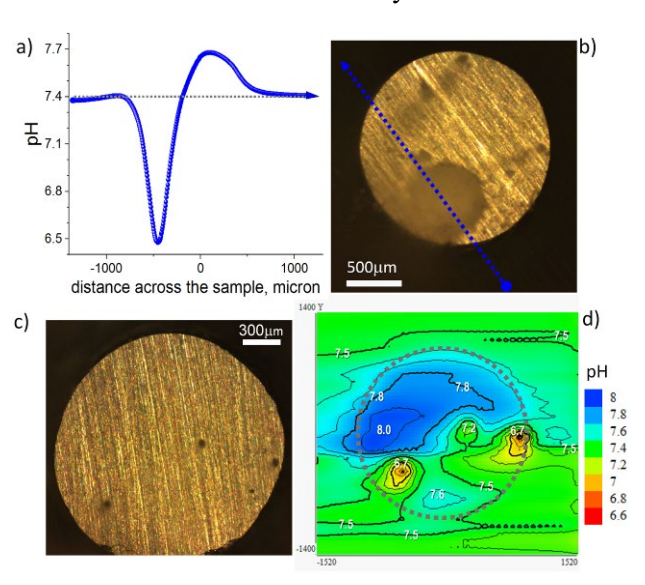


Fig. 1: a) pH profile across Zn sample taken after 24 hours of immersion in SBF at the location shown in the optical micrograph b). c) shows the appearance of the Zn-4Mg sample after 4 hours of immersion and d) corresponding pH mapping.

**REFERENCES:** <sup>1</sup> D. Vojtěch, et al. (2011) Acta Biomat. 7(9): 3515-22. <sup>2</sup> E. Mostaed, et al. (2016). J. Mech. Beh. Biomed Mat. **60**: 581-602. <sup>3</sup> X. Liu, et al. (2016). Mat. Lett. **162**:242-245. <sup>4</sup> D. Persson, et al. (2017). Corr.Sci.**126**: 152-65. <sup>5</sup> S.V.Lamaka, et al. (2010) In-situ visualization of local corrosion by Scanning Ionselective Electrode Technique (SIET). in: A. Mendez-Vilas, J. Diaz (Eds.), *Microscopy: Science, Technology, Applications and Education* **3**: 2162-73.

## Optimisation of the corrosion rate of iron-based alloys for bioresorbable stent applications by surface acidification

S Reuter<sup>1</sup>, C Georges<sup>2</sup>, P J Jacques<sup>1</sup>

INTRODUCTION: Biodegradable materials progressively become of interest for stent applications. Indeed, a stent is not needed anymore after 6-12 months due to artery remodelling. Bioresorbable stents could prevent complications such as late thrombosis [1]. Stents need to be mechanically strong, making steel a good candidate. But steel does not corrode sufficiently fast. Furthermore, during corrosion in the blood environment, different layers form on top of the metal. This hinders the oxygen diffusion towards the metal, slowing down the corrosion [2]. Therefore, a way to increase the corrosion rate needs to be found. The pH of the environment greatly influences the presence of these layers; an acidic pH favours their dissolution [2,3,4], which could help in activating the corrosion. However, the blood environment needs to keep a pH close to physiological pH (7.4) and thus only the near stent surface can undergo an acidification without affecting the blood system too much. The present work investigates different methods that can influence the pH on Fe-based alloys surfaces; especially hydrogen addition in the steel and polymer coating.

METHODS: Hydrogen charging was conducted either electrochemically, thermally or chemically on Fe-based alloys. The influence of the hydrogen concentration on the corrosion mechanism in SBF (simulated body fluid) is assessed by means of immersion tests. These tests allow to mimic closely what happens in vivo. Potentiodynamic polarisation tests were also conducted to highlight the influence of the chemical composition on the corrosion rate. Tensile tests were also carried out. The polymer was coated on the steel by dip coating and the influence of this polymer addition on the corrosion rate was assessed by immersion tests as well as potentiodynamic polarisation tests.

**RESULTS:** Samples that were electrochemically charged with hydrogen show an increased corrosion for higher hydrogen contents after one day of immersion. However, after three days of immersion, the corrosion rate is similar for different hydrogen contents (Figure 1). On Figure 2, one can see the amount of hydrogen present at time 0 in the steel and after three days at room temperature. Polymer

coated samples lead to an increased corrosion rate during immersion tests.

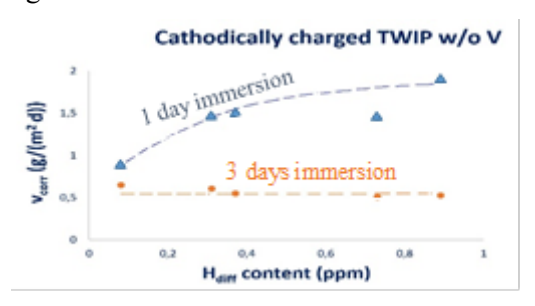


Fig.1:Corrosion rate after 1 and 3 days for different hydrogen content charged electrochemically.

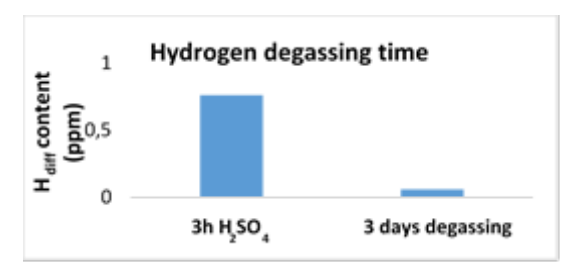


Fig. 2: Hydrogen content at time 0 and after three days at room temperature.

#### DISCUSSION & CONCLUSIONS:

Electrochemically charged hydrogen disappears in between three days of charging. This explains the similar corrosion rate after three days immersion. The presence of a polymer (PLA) coating leads to an increased corrosion rate due to the polymer hydrolysis that acidifies the surface [2]. Bioresorbable stents made of steel could become a solution to avoid late complications due to the presence of a foreign body in the blood environment. In order to accelerate the corrosion of steel, surface acidification can be implemented, leading to a dissolution of the corrosion layers that hinder the oxygen transport and thus decrease the corrosion rate.

**REFERENCES:** <sup>1</sup> T. M. Jeewandara, et al. (2014) *Materials* **7**(2):769–786. <sup>2</sup> A. H. Md. Yusop, et al. (2015) *Scientific Reports* **5**:11194. <sup>3</sup> M. Z. Yang, et al. (1999) *Journal of the Electrochemical Society* **146**(6):2107-2112. <sup>4</sup> J. Flis, et al. (1999) *Electrochimica acta* **44**(23):3989-3997.

**ACKNOWLEDGEMENTS:** The FRIA and ARC are thanked for funding this research.

<sup>&</sup>lt;sup>1</sup> Université catholique de Louvain, Institute of Mechanics, Materials and Civil Engineering, IMAP, Louvain-la-Neuve, Belgium <sup>2</sup> Centre for Research in Metallurgy – CRM Group, Liège, Belgium

## Hunting individual atoms – Challenges for the determination of low concentrations in small sample amounts

J. Bode<sup>1</sup>, F. Zimmermann<sup>2</sup>, M. Rinne<sup>2</sup>, S. Meerwald<sup>2</sup>, C. Vogt<sup>1</sup>

<sup>1</sup> TU Bergakademie Freiberg, Faculty for Chemistry and Physics, Institutte for Analytical Chemistry, Leipziger Str. 29, 09599 Freiberg, Germany

<sup>2</sup> University of Hannover, Institute for Inorganic Chemistry, Callinstr. 9

30167 Hannover, Germany

When degradation of metallic bioresorbable implants is monitored background values for the implant components and concentration of released metals have to be determined. Often only small sample amounts are available for this analysis and in these samples low or very low concentrations in the µg/kg to ng/kg range have to be determined. An overview will present analytical methods which could be applied for this task using solid state analysis or the analysis of liquid samples after decomposition of the tissues. In addition conditions for sampling, sample preparation and the measurement procedure, necessary to obtain reliable results, will be discussed, emphasizing the most critical conditions. Finally, an example will be given how much sample is necessary for the analytical procedure using a certain analytical method to produce reliable concentration data.

## 3D printed silicone vascular and heart model for biodegradable endovascular device characterization

H Gong<sup>1,2</sup>, M Mao<sup>1,2</sup>, F Xu<sup>1,2</sup>, K Ying<sup>2</sup>

<sup>1</sup> <u>State Key Lab of Manufacturing Systems</u>, School of Mechanical Engineering, Xi'an Jiaotong University, Xi'an, Shaanxi, China. <sup>2</sup> <u>Trandomed, Inc.</u>, Ningbo, Zhejiang, China.

**INTRODUCTION:** In vitro characterization of biodegradable endovascular device remained as a challenge due to lack of high-fidelity testing environment<sup>1</sup>. 3D printing technology allows high precision reproduction of human vascular anatomy, but current 3D printed human vascular models are rigid and have no pulsatile motion and blood flow<sup>2</sup>. In this paper, we explored an integration of silicone 3D printing technology, flow behaver controlling method and smart sensor technology. The goal is to simulate both of anatomy and physiology of human vessels and heart for in-vitro characterization of biodegradable endovascular device.

METHODS: The silicone ink for 3D printing was prepared by mixing Sylgard 184 (Dow Corning) and curing agent by the ratio of 10:1. A heat-curing 3D printing process was utilized. Finest line was 30um, and precision was 200um. To print multi-material samples, a multi-head printer was developed and controlled by CMKY algorithm. A complex pumping system was developed to control flow behaviours within elastic structures. The pumping system can control temperature, pressure, flow rate in real-time. Pulse rate range was set between 20-200 pulse/min. Max flow rate was 120 mL/beat and max pressure was 240 mmHg.

RESULTS: A biodegradable Magnesium alloy coronary stent was tested in a 3D printed silicone coronary artery model (Fig.1). Results showed that the stent was delivered and deployed in a safe, consistent and accurate manner within the intended implant site and with intended use conditions. Physiological pulsatile flow and pressures were replicated (Fig.2) for in-vitro degradation test under pulsatile flow condition after clinical-relevant delivery and deployment process. Besides degradation test, other testing targets include pulsatile flow interactions, deployment accuracy, sizing, conformability, trackability and pushability, and torquability.

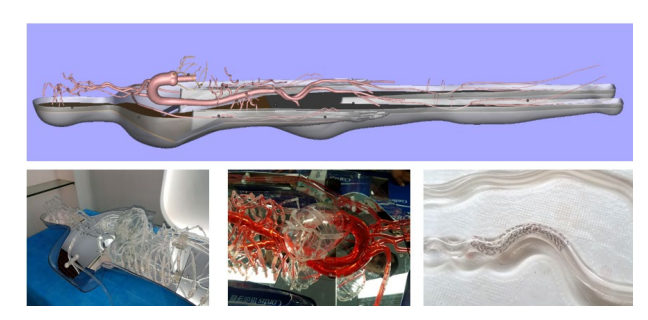


Fig. 1: 3D printed silicone artery model system.

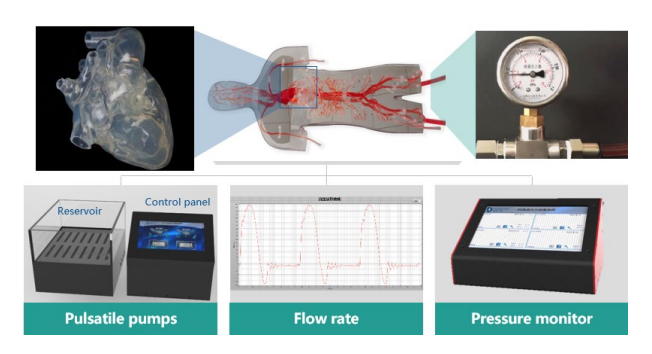


Fig. 2: A complex pumping system was built to simulate physiological pulsatile flow and pressures with programmable waveform.

DISCUSSION & CONCLUSIONS: In this paper a novel 3D silicone model system was developed to simulate the human vascular system by using advanced 3D printing technology. Realistic clinical scenarios can be replicated for in-vitro characterization of biodegradable endovascular devices. Numerous physiologically normal or abnormal functions can be replicated such as tortuosity, stenosis and other anomalies.

**REFERENCES:** <sup>1</sup> https://www.texasheart.org/thi-explores-advanced-3d-printed-silicone-technologies/ <sup>2</sup> Wang, J., Giridharan, V., Shanov, V., et. al (2014). *Acta biomaterialia*, *10*(12), pp.5213-5223.

**ACKNOWLEDGEMENTS:** This research is supported by The National Key Research and Development Program of China (Project Number: 2018YFB1107100).

### Degradation studies of Mg membranes for dental surgery

H Hornberger<sup>1</sup>, M Trahanofsky<sup>1</sup>, A Sudermann<sup>1</sup>, F Kneissl<sup>1</sup>

<sup>1</sup> <u>Biomaterials Lab</u>, Faculty Mechanical Engineering, OTH Regensburg, Germany

**INTRODUCTION:** Magnesium foils offer new applications in oral and facial surgery as degradable membranes. Conventional products in this area are resorbable collagen membranes or not-degradable metallic grids. Especially before and during implantation of dental implants resorbable collagen membranes are applied to stabilize defect tissue, to support the formation of bone and to avoid overgrowth by connective tissue. However, the mechanical stability of collagen membranes is very low. Metallic membranes in facial surgery, e.g. Ti, are not degradable but show typically grid structures to ensure the adaption to the tissue. The aim of the study was to evaluate the degradation behaviour of Mg foils for dental and facial surgery, which can be applied as resorbable membranes having high mechanical stability compared with collagen.

**METHODS:** Simple Mg foils (Ø 8mm, d=1mm, Goodfellow) were used to allegorize dental membranes. Bioactivity study was performed according to Kokubo [l]. Polarisation curves were conducted in D-MEM using the Mini cell system. Microsensor (Presens) was applied for pH-measurements in various distances from the surface.

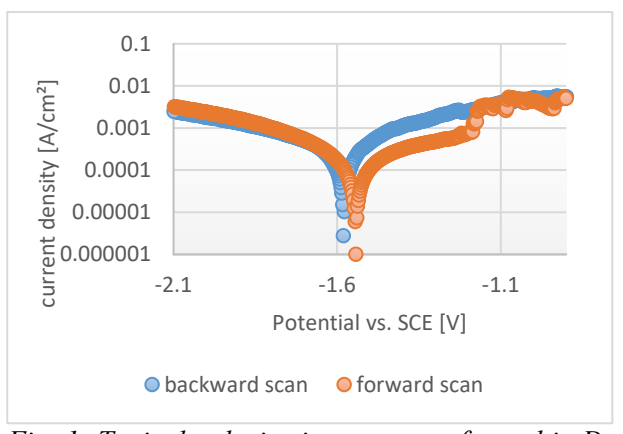


Fig. 1: Typical polarisation curve performed in D-MEM on Mg foil surface



Fig. 2: Image of laser scanning microscopy after immersion tests according to Kokubo [1]

**RESULTS:** Current potential curves including forward and backward scans (Fig. 1) demonstrate the pitting corrosion behaviour. That was also shown in μCT studies. Bioactivity of Mg was compared to the one of Ti very high, laser scanning microscopy reveals formation of Ca-P-layers (Fig. 2). The pH change during corrosion in dependence of time and distance to the reacting Mg surface is shown in Fig 3.

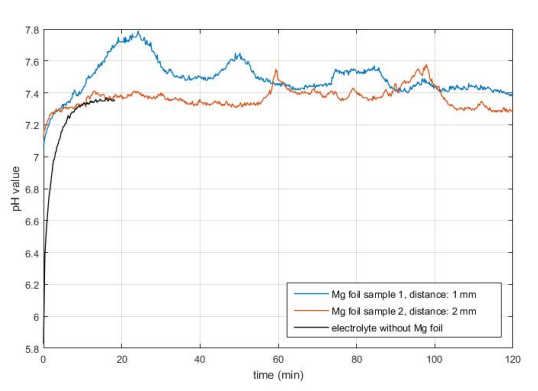


Fig. 3: Increase of pH during immersion of Mg foils in PBS (pH = 7.4)

**DISCUSSION & CONCLUSIONS:** The results show that the Mg degradation has an impact on mechanical stability as well as on biocompatibility. The bioactivity on Mg surfaces was remarkably high and indicates that the adaption to the tissue in vivo can proceed very well. Furthermore, the common grid structure of conventional metallic membranes is possibly not necessary for Mg. The pH in various distances indicate a very local (1mm) sudden change in the first 20 min, which might damage surrounding tissue. The pitting behaviour of Mg can cause problems of the mechanical stability, if the progression of corrosion is already reached before the bone formation is completed. Negative effects by pitting behaviour or by sudden pH increase can be reduced by appropriate surface modifications [3].

**REFERENCES:** <sup>1</sup> T. Kokubo and H. Takadama (2006) *Biomaterials* **27**: 2907-2915. <sup>2</sup> W.-D. Müller and H. Hornberger (2014) *Int J Mol Sci* **15**:11456-11472. <sup>3</sup> H. Hornberger, S. Virtanen, A.R. Boccaccini (2012) *Acta Biomaterialia* **8**: 2442-2455

**ACKNOWLEDGEMENTS:** We thank gratefully the company Presens (Regensburg, Germany) for gentle provision of the microsensor including micromanipulator and helpful guidance.

### Cytotoxicity of Ceramic-coated Mg-1.2Zn-0.5Ca-0.5Mn Resorbable Skeletal Fixation Hardware

D Dean<sup>1</sup>, H Ibrahim<sup>2</sup>, T McManus<sup>1</sup>, A Dehghan<sup>2</sup>, T MacDonald<sup>1</sup>, J Lammel<sup>1,4</sup>, MB Wandel<sup>1</sup>, A Luo<sup>3</sup>, R Advincula<sup>5</sup>, M Elahinia<sup>2</sup>

<sup>1</sup>Osteo Engineering Laboratory, The Ohio State University, Columbus, OH, USA. <sup>2</sup>Dynamic and Smart Systems Lab, University of Toledo, Toledo, OH, USA. <sup>3</sup>Light Metals and Manufacturing Research Laboratory, The Ohio State University, Columbus, OH, USA. <sup>4</sup>Escuela de Ingenieria, Tecnologico de Monterrey. Nuevo Leon, Mexico. <sup>5</sup>Advincula Research Group, Case Western Reserve University, Cleveland, OH, USA

INTRODUCTION: Ti-6Al-4V (Surgical Grade 5 titanium) is the standard of care material for fixation devices used to immobilize bones during the healing process following reconstructive surgery. These devices are usually left in the patient after the fractured and/or grafted bone has healed. Thereafter this extremely stiff fixation hardware can interrupt the bone's loading pattern. Stress concentrations can lead to device failure and stress shielding can lead to bone resorption. Biofilm formation, infection, and/or irritation of adjacent soft tissues are other possible problems.

While a topic of longstanding interest, it is has only been in the past decade that resorbable Magnesium (Mg) alloys have begun to be used clinically for the production of skeletal fixation devices. In addition to their bioresorbability, their low density and biocompatibility make these alloys useful for bone fixation applications. However, it has been difficult to simultaneously increase strength, retain useful resorption rates, and maintain biocompatibility. We strengthen our alloy with heat treatment. The surface is then passivated with Micro Arc Oxidation (MAO). That creates a pitted surface that binds well with a ceramic coating process where we use a Sol Gel to deliver a biphasic, hydroxyapatite and tricalcium phosphate, coating. [1] We report here on our effort to ensure the biocompatibility of Mg-1.2Zn-0.5Ca-0.5Mn skeletal fixation devices following these treatments.

METHODS: This study looked at six of each of the following specimens: pure Mg, our alloy (Mg-1.2Zn-0.5Ca-0.5Mn) "As Cast", our alloy after Heat Treatment, our alloy after MAO coating, and our alloy after Sol Gel coating with a sealing layer of TiO2 and entrapped hydroxyapatite and tricalcium phosphate nanoparticles. After soaking coupons for 3 days we ran live/dead assays on undiluted effluent or effluent diluted 2.5, 6, or 10 times. All coupons were introduced to complete media (89% MEM, 10% Horse Serum, and 1% Penicillin Streptomycin)

according to their weights at a ratio of 0.2g/mL. Incubated (37°C and 5% CO2) for 72 hours. 100,000 L929 murine fibroblasts were seeded into wells. Baseline cell numbers were recorded (t=0) using the PrestoBlue Metabolic Assay. Cells were then introduced to metal extract dilution (n=4 sample size of 96), and cell numbers were recorded at 24 and 72 hours.

**RESULTS:** Our preliminary results found the pure

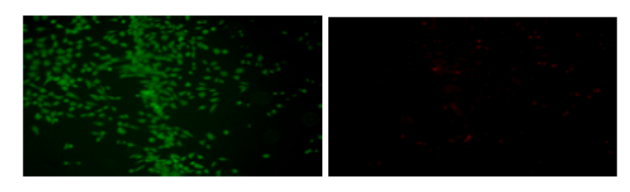


Figure 4. Live/Dead Images of L929 cells exposed to effluent samples for 24 hours.

Mg group was not safe (i.e., it was cytotoxic) at any dilution. The "As-Cast" group was safe at 6X dilution and the MAO-coated specimens were nearly safe at 2.5X dilution. Sol Gel-coated specimens were nearly safe without dilution.

**DISCUSSION & CONCLUSIONS:** These preliminary results suggest that only the Sol Gelcoated group would be safe on implantation. We will verify these preliminary results and will test the effect of pre-soaking specimens on safety. Work on determining the resorption rate of the Sol Gel coating is needed to determine a time certain when the coating is breached and the underlying Mg alloy specimen can be expected to begin losing mass and its mechanical properties.

**REFERENCES:** <sup>1</sup>H. Ibrahim, S.N. Esfahani, B. Poorganji, D. Dean, and M. Elahinia (2017) *Mater Sci Eng C Mater Biol Appl.* **70**(Pt 1):870-88.

**ACKNOWLEDGEMENTS:** Partial support for was provided by the Departments of Materials Science and Engineering and Plastic Surgery at The Ohio State University, Columbus, OH.

### A Smart Self-Healing Coating on Mg-1Ca Alloy for Bone Implants

Pan Xiong<sup>1</sup>, Yufeng Zheng<sup>2</sup>, Yan Cheng<sup>1</sup>

<sup>1</sup> BioMed-X Center, Academy for Advanced Interdisciplinary Studies, Peking University, Beijing 100871, China <sup>2</sup> Department of Materials Science and Engineering, College of Engineering, Peking University, Beijing 100871, China

**INTRODUCTION:** Surface modification have attracted considerable recent research interest, due to the poor corrosion resistance of magnesium alloys. (Hornberger *et al.*, 2012). The self-healing coatings are developed to heal the defects during the early degradation (Borisova *et al*, 2013). In the present work, a self-healing coating was fabricated by silk fibroin, while phytic acid was as the corrosion inhibitor. The self-healing property was studied by SVET (Scanning Vibrate Electrode Technique).

METHODS: The extruded Mg-1Ca alloy (wt.%) bar with a diameter of 12 mm was cut into 2mm thick slices, ground by up to 2000 grit SiC paper, and ultrasonically cleaned in acetone and ethanol, deionized water, respectively. The specimens were pre-treated by fluoride treatment and followed by coating of silk fibroin and phytic acid composite coating with spin-coating method (termed as Silk-PA). The *in vitro* corrosion resistance and biocompatibility measurements were studied. And the SVET was adopted to evaluated the self-healing property in Hank's solution.

#### **RESULTS:**

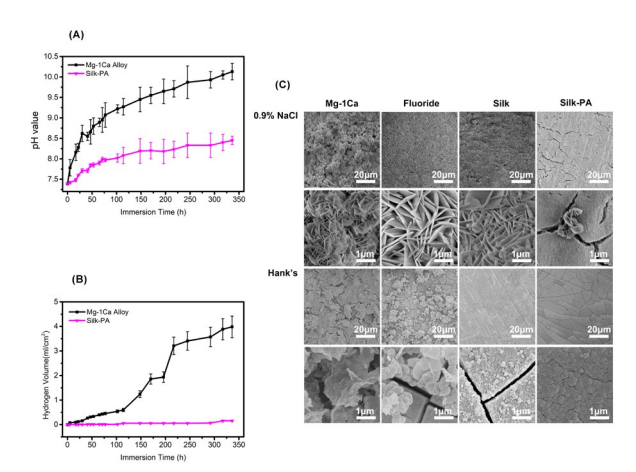


Fig. 1: Images of (a) pH value and (b) the variation of Hydrogen evolution volume immersed in Hank's solution for 14 days. (c) the surface morphologies immersed in Hank's solution and 0.9% NaCl solution for 7 days.

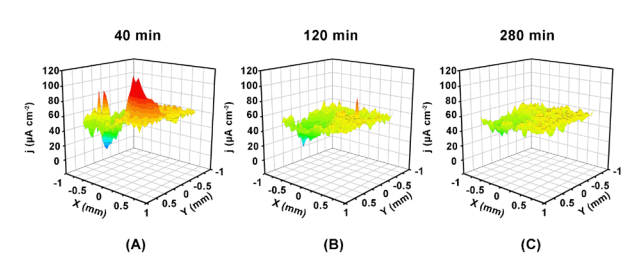


Fig. 2: SVET 3D maps of Silk-PA coating immersed in Hank's solution.

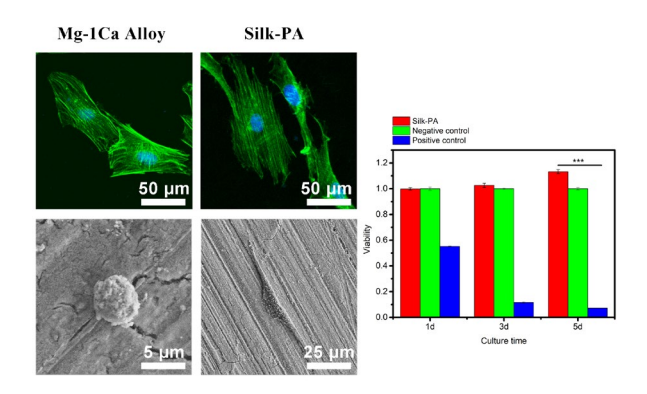


Fig. 3: The images of cell morphologies after cultured for 12 h on bare and Silk-PA; Actin-nucleus co-staining of cells cultured for 12h in the extracts; Viability of cells cultured in the extracts of each samples at 1, 3, 5 days by the CCK-8 assay kit;

**DISCUSSION & CONCLUSIONS:** Our study suggested that the silk fibroin and phytic acid composite coating could be self-healing during the degradation as well as decreased the corrosion rate of Mg-1Ca alloy and improved the surface biocompatibility, which would be a promising candidate for biomedical magnesium alloys surface modification.

**REFERENCES:** Borisova D, Akçakayıran, D Schenderlein, M, Möhwald H, Shchukin D G. Adv Func Mater **30** (23): 3799-3812.

ACKNOWLEDGEMENTS: This work was supported by the National Key Research and Development Program of China (2016YFC1102402).

## Epigallocatechin gallate (EGCG) induced chemical conversion coatings for surface modification of biomedical MgZnMn alloys

Jin Wang<sup>1\*</sup>, Hao Zhang<sup>1</sup>, Rifang Luo<sup>2</sup>, Xiaolong Shen<sup>1</sup>

<sup>1</sup>Key Lab. of Advanced Technology for Materials of Education Ministry, Southwest Jiaotong University, China

<sup>2</sup>National Engineering Research Center for Biomaterials, Sichuan University, China

INTRODUCTION: Magnesium and its alloys are generally known to degrade in aqueous environments via an electrochemical reaction by producing hydrogen gas and magnesium hydroxide. Unfortunately, the intrinsic drawback magnesium and its alloys is the low control of the corrosion speed, which makes the degradation too quick and the implant loses its function before sufficient healing. Surface modification is one of the most straightforward and effective methods for protection corrosion and improving biocompatibility simultaneously. Desired coatings on Mg-based implants should be environmentally friendly, biodegradable and biocompatible in the local tissue environment. The present study aimed to provide a simple and effective epigallocatechin gallate (EGCG) conversion coating to control the rapid biodegradation of MgZnMn. EGCG, the major catechin in green tea, is known to possess strong antioxidant ability and can suppress the inflammatory processes. As an organic compound with phenol hydroxyl (OH) groups, it was speculated to chelate with metal ions and form EGCG-metal complexes in the conversion coating on MgZnMn alloys. The corrosion resistance, cytocompatibility and tissue response to the EGCG conversion coated samples were systematically investigated.

METHODS: The MgZnMn samples were immersed into the conversion solution with a surface/volume ratio about 0.08 cm²/mL and incubated for 12 h at 22°C. Coated MgZnMn samples were rinsed thoroughly with deionized water, then dried in air and kept in a vacuum drying, oven at room temperature. Coatings were assigned as MgZnMn–0.1, 0.5 and 2.5EGCG (i.e. MgZnMn was coated in 0.1, 0.5 and 2.5 mg/mL EGCG solution) and MgZnMn–Tris represented the sample prepared in Tris buffer for 12 h at room temperature, while uncoated MgZnMn was served as a control.

**RESULTS:** Fig. 1(A) shows the PDP curves of the samples. The *i<sub>corr</sub>* values of the EGCG coated

samples were significantly lower than that of the control. Fig. 1(B) showed the hemolysis ratio of the samples, the EGCG coated samples decreased the hemolysis ratio compared with MgZnMn. As shown in Fig. 1(C), the MgZnMn, MgZnMn-ECGG did not induce local toxic effects and obvious local tissue reaction. The differences of fibrous capsule thickness among the samples were observed by microscopic evaluation. The thicker fibrous encapsulation implies more serious tissue response. The introduction of EGCG conversion coating improved the corrosion resistance of the substrates, which attenuated the fibrous capsule formation

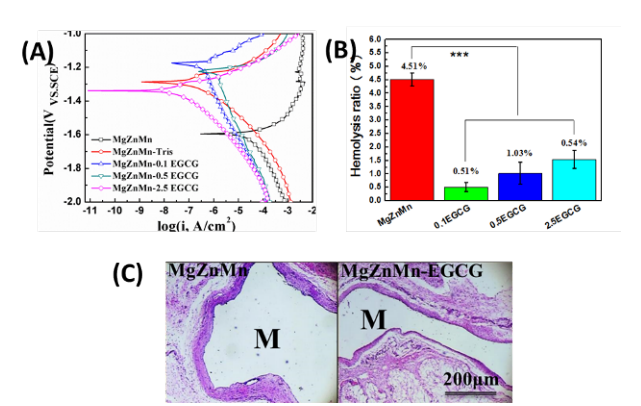


Fig. 1: (A) PDP curves,(B) hemolysis ratio and (C) HE staining of subcutaneous tissues around MgZnMn and EGCG coated MgZnMn.

**DISCUSSION & CONCLUSIONS:** An EGCG conversion coating was developed on magensium alloy successfully. The EGCG conversion coating on magnesium alloy can improve corrosion resistance and histocompatibility.

**REFERENCES:** <sup>1</sup> F. Witte, N. Hort, C. Vogt, etal. Curr. Opin. Solid State Mater. Sci. 12, 63–72, 2008. <sup>2</sup>J. Wang, V. Giridharan, V. Shanov, etal. Acta Biomater. 10, 5213–5223,2014.

**ACKNOWLEDGEMENTS:** This work was financially supported by the National Natural Science Foundation of China (Nos. 81330031, 51173149).

### Preliminary results of Y- and Nd-ion implantation on pure Mg

P Maier<sup>1</sup>, C Lux<sup>1</sup>, M Polak<sup>2</sup>, N Hort<sup>3</sup>, M Fröhlich<sup>4</sup>

<sup>1</sup>University of Applied Sciences Stralsund, <sup>2</sup>Coldplasmatech GmbH, <sup>3</sup>Helmholtz-Zentrum Geesthacht, MagIC, <sup>4</sup>Leibniz Institute for Plasma Science and Technology (INP), Greifswald – Germany.

INTRODUCTION: Especially the surface of an implant giving the direct contact to human bone cells must designed to act as a shield for unwanted corrosion rate (CR) and morphology. Plasma-immersion ion implantation (PIII) is one way to decrease initial corrosion remarkable [1]. Once pitting corrosion has started during the initiation phase, it will propagate and increase stress intensity by the notch effect causing undesirable failure of the implant. Chu et al. [2] has shown improvement of cytocompatibility and corrosion resistance by plasma-based surface modification applying ion implantation. However, PIII of Ca and Zn in Mg has shown no positive effect [3].

MATERIAL & METHODS: In this study. extruded pure Mg (0.00565wt.% Cu, 0.00247wt.% Fe, less than 0.0002wt.% Ni) was implanted with Yand Nd-ion, based on WE43. Prior to PIII, the samples were ground to 1200 grit SiC paper and then polished with diamond paste. PIII was performed in an INP in-house ultra-high vacuum reactor. The applied pulsed voltage amounted to 2keV and the working pressure was 0.3Pa. The pulses for the Y- and Nd-PIII had a short rise time in the range of 4ms, a repetition rate of 50kHz and a pulse length of 2µs. These parameters induced a mean implantation current of about 4mA. The temperature of the sample stayed below 50°C. PIII treatment was carried out for 2, 4 and 6min. Potentiodynamic tests were done in Ringer solution according to [3]. Polarization curves are used to monitor the ability of passivation and the pitting factor (PF) is used to describe the morphology by dividing the deepest pit by the mean average corrosion depth. The corrosion behaviour of the modified Mg-alloy is compared to the extruded untreated pure Mg, see here [4].

**RESULTS:** The enrichment of Y and Nd is only in a depth of 50 nm. **Fig. 1** shows the chemical content near the surface of the Y- and Nd-ion implanted Mg-alloy at three treatment times (2, 4, 6 min) compared to an extruded WE33 [5]. Decreasing the treatment time leads to less amount of Y and Nd. However, the content is still higher than in WE33. The current density - voltage curves do not differ a lot in dependence on the treatment time and its resulting Mg surface content.

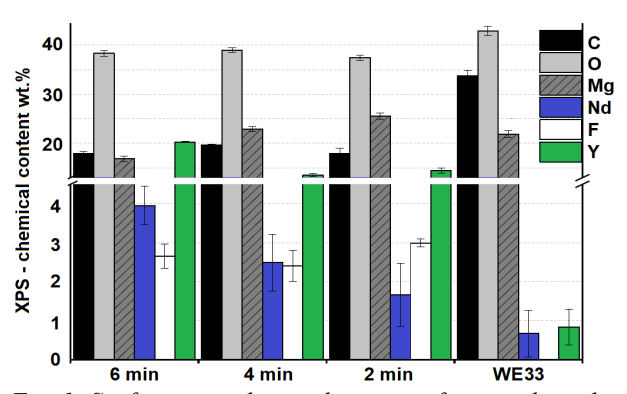


Fig. 1: Surface near chemical content of ion implanted Mg at 3 treatment times compared to WE33 [5]

**Fig. 2** shows the corrosion data evaluated from cross-sectional micrographs of pure and modified Mg compared to WE33. Implantation of Y- and Ndions over 6 and 4 min reduces the PF slightly. PIII over 2 min decreases the PF, but leads to an increase of the corroded area. The PF of WE33 in the 3 different conditions: extruded, T4 and T6 [5] is found higher; the highest CR appeared for T4.

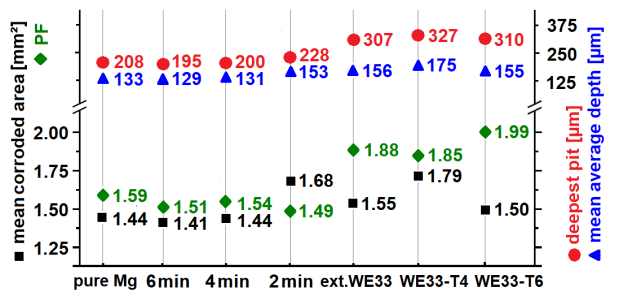


Fig. 2: Corrosion data evaluated from micrographs of pure Mg and modified Mg compared to WE33 [5]

DISCUSSION & CONCLUSIONS: The amount and size of second phases control the corrosion behaviour. PIII results in solid solution rather than in forming precipitates. The enrichment of Y and Nd by PIII seems to act positively on the corrosion behaviour if higher treatment times are applied. Over all: grain size, impurities, residual stresses, manufacturing route, volume fraction and size of precipitates need to be addressed to discuss beneficial improvement by PIII.

**REFERENCE:** <sup>1</sup>U. Walschus et al. J. Funct. Biomater. 2017(8):30. <sup>2</sup>Paul K. Chu Magnesium Technology 2016:329-330. <sup>3</sup>S. Somasundaram et al. Metals 2018(8):30. <sup>4</sup>P. Maier et al. Magnesium Technology 2017:429-437. <sup>5</sup>P. Maier et al. TMS Annual Meeting & Exhibition Supplemental Proceedings 2018.

### New in vitro set-up to evaluate the corrosion mechanisms of biodegradable metals

A. Bruinink<sup>1</sup>, D.Hahn<sup>1,2</sup>, N.G. Grün<sup>2</sup>, AM.Weinberg<sup>2</sup>, P. Schmutz<sup>1</sup>

<sup>1</sup> <u>Laboratory for Joining Technologies & Corrosion, Empa</u>, Dübendorf, CH. <sup>2</sup> <u>Department of Orthopedics and Trauma Surgery</u>, Medical University of Graz, Austria

**INTRODUCTION:** Permanent implants which are only needed during the healing process but without function afterwards may be deleterious at these later stages. This is the reason why, if possible, these are removed in a second operation. Because of the related inconveniences for the patients, large efforts are currently made to develop and produce, for certain applications such as stents and screws, implants made of degradable materials. To introduce a biomaterial into the body, an acute wound has to be made in nearly all cases. Thereafter, the implant is positioned inside this acute wound. During inflammation, activated macrophages will interact with the implant. In case of encapsulation/integration (during the last phase), the implant will be surrounded by interstitial fluid, extracellular matrix and cells. Not only the pH of the surrounding fluid will vary during these phases but also the fluid composition will change, i.e. from blood serum to interstitial fluid <sup>1</sup>. To maximally mimic the in vivo situation, we defined a new simulated body fluid based on the interstitial fluid composition consisting of the main electrolytes and additionally glucose and albumin. Furthermore, a new flow chamber based set-up to evaluate in vitro with a combination of analytical characterization the degradation of magnesium based materials was developed. In addition the same magnesium samples were evaluated in vivo using the rat as an animal model.

METHODS: A set-up composed of a flow-chamber with an inlet and an outlet as well as two openings (one to place the Mg sample and the second one to place a pH electrode to monitor online the changes evoked by the Mg dissolution) has been designed. On top of the outlet, a device is placed to quantify the H<sub>2</sub> gas release. Upstream of the Mg sample reference and counter electrodes are placed allowing to perform a full electrochemical characterization. The degradation evoked change in OCP (open circuit potential) and EIS

(electrochemical impedance spectroscopy) characteristics of the Mg surface. At the end of the experiment, the morphology and chemical composition of the sample surface can be evaluated

by SEM/EDX surface and cross section analysis of the corroded Mg.

In order to assess the correctness of the *in vitro* setup magnesium samples are evaluated in rats. Therefore, pin-shaped Mg implants are bicortically implanted into the diaphyseal area of the femurs or serve as sham control. One and two weeks after implantation animals are sacrificed and femurs are excised. Micro-computed tomography ( $\mu$ CT) is performed to investigate implant surface and degradation rate.

**RESULTS:** The set-up is designed to monitor changes over a period of several days. First results show that the stability of the pH sensing system is affected by the presence of proteins. Several solutions to overcome this issue were evaluated and the best was implemented in the system. In addition a steering device was developed enabling the monitoring and data saving of a battery of 10 flow-chambers. The latter is a premise to enable a statistical analysis of the outcome.

To investigate implant surface and degradation rate, gathered µCT data was converted to DICOM format and post processing was done with Materialise MIMICS® ver. 20. Results obtained from *in vivo* animal study are compared to *in vitro*.

**DISCUSSION & CONCLUSIONS:** First results show the clear advantages of the current set-up in comparison to the simple set-up based on static immersion of a sample in immersion fluid.

**REFERENCES:** <sup>1</sup> A. Bruinink (2019) Body fluids and simulated body fluids used for in vitro degradation tests, in Biomaterials Handbook (eds P.L. Granja, D. Mantovani, H. Engqvist) Wiley (submitted).

### Corrosion and microstructure of hot extruded ZX11 compared to WE43 in Hanks' solution

D. Zander<sup>1</sup>, V.F. Chaineux<sup>1</sup>, N.A. Zumdick<sup>1</sup>, C. Ptock<sup>2</sup>, A. Kopp<sup>2</sup>

<sup>1</sup> <u>Chair of Corrosion and Corrosion Protection</u>, RWTH Aachen University, Germany, <sup>2</sup> <u>Meotec GmbH & Co.KG</u>, Aachen, Germany

INTRODUCTION: Up to now Magnesium-Yttrium-Rare Earths alloys are commonly used as clinical implants [1]. However, low alloyed Magnesium-Calcium-Zinc alloys are a promising alternative due to the use of potential biocompatible alloying elements and beneficial mechanical properties and corrosion behaviour [2]. The aim of this work is to investigate the corrosion behavior of hot extruded ZX11 alloy in comparison to WE43 in Hanks' solution and to clarify the effect of extrusion deformation on the microstructure and corrosion mechanism.

**METHODS:** The extruded samples of WE43 alloy, consisting of Mg-4wt.%Y-3wt.%RE, and the ZX11 here Mg-0,6wt.%Ca-0,8wt.%Zn, produced without homogenization treatment from poured material [3] by indirect extrusion at 420 °C and 0.01 mm/s. The corrosion analysis was carried out by a five-day immersion testing. The modified experimental set-up [4] monitors the evolved hydrogen in Hanks' balanced salt solution without glucose (HBSS) [5] at 37 °C. The simulated body fluid was prepared with bi-distilled water and highpurity chemicals. The pH was adjusted frequently to  $7.2 \pm 0.5$ . To analyse the microstructure of the polished and colour etched samples a Zeiss optical light microscope (Zeiss Apollo) and a Zeiss scanning electron microscope (Zeiss Ultra 55) were used. A Panalytical Empyrean X-ray diffractometer with Cu Ka radiation (40 kV, 40 mA) was used for phase analyses.

**RESULTS:** ZX11 and WE43 exhibit not only a fine microstructure and distribution of segregations but process-related elongated grains. phenomena of crystallization along the grain boundaries of a secondary phase was observed only for ZX11 by means of scanning electron micrographs. X-Ray diffraction revealed the formation of Mg and Mg<sub>2</sub>Ca for ZX11. The WE43 exhibited the Mg41Nd5 phase. Corrosion was investigated by immersion testing in HBSS. The mass loss-curves obtained by the hydrogen evolution method of both alloys show at the beginning of the test a positive steep ascent and subsequent after ca. five hours a lower ascent of the curves. However, the mass-loss per unit time is significantly higher for WE43 than for ZX11, see

Figure 1. In addition, a strong deviation of the mass loss was observed for both alloying systems.

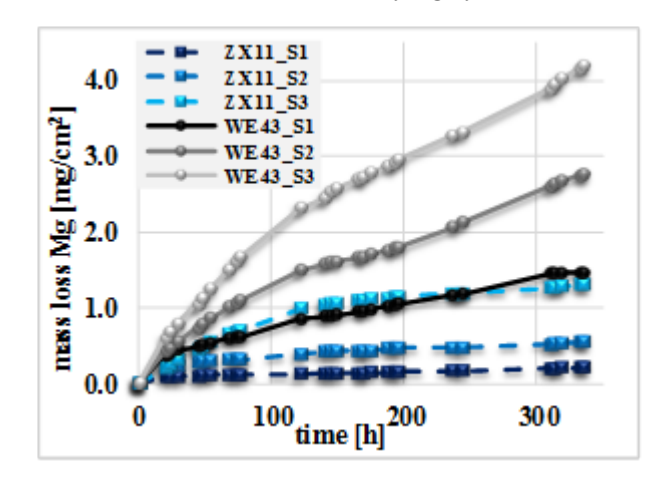


Fig. 1: Mass-loss curves of ZX11 and WE43.

DISCUSSION & CONCLUSIONS: The fine distribution of segregations and the process-related elongated grains leads to a general high mass loss for both alloys which can be related to the formation of micro-galvanic elements between the less noble secondary phases compared to the Mg matrix. It is assumed that the change in the degradation rate starting with fast-initial corrosion relates to the formation of micro-galvanic elements and the "steady state" corrosion to the formation of protective passive layers. However, the lower mass loss of ZX11 compared to WE43 is assumed to be influenced by the different electrochemical potentials of the secondary phases and segregation mechanism along the grain boundaries.

REFERENCES: <sup>1</sup> B.J. Luthringer, F. Feyerabend, R. Willumeit-Römer (2014) *Mg Research*, **27**: 142-154. <sup>2</sup>J. Hofstetter, M. Becker, E. Martinelli, et.al. (2014) *JOM* **66**: 566-572. <sup>3</sup>D. Zander, N.A. Zumdick (2015) *Corr. Sci.* **93**: 222-33. <sup>4</sup>G. Song, A. Atrens (2003) *Adv. Eng. Mater.* 5: 837-858. <sup>5</sup>J.H. Hanks, R.E. Wallace (1949) *Exp. Biol. Med.* **71**: 196–200.

**ACKNOWLEDGEMENTS:** The authors like to thank the ZIM (The central Innovation Programme for SMEs) for the financial support under the project KF2461807SU4.

## The effect of magnesium-degradation products can be influenced by hypoxia in the coculture of endothelial and mesenchymal stem cells

Lei Xu<sup>1</sup>, Regine Willumeit-Römer<sup>1</sup>, Bérengère Luthringer – Feyerabend<sup>1</sup>

<u>Institute of Metallic Biomaterials</u>, Institute of Materials Research, Helmholtz-Zentrum Geesthacht Centre for Materials and Coastal Research, Max-Planck-Straße 1, 21502 Geesthacht, Germany

**INTRODUCTION:** Bone healing process involves hematoma. inflammation. callus and remodelling. With callus formation, angiogenesis defines new blood vessels formed by endothelial cells (EC), which can support bone repair by supplying oxygen and cells [1]. Hypoxia, induced by hematoma, plays an essential role in coordinating bone formation (osteogenesis) and angiogenesis via cytokines [2]. As biodegradable material, magnesium (Mg) has been known to improve osteogenesis and angiogenesis by influencing numerous cellular enzymatic reactions and cytokines expression. Several coculture reports indicate the communications between EC and mesenchymal stem cells (MSC) can support the formation of stable vascular networks and stimulate cell proliferation [3]. Thus, we applied a transwell coculture of human umbilical cord vein endothelial cells (HUVEC) and human umbilical cord perivascular (HUCPV) cells under hypoxia to explore the interaction between Mg, osteogenesis and angiogenesis in bone fracture.

METHODS: HUVEC and HUCPV were isolated and their phenotypes characterised by the expression of specific surface markers (CD 90 and CD 31, for HUVEC and HUCPV, respectively, via flow cytometry). Tube formation was performed by seeding HUVEC on reconstituted matrix membrane (Geltrex® LDEV-Free Reduced Growth Factor Basement Membrane Matrix, Thermo Scientific - Fisher Scientific GmbH, Schwerte, Germany) for 6 hours. HUCPV and HUVEC were seeded respectively on upper membrane and lower chamber of 24-transwell-plate for 1 day. Ribonucleic acids (RNA) was extracted (RNeasy

Mini kit, Qiagen, Hilden, Germany) and real-time polymerase chain reaction (RT-qPCR) was performed (Omniscript Reverse Transcription Kit, Qiagen). All data were acquired from two independent experiments (3 donors) with at least 2 technical replicates. Statistical analysis was performed by one-way ANOVA ( $p \le 0.05$ ).

**RESULTS:** Cocultured with HUCPV, tube formation of HUVEC was significantly decreased in Mg degradation products with 20% O<sub>2</sub> but such effects were obviously diminished under 5% O<sub>2</sub>. During coculture in Mg degradation products with 20% or 5% O<sub>2</sub>, migration, collagen degradation,

adhesion and angiogenesis regulation related genes (chemokine (c-c motif) ligand 2, c-x-c motif chemokine ligand 8, matrix metallopeptidase 13, metallopeptidase inhibitor 1, integrin alpha-1, vascular endothelial growth factor b and hypoxia-inducible factor 2) of HUCPV and HUVEC were remarkably upregulated in Mg degradation products under 20% O<sub>2</sub>. Regulation of these genes were extenuated or downregulated under hypoxia both in HUVEC and HUCPV.

DISCUSSION & CONCLUSIONS: Mg degradation can enhance osteogenesis and angiogenesis by upregulating the related genes in coculture. Hypoxia could affect the influence of Mg and play a core coordination between the interaction of angiogenesis and osteogenesis. The expression of corresponding cytokines need to be further investigated.

**REFERENCES:** 1 Ghiasi, M.S., et al. (2017) *Bone Reports* **6**:87-100. 2 Xie, Q., et al. (2016) *Cell Prolif* **49**:236-45. 3 Zhang, X., et al. (2017) *Acta Biomater* **59**:317-326.

### Porous Zn-based scaffold for bone regenerations

I Cockerill<sup>1</sup>, Y Su<sup>1</sup>, M Young<sup>1</sup>, Y-X Qin<sup>2</sup>, Y-F Zheng<sup>3</sup>, D Zhu<sup>1</sup>

<sup>1</sup>University of North Texas, TX, USA. <sup>2</sup>University of Stony Brook, New York, USA. <sup>3</sup>Peking University, Beijing, China.

**INTRODUCTION:** Zn biomaterials attract strong attentions recently for load-bearing medical implants because of their mechanical properties similar to bone, biocompatibility, and degradability at a more matched rate to tissue healing. It has been shown previously that Zn alloys are beneficial for bone regeneration, thus we developed novel porous Zn foam-based scaffolds and studied their potential for bone regeneration both in vitro and in vivo.

**METHODS:** Zn foams were produced using a novel casting method involving a salt-preform method which was preceded by a polymeric-foam structure produced using a 3D printer. Then we used human bone marrow mesenchymal stem cells (hMSC) to study cell-Zn material interaction in vitro. Lastly, in vivo performance and biocompatibility of the scaffold was evaluated using a femoral condyle implantation model.

**RESULTS:** The resulting textured and porous Zn structures exhibit a controlled regular spacing based on an initial 3D polymer structure and a textured surface based on the initial salt size and morphology (Fig. 1).

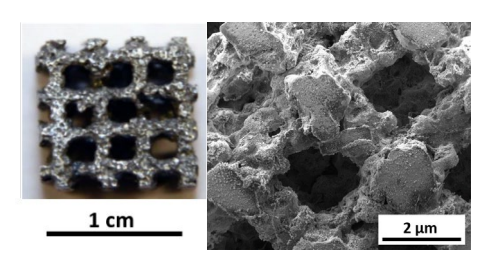


Fig. 1: Image of Zn foam and detailed view of Zn strut showing textured surface.

biomaterials hMSC adhesion, Zn support proliferation. and motility (Fig. 2-3). Mineralization of ECM and hMSC osteogenic differentiation are significantly enhanced when cells are cultured on Zn with increased expression of bone-related genes including ALP, collagen I, and osteopontin. Animal studies showed that porous Znscaffold cause minimal immune responses and promoted bone regenerations.

**DISCUSSION & CONCLUSIONS:** Porous Zn foam based scaffold for bone regenerations can be fabricated using 3D printing and salt-preform technology. Zn-based scaffold would lead to

enhanced differential regulation of genes, cell survival/growth and differentiation, ECM mineralization, osteogenesis, and other activities. These porous Zn foam-based scaffold will have a strong potential for bone regenerations.

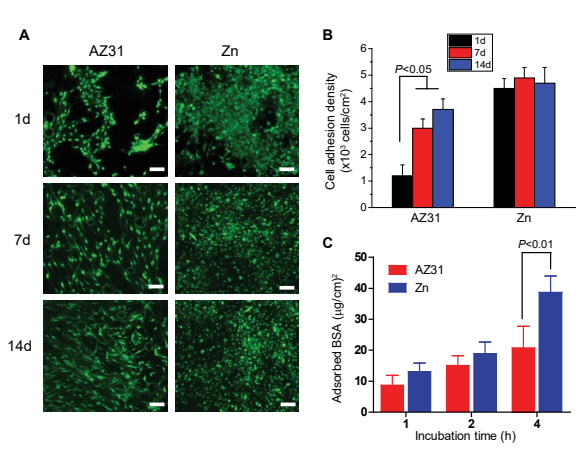


Fig. 2. Direct culture of hMSC on surfaces of Zn materials for a time course of 14 d.

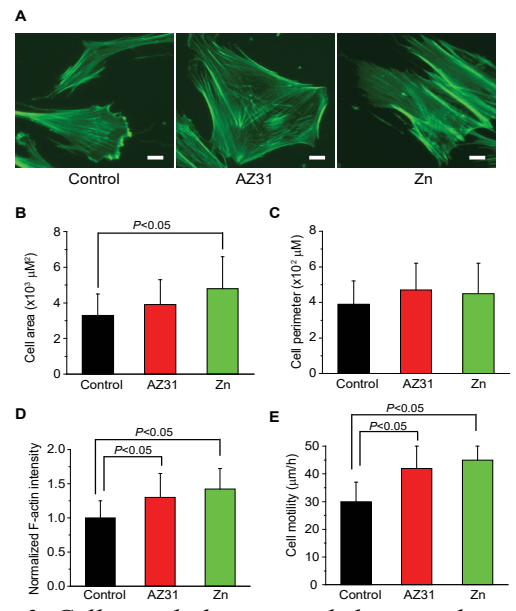


Fig. 3. Cell morphology, cytoskeleton and motility on Zn materials.

**ACKNOWLEDGEMENTS:** This work was supported by National Institutes of Health [grant number HL140562]. The content is solely the responsibility of the authors and does not necessarily represent the official views of the National Institutes of Health.

### DFT study of the adsorption of short peptides on Mg and Mg-based alloy surfaces

SK Guan<sup>1</sup>, Z Fang<sup>1</sup>, JF Wang<sup>1</sup>, LG Wang<sup>1</sup>

<sup>1</sup>Research Centre for Materials, School of Material and Science, Zhengzhou University, China

INTRODUCTION: The simulations of novel biomolecular coating on Mg-based alloy surfaces at the atomic scale play an important role in understanding the experimental advancements. For this presentation, we performed the first-principles calculations based on density functional theory (DFT) to investigate the adsorption of di- and tripeptides on the clean Mg (0001) and Zn, Y and Nddoped surfaces (models of Mg alloys) on the basis of our previous work [1]. The purpose of the present work was to analyse the adsorption mechanism and the phenomenon of different peptides with different length of backbone chain on the surfaces, and to reveal the effect of the doping Zn, Y and Nd elements on the adsorption of the peptides [2].

**METHODS:** All calculations are performed by the Vienna *Ab initio* Simulation Package (VASP) with the projector augmented wave (PAW) method. To simulate the adsorption of the isolated short peptides on Mg (0001) surface, the 8 × 8 supercell containing 4 Mg layers was selected as the slab model. The 20 Å vacuum was adopted to avoid the interactions of adsorbed peptides with the periodic slab. A single k-point was sampled for the surface Brillouin zone. The plane-wave basis is set up with cut-off energy of 400 eV.

**RESULTS:** The adsorption energy ( $E_{ads}$ ) of short peptides on the substrates are obtained by the following equation:

$$E_{ads} = E_{mol+sub} - E_{mol} - E_{sub} \tag{1}$$

where  $E_{mol+sub}$ ,  $E_{mol}$ , and  $E_{sub}$  represent the total energy of the stable adsorption systems, the energy of the optimized peptides, and the energy of the substrates, respectively.

Short peptides have three potential metal-binding groups: the guanidyl ( $-\text{CN}_3\text{H}_4$ ), amino ( $-\text{NH}_2$ ), and carboxyl (-COOH), and they prefer to lie on the surface in a flat way. The optimized structures of RGD tripeptide on the substrate are shown in Fig. 1, and the PDOS of the configuration ( $a_6$ ) in Fig. 1 for the before and after adsorption process are depicted in Fig. 2.

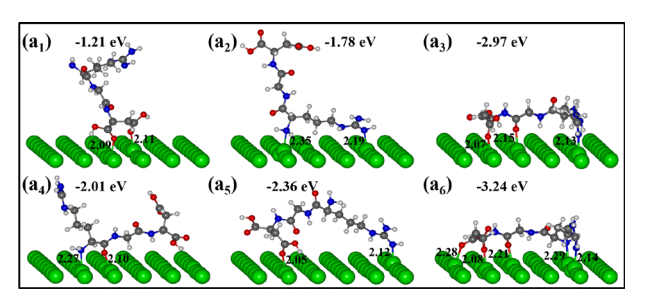


Fig. 1: Six optimized adsorption configurations of RGD tripeptide on Mg (0001) surface. Adsorption energies (in eV) and bond lengths (in Å) are also listed.

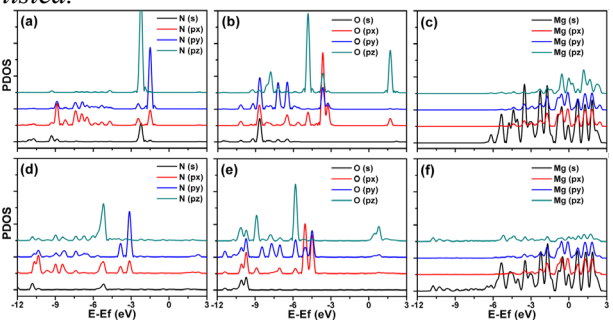


Fig. 2: The PDOS of the binding atoms (a) three O atoms, (b) two N atoms in the isolated RGD tripeptide and (c) five Mg atoms in the substrate before adsorption; (d), (e) and (f) are the PDOS of the corresponding atoms in the adsorption systems after the adsorption process.

**DISCUSSION & CONCLUSIONS:** The binding of short peptides with substrates are combined through covalent bond. The Zn element improves the bond strength between molecules and substrates, while the Y (Nd) element presents the opposite effect. These results will provide some guidance in understanding and improving the application prospects of the RGD-based peptide coating in the biomimetic fields.

**REFERENCES:** <sup>1</sup> Z. Fang, J.F. Wang, S.K. Guan, et al (2017) *Appl Surf Sci* **409**:149-155. <sup>2</sup> Z. Fang, J.F. Wang, S.K. Guan, et al (2018) *Phys Chem Chem Phys* **20**:3602-3607.

**ACKNOWLEDGEMENTS:** Authors are grateful for the National Key R&D Program of China (No. 2017YFB0702504).

## Effects of continuous degradation and Cu<sup>2+</sup> release on anti-infection mechanism of Fe-Mn-C-Cu alloys

Zheng Ma<sup>1</sup>, Lili Tan<sup>1</sup>, Ke Yang<sup>1</sup>

<sup>1</sup>Institute of Metal Research, Chinese Academy of Sciences, Shenyang, China

**INTRODUCTION:** The implantation materials related infection and lithangiuria influences the effectiveness of implantation and may result in consequences including re-operation, amputation, and death in extreme case, during the urinary reconstruction operation. The inhibition of bacterial biofilm and crystal deposition from the material itself is an effective measure to solve the urinary tract infection and calculus of the implant material.

METHODS: In this project, combining the antiinfection and anti-encrustation effect of Cu2+ and bio-degradable property of Fe and mechanical strengthening, degradation accelerating and austenitization expanding effects of Mn and C, the Fe-Mn-C-Cu alloys were designed and prepared based on proper addition of Cu, Mn, C elements into Fe. As an implant material, Fe-Mn-C-Cu implantation can shorten the operation time and inhibit bacterial infection and stone formation. When the body's diseased tissue is repaired or healed, it can be gradually biodegraded in the body and disappear, eliminating the need for secondary surgery. The study reveals the relationship between corrosion property of Fe-Mn-C-Cu alloy and the phase composition of the alloying elements, the microstructure and the second phase of the alloy, revealing the degradation mechanism of Fe-Mn-C-Cu alloy in the service environment and can effectively regulating the degradation rate.

The study also reveals the anti-infection a mechanism of Fe-Mn-C-Cu alloy under the double effect of degradation and Cu<sup>2+</sup>. It will provide a scientific basis and new ideas for the development of new Fe-based materials and the treatment of urinary tract infections and stones in the urinary system.

**RESULTS:** Antibacterial experiments showed that the Fe-Mn-C-Cu alloy has a strong antibacterial effect (Fig. 1e) with a sterilization rate of 99%. Live dead-staining experiments showed that the Fe-Mn-C-Cu alloy can destroy the bacterial cell wall

because the red fluorescent agent PI can only cross the incomplete cell wall and behaves as a red dead bacterium (Fig. 1e). SEM observation showed that Staphylococcus aureus was spherical and full in shape on the surface of pure Fe, resulting in polysaccharide mucosa, forming bacterial biofilm (Fig. 1c); while Fe-Mn-C-Cu surface bacteria were rare and sparsely distributed, no trend of bacterial biofilm formation (Fig. 1f).

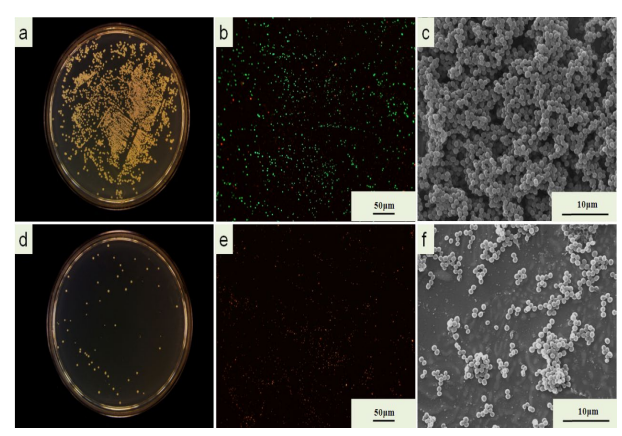


Fig. 1: Representative photos of bacteria colonization, the live/dead and SEM micrographs of S. Aureus of pure Fe(a) (b) (c) and Fe-Mn-C-Cu (d) (e) (f)

**DISCUSSION & CONCLUSIONS:** Fe-Mn-C-Cu alloy has good mechanical properties and tissue compatibility, can inhibit bacterial infections and stones, and can be degraded and absorbed in vivo.

**REFERENCES:** <sup>1</sup> J Zhao, L Ren, et al (2016) *Mater Sci Eng C*, **68**:221-29. <sup>2</sup> M Peuster, C Hesse, T Schloo (2006) *Biomaterials*, **27**: 4955-62. <sup>3</sup> I Burghardt, F Lüthen, C Prinz, (2015). *Biomaterials*, **44**:36-44.

**ACKNOWLEDGEMENTS:** The authors would like to thank the financial supports from National Natural Science Foundation of China (Nos. 81271957, 51501218, 81572113, 51631009, 2012CB619101 and 2012CB619102).

### The degradation behaviour and the rapid re-endothelialization effect of Atorvastatin-eluting magnesium-based stents

Ansha Zhao<sup>1</sup>, Changrong Ye<sup>1</sup>, Juan Wang<sup>1</sup>, Dan He<sup>1</sup>, Wangjin<sup>1</sup>, Nan Huang<sup>1</sup>

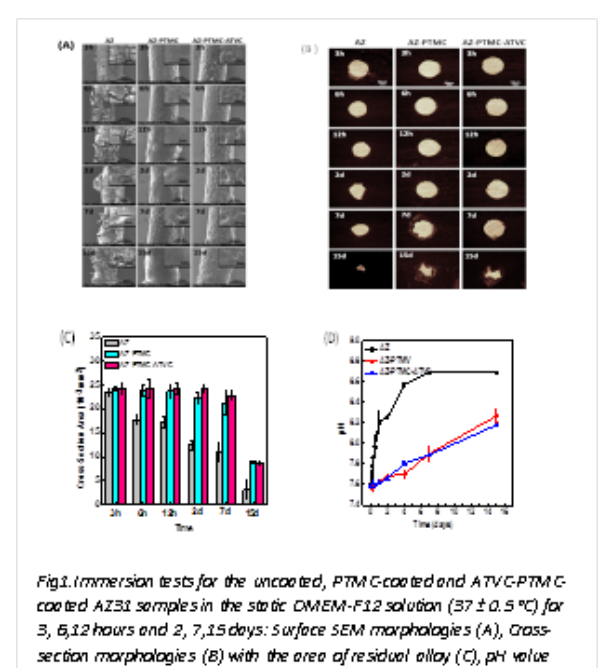
\*\*IKev Laboratory of Advanced Materials Technology of Ministry of Education, Department of

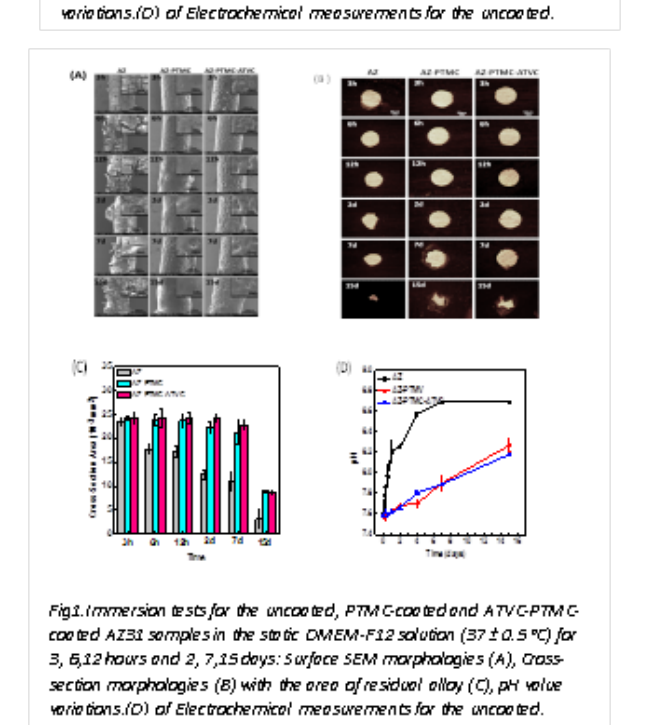
Materials Science and Engineering, Southwest Jiaotong University, Chengdu 610031, China

INTRODUCTION: Magnesium (Mg) based stents are opening a new horizon in the vascular therapeutic field. They grant physicians a new option for treating coronary artery disease without leaving a permanent implant behind. Statins as a kind of oral medication have been found to reduce cardiovascular disease (CVD) and mortality in those who are at high risk of cardiovascular disease and used widely. In this study, the direct therapeutic effect of statins on damaged vascular when applied on mg-based stents was discussed and demonstrated.

METHODS: To better simulate the degradation behavior of vascular stents, Mg-based alloy (AZ31) wires with a diameter of 1000 μm were gradually drawn to 175 μm by Cold Drawing Instrument, PTMC or PTMC with atorvastatin solution were sputtering on the wires. FTIR and SEM were performed to characterize the chemical structure and morphology of the wire. Also the degradation behavior of the wire including the pH value, cross-section morphologies and mg ions concentration were analyzed in different period. Microfluidic was applied to study the interaction between mg-wire and endothelial cell in vitro. Furthermore, the animal implantation test was used to demonstrate this drug-eluting stent's therapeutic effect.

RESULTS: The uncoated, PTMC-coated and ATVC-PTMC-coated AZ31 samples were immersed in the static DMEM-F12 solution (37  $\pm$ 0.5 °C) for different time. The surface and crosssection morphologies were observed by SEM and optical microscope as presented in Fig. 1A, 1B. The serious degradation happened on the AZ31 alloy surface with the increase of the time. But the surfaces of PTMC-coated and ATVC-PTMCcoated AZ31 samples were stable until 15 days. Also, the pH value variations for each sample were consistent with the above data in Fig. 1C.1D. Furthermore, the in vivo and in vitro test also show the ATVC-PTMC-coated AZ31 group has the potential to promote the endothelial cell growth as showed in Fig2A,2B.





**DISCUSSION & CONCLUSIONS:** Our results highlight the Atorvastatin eluting magnesium stent's promising role to promote vascular reconstruction.

**REFERENCES:**  $^{1}$  YF Zheng et al (2014) *Mat Sci Eng R* 77:1-34  $^{2}$  F. Witte (2010) Acta Biomater **6**:1680-92.

### An ex vivo vessel culture model to study the cellular response to magnesiumbased stent

J Wang<sup>1</sup>, M H Kural<sup>1</sup>, P Ling<sup>3</sup>, G Li<sup>2</sup>, N Huang<sup>3</sup>, L Niklason<sup>1</sup>

<sup>1</sup>Department of Anesthesiology and <sup>2</sup>Department of Surgery, School of Medicine, Yale University, CT. <sup>3</sup>School of Materials and Engineering, Southwest Jiaotong University, Sichuan.

**INTRODUCTION:** Absorbable stents grant physicians a new option for treating stenotic artery disease. Magnesium (Mg)-based stents have been studied for several years in animal and pre-clinical models with encouraging results. However, no correlation or preferred method currently exists for an in vitro prediction of in vivo cellular response to absorbable metals. Thus, accurate assessment is urgently required to provide insight into consideration of cellular response to stent in new testing standards for ASTM and ISO approval and future safety testing of absorbable metallic stents.

METHODS: MgZnMn stents with the diameter of 2 mm and the length of 18 mm were used in this study (Fig. 1a). The porcine coronary arteries were freshly isolated and stents was deployed in to the vessels by a balloon with the diameter of 2.75 mm. Then the vessels were mounted to perfusion bioreactors (Fig. 1b). The SMC-EC co-culture media consisted of Vasculife: DMEM (1:1) with 10 % FBS, 1% Antibiotic-Antimycotic and Dextran (30 g/L) as a pseudo-physiological medium in perfusion bioreactors. The medium was changed every two days. During the 7 days of culture, the flow rate of the circulating medium was 7.5 mL/min. The O<sub>2</sub>, glucose and lactate level kept at 120-140 mm Hg,150-250 mg/dL and less than 13.0 mmol/L, respectively. The pH kept in the range of 7.35-7.50. As controls, the vessels without stent in the perfusion bioreactor, and the vessels with and without stent in the flasks (static condition) were cultured.

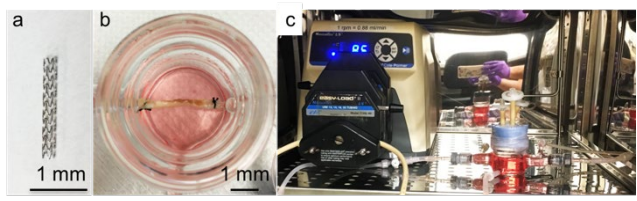


Fig.1: a. MgZnMn stent; b. Vessel with stent in the bioreactor; c. Bioreactor system.

**RESULTS:** The stented vessels had thicker vessel wall and higher viability after 7 days of culture in perfusion bioreactors than those in static culture (Fig. 2 c and d). TUNEL stain showed that  $\sim 97\%$  of the live cells in the stented- and perfused-cultured vessels, while 65% of the apoptosis cells in the

stented- and statically-cultured vessels (Fig. 3). The arrows indicate the luminal areas repressed by the stent (Fig. 2 c and d). Compared with the non-stented vessel in the perfusion bioreactor, the stent reduced intimal hyperplasia (Fig. 2 b and d).

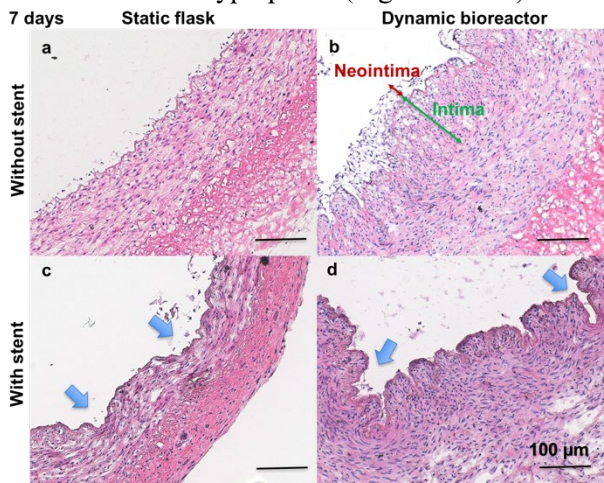


Fig. 2: H&E staining of the vessels with and without stent at the static flasks and dynamic bioreactors for 7 days. Blue arrows: stent struts.

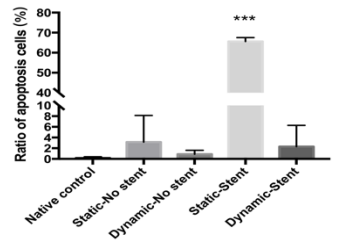


Fig.3: Ratio of apoptosis cells of the vessels with and without stent at the static flask and dynamic bioreactor by TUNEL staining for 7 days.

**DISCUSSION & CONCLUSIONS:** Ex vivo vessel culture system provides a mass transfer model for the study of cellular response to Mgbased stent including the cytotoxicity and intimal hyperplasia. It eliminates the high local pH and ions release form stents in conventional static approaches. This model is a closer simulation of the in vivo vessel environment to study absorbable stents.

**REFERENCES:** <sup>1</sup> ISO/TS 17137:2014(e), cardiovascular implants and extracorporeal systems — cardiovascular absorbable implants. **ACKNOWLEDGEMENTS:** American Heart Association Postdoctoral Fellowship (17POST33661238) and National Natural Science Foundation of China (31600766).

## In vitro degradation behaviour, drug release properties, and biocompatibility of iron oxide nanostructured arrays coated with polycaprolactone

JC Zhou<sup>1</sup>, YY Yang<sup>1</sup>, S Virtanen<sup>1</sup>

<sup>1</sup> <u>Institute for Surface Science and Corrosion</u>, Department of Materials Science and Engineering, University of Erlangen-Nuremberg, Erlangen, Germany

INTRODUCTION: Due to excellent mechanical properties and the relatively stable biodegradation process, iron-based materials have been considered as a promising candidate for the biodegradable implant material. To meet complex clinical demands, the surface functionalization for implants is necessary. The unique morphologies of nanostructures can act as a matrix for various functionalizations, and naturally, iron oxide nanostructured arrays are the ideal functionalization matrix for iron-based materials, since such arrays can be built directly on the iron substrate. In this work, two nanostructures, nanopore and nanotube, are developed, and polycaprolactone (PCL) is used to fabricate PCL coatings on the top surface of nanostructured arrays. PCL coatings not only improve the stability of iron oxide nanostructure arrays but also can function as a barrier for a drug release system. Moreover, in vitro biocompatibility of iron oxide nanostructures with/without PCL coatings is studied.

METHODS: The iron oxide nanopore and nanotube arrays were fabricated on pure iron foils by anodization in two fluoride-containing ethylene glycol (EG) electrolytes containing a different concentration of H<sub>2</sub>O and NH<sub>4</sub>F. Subsequently, PCL coatings were fabricated on the surface of the nanostructured arrays by spin-coating. Electrochemical and immersion tests were conducted to evaluate the corrosion resistance of samples, and morphology and composition of nanostructured arrays were characterised. Drug release behaviour was investigated with model drug tetracycline, and the biocompatibility of samples was investigated with human osteosarcoma cell line MG-63 MG-63 cells and adipose-derived stem cells (ADSCs).

**RESULTS:** By anodising in the two electrolytes, nanopore and nanotube arrays can be fabricated, and the thickness of arrays depends on the anodization time. Different surface morphologies could lead to diverse cellular responses. The morphology of the

PCL coatings is also affected by the surface morphologies of the underlying nanostructured arrays, and can moreover be modified by changing the PCL concentration in the spin coating solution and the rotation speed. In this work, discontinuous and continuous PCL coatings with different thickness were studied. Electrochemical impedance spectroscopy (EIS) and potentiodynamic polarisation tests show that the corrosion resistance of the iron substrate is not increased by nanostructured arrays, which is appreciated due to the fact that the degradation rate of iron-based materials is considered too low for the clinical application. For samples with PCL coatings, the corrosion resistance is only slightly increased compared to bare nanostructured arrays. After immersion, elements P and Ca can be found on surfaces of all samples, while the highest concentration is found in samples discontinuous PCL coatings. The bare iron oxide nanostructured arrays start to peel off after 15 days of immersion, while samples with PCL coatings show better stability. Due to the different morphologies and thickness of PCL coatings, the drug release behaviour can be adjusted. In general, thick continuous coatings can effectively delay the drug release rate. In an indirect assay, the extraction media from nanostructured arrays present no cytotoxicity compared to the control, which indicates that iron ions released from samples bring no adverse effect to MG-63 cells. In a direct assay, compared to bare nanostructured arrays, samples with PCL coatings present better osteogenic differentiation (more collagen type I produced) and less cytotoxicity to ADSCs (growth condition is better).

DISCUSSION & CONCLUSIONS: Iron oxide nanopore and nanotube arrays with PCL coatings are fabricated. The stability of nanostructured arrays can be improved by PCL coatings with a limited improvement of corrosion resistance. Different PCL coatings can cause various drug release behaviour and bring distinct influence on the biocompatibility of iron oxide nanostructured arrays.

### Cytotoxicity and hemocompatibility of magnesium alloys

N.D.H Munroe<sup>1</sup>

<sup>1</sup> Florida International University, Department of Mechanical and Materials Engineering, Miami, Florida, USA

INTRODUCTION: The usage of biodegradable alloys and coatings for the manufacture of stents obviate the need for repeat surgical procedures. Biodegradable magnesium alloys may possess elements that are essential in human metabolic and healing processes. Additionally, biocompatibility and corrosion rate are dependent on basic surface characteristics, such as elemental composition, nature and thickness of the oxide/polymer layer, surface morphology, surface charge and wettability that are modified by surface treatments. For example, a biodegradable co-polymer coating (poly glycolide-co-caprolactone (10:90)) is applied to delay the initial degradation rate of the alloy.

METHODS: The current research is focused on assessing corrosion rates, cytotoxicity and hemocompatibility of magnesium alloys that are subject to various surface treatments including acid etching, anodization and polymer coating with PGCL [1.2]. The magnesium alloys were manufactured in an ARC furnace by ACI Alloys, Inc. Ingots were cast in a water-cooled copper mold and heat treated at 350 °C and water quenched. Surface characteristics of acid etched and anodized samples such as surface morphology, roughness, wettability and surface chemistry were compared with those of mechanically polished samples.

A sulforhodamine B (SRB) assay (*In-vitro* Toxicology Assay Kit, Sulforhodamine B based-TOX6, Sigma-Aldrich, Saint Louis, MO) was conducted to assess cell viability in the presence of metal ions leached during corrosion.

Hemocompatibility was evaluated by passage of porcine blood (platelets) over alloys using a custom-built, multi-specimen, laminar flow chamber. The number of adhered platelets was counted using an image analysis software (Image J, NIH, Bethesda, MD). A statistical analysis was performed on platelet adhesion data using a one-way ANOVA analysis, followed by post-hoc testing (Tukey HSD). A significant difference between materials was interpreted to occur at p < 0.05.

**RESULTS:** A comparison between the average concentrations of dissolved metal ions (Mg, Ca and Zn) in PBS after corrosion tests with bare metal

MZC and surface treated MZC coated with PGCL are displayed in Fig.1.

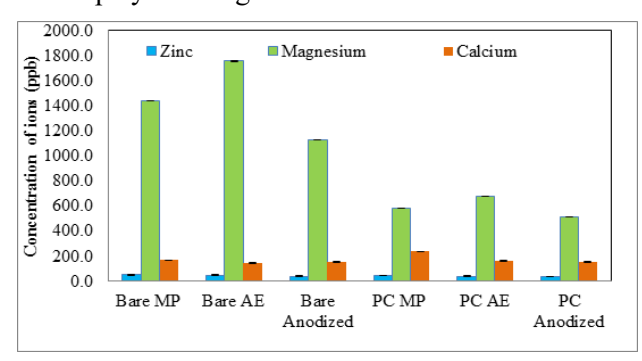


Fig. 1: Mg, Zn and Ca ions in PBS after corrosion.

These results indicated that acid etched MZC had the highest concentration ( $\sim$ 1758.1 ppb) of Mg<sup>2+</sup> ions as compared with that from mechanically polished ( $\sim$ 1442.9 ppb) and anodized ( $\sim$ 1129 ppb) MZC. The elevated Mg<sup>2+</sup> ion content was attributed to galvanic corrosion induced by the presence of secondary phases (Mg<sub>2</sub>Ca).

DISCUSSION & CONCLUSIONS: This research focused on investigating an optimal biodegradable stent material that initially has a slow degradation performance (to ensure total mechanical integrity) but degrade over time while the tissue has healed. The results indicates that anodization with biodegradable PGCL coating has great potential for cardiovascular stent applications with improved corrosion resistance, biocompatibility and mechanical integrity.

**REFERENCES:** <sup>1</sup> **S.** Amruthaluri (2014) *An Investigation on Biocompatibility of Bi-Absorbable Polymer-coated Magnesium alloys, PhD Thesis, Florida International University. <sup>2</sup> P. S. Gill (2012) <i>Assessment of biodegradable magnesium alloys for enhanced mechanical and biocompatibility properties*, PhD Thesis, Florida International University.

**ACKNOWLEDGEMENTS:** FIU DYF & DEA fellowships, Bezwada Biomedical, LLC, AMERI, FCAEM, ACI Alloys.

## Effect of Osmolality and Mg Ions on Viability, Proliferation and Migration of Human Gingival Fibroblast (HGF)

R Amberg<sup>1</sup>, A Elad<sup>2</sup>, F Witte<sup>1,2</sup>

<sup>1</sup> <u>Julius Wolff Institute</u>, Berlin-Brandenburg Center for Regenerative Therapies, Charité Universitätsmedizin, Berlin, <sup>2</sup> <u>Botiss GmbH</u>, Berlin

INTRODUCTION: Since more than a decade there is a high interest in magnesium as biodegradable metal implants due to their excellent biocompatibility, biodegradability and their low elastic moduli similar to natural bone [1]. During the degradation process the local Mg ion concentration, the osmolality and the local pH are enhanced [1]. Changes in pH are balanced by the buffer capacity of the tissue, but the effect of increased osmolality and Mg ion concentration on cells are not fully investigated.

#### **METHODS:**

A confluent monolayer of primary HGF, labelled with fluorescent dye CellTracker Red were scratched with a pipette tip to get a cell free area. After washing the cells various altered cell culture medium (CCM, reached by adding mannitol, magnesium chloride and sodium chloride respectively) were added. Wound closure were observed using an inverted microscope with a live cell imaging system over a period of 65 hours. To investigate the proliferation and viability of the HGF in altered CCM, cells were subjected to the BrdU- and MTT-assay. Effect of magnesium ions on cell adhesion were analyzed by treating the cells with 25mM and 75mM magnesium chloride for 24 h and staining vinculin, actin and nucleus.

#### **RESULTS:**

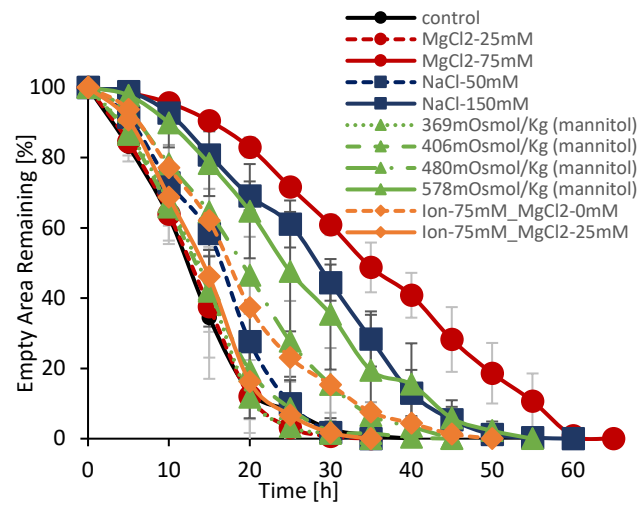


Fig.1: Wound closure of HGF over time, exposed to various altered CCM. Ion: same ionic strength and osmolality

(447mOsmol/Kg), adjusted with mannitol and NaCl. Control: unaltered CCM (n=4).

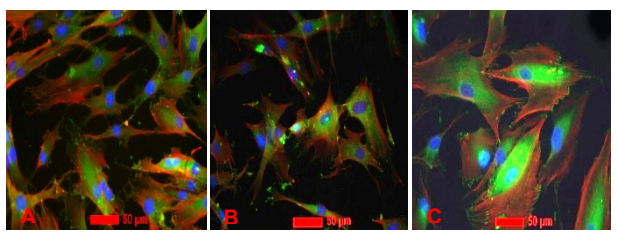


Fig. 1: HGF in 80% confluent 48well-plate, treated with CCM (A), containing additionally 25mM (B) and 75mM MgCl<sub>2</sub> (C) for 24 h and stained vinculin (green), actin (red) and nucleus (blue).

#### **DISCUSSION & CONCLUSIONS:**

MgCl<sub>2</sub> has no effect on cell migration & proliferation up to 25mM, but cell migration & proliferation is reduced at 75mM (Fig.1). The observed effect of MgCl2 is not dependent on the osmolality, nor its Cl<sup>-</sup> concentration, but rather on the Mg<sup>2+</sup> concentration. Similar osmolalities adjusted with NaCl and mannitol, respectively, show similar cell migration and proliferation behaviour, which confirms, that Cl aren't responsible for the effect of MgCl<sub>2</sub>. All tested ion solutions and osmolalities have no negative effect on cell viability. Cell proliferation was decreased to 15% at concentration of 75mM MgCl<sub>2</sub>, 150mM NaCl and 578 mOsmol/Kg (mannitol), compared to CCM (control). Media with same ionic strength show increased proliferation up to 145 %. At elevated Mg<sup>2+</sup> concentration (75mM MgCl<sub>2</sub>) more focal adhesion point can be found per cell (Fig.2) compared to CCM and 25mM MgCl<sub>2</sub>, which leads to reduced cell migration as reported by other authors [2]. Therefore, the initial corrosion rate of biodegradable magnesium implants needs to be controlled for optimal wound closure rates over corroding magnesium implants.

**REFERENCES:** 1 Y. F. Zheng et al (2014) *Mat Sci Eng R* 77:1-34 2 T. S. Lange et al (1995) *Clin Exp Dermatol* 4:130-137

**ACKNOWLEDGEMENTS:** This project was supported by AIF-ZIM (ZF4122205AK6) and BMBF SynGoMag

### Reduction of magnesium-induced biomineralization using matrix GLA protein

D Hong<sup>1</sup>, S Zaky<sup>2</sup>, R Chong<sup>2</sup>, K Verdelis<sup>2</sup>, F Witte<sup>3</sup>, C Sfeir<sup>1, 2</sup>

<sup>1</sup> <u>Department of Bioengineering</u>, University of Pittsburgh, Pittsburgh, PA. <sup>2</sup> <u>School of Dental Medicine</u>, University of Pittsburgh, Pittsburgh, PA. <sup>3</sup> <u>Julius Wolff Institute and Center for Musculoskeletal Surgery</u>, Charité - Universitätsmedizin Berlin, Germany.

INTRODUCTION: Magnesium (Mg) based stent has been approved for commercial use by the CE mark in 2016. However, as shown both in vivo and in vitro, Mg degrades spontaneously in biological environment, triggering the deposition biominerals on the metal, which could be harmful when implanting in soft tissue<sup>1, 2</sup>. Hence, the **goal** of this study is to locally inhibit the biomineralization induced by Mg degradation process, by coating matrix GLA protein (MGP) exterior of Mg metal implant. MGP is a small secretory protein that has shown to inhibit soft tissue calcification<sup>3</sup>. We hypothesize that less minerals would be deposited on Mg metals in the presence of MGP. This study also explored the relation between Mg degradation products and corrosion rate for the first time.

**METHODS:** Pure Mg rods of 1.6mm in diameter and 5mm in length were etched and polished. MGP plasmid was stably transfected into mammalian cells. Sterilized Mg rods were placed on inserts and suspended in medium culturing cells secreting MGP for 5 days. Samples were imaged and analysed by SEM and EDS for mineral deposition. MGP transfected cells were seeded into cylindrical collagen scaffolds, enclosing the Mg rod in the middle of the scaffold (group MGP). Three control groups were designed: Mg rod only (Mg only), Mg rod enclosed by collagen scaffold (gel), Mg rod enclosed by scaffold seeded with unmodified cells (293). Constructs were implanted intramuscularly on the left and right dorsal side of each mouse for four and six weeks. Explanted samples were embedded in PMMA for histology, microCT, and EDS analyses.

**RESULTS:** *In vitro* submersion test showed that significantly lower weight percent of calcium and phosphorous were deposited on the surface of Mg rods that were immersed in MGP secreting cells. Alizarin red (figure 1) and von Kossa staining revealed the least minerals from cross sections of Mg rods in MGP group from *in vivo* study. EDS scanning of Mg rods and surrounding tissues extracted from *in vivo* study verified results from *in vitro* test, showing the lowest weight percent of Ca

and P in MGP group, especially at the latter time point (figure 2).

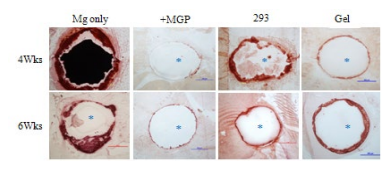


Fig. 1: Representative images of Alizarin red stain on cross sections of Mg rod from all groups.

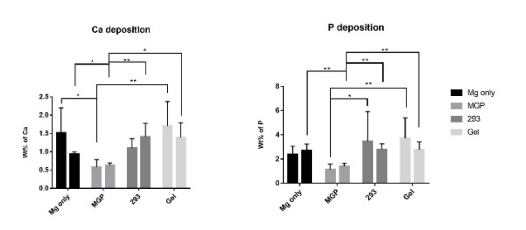


Fig.2: Cross sections of Mg rods from all groups were scanned with EDS to assess Ca & P weight percent at both time points.

MicroCT analysis demonstrated that the percentage of rod volume loss was the highest in MGP group at both time points, and the lowest at Mg only group.

both *in vitro* and *in vivo* tests confirmed that minerals triggered by degradation deposited on Mg metal surface were reduced by MGP. Although this study proved the concept for the efficacy of protein functioning on an exogenous implant, a better model for protein delivery will be developed to diminish the gap between the bench and bed side. Furthermore, since this is the first study to inhibit mineralization on Mg surface, we were able to exam its effect on metal corrosion rate. We could interpret the large volume loss in MGP group as that mineral layer serves as a protection layer to slow down the corrosion, as proposed in various reports.

**REFERENCES:** <sup>1</sup>E. Wittchow, J. Riedmuller, et al (2013) *EuroIntervention* **8**:1441-1450. <sup>2</sup>Y. Yu, J. Sun. (2018) *Acta Biomaterialia* In Press Available online. <sup>3</sup>L. Schurgers, C. Reutelingsperger. (2013) *Trends Mol Med* **19**: 217-26.

**ACKNOWLEDGEMENTS:** We would like to acknowledge NSF-ERC for funding this project. Gratefully thank Dr. Mike Epperly for gamma sterilizing the samples.

#### 3D cell culture to test novel implants

N Donohue<sup>1</sup>, B Lohberger<sup>1</sup>, N Gruen<sup>1</sup>, A Weinberg<sup>1</sup>

<sup>1</sup> <u>Medical University of Graz</u>, Department of Orthopedic Surgery, Austria.

INTRODUCTION: Biodegradable magnesium (Mg) is a promising alternative to steel or titanium implants in orthopaedic surgery. Mg gradually degrades in contact with body fluids, while supporting bone regeneration. However, novel Mg alloys require extensive testing to evaluate their biosafety and capabilities. In this work, 3-dimensional cell culture of human mesenchymal stem cells is used to establish an in vitro model of the interface between bone and Mg implant material. This model allows fundamental research to be conducted on implant safety and Mg-induced bone healing.

METHODS: Human mesenchymal stem cells (hMSCs) were isolated from femoral heads collected during hip operations, or surgically removed polydactyl fingers. Following expansion, differentiated osteoblasts, cells were into chondrocytes and adipocytes. Successful differentiation was visualized by histological staining, using Alizarin Red, Alcian Blue and Oil Red O dyes, respectively. Fluorescent Assisted Cell Sorting (FACS) was performed to evaluate cell surface markers according to the criteria established by<sup>1</sup>. 3D cell culture was performed using a gel matrix derived from human platelet lysate.

**RESULTS:** Six cell lines were fully characterized as hMSCs by differentiation (Fig. 1 and 2) and FACS, according to which the cell lines were positive for markers CD90, CD105 and CD73 as well as negative for CD14, CD45, CD34 and CD19. Substantial differences were observed between hMSCs isolated from young (<1 year) and old patients (>50 years), in terms of growth rate, differentiation and expression of osteogenic markers (Fig. 1 and 2).

DISCUSSION & CONCLUSIONS: 3D cell culture using adult and juvenile hMSCs is currently ongoing. Degradable Mg discs will be inserted into the 3D culture and the effects on cells will be determined by RNA and protein expression analysis. This work will focus on determining the molecular pathways that are responsible for the bone regeneration properties of Mg and in particular

how microRNAs affect major osteogenic regulators such as RUNX2 during this process.

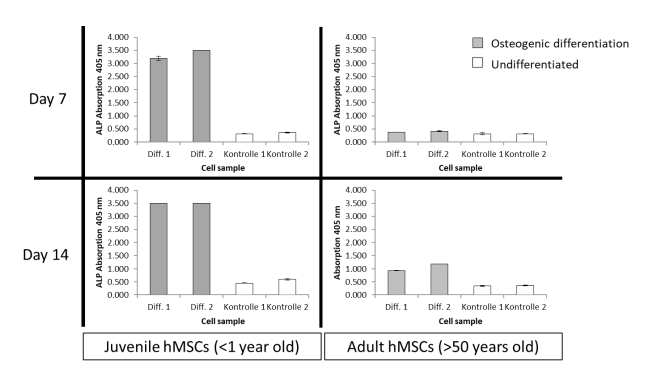


Fig. 1: Comparison of Alkaline Phosphatase expression between hMSCs isolated from adult and juvenile patients after 7 and 14 days of osteogenic differentiation.

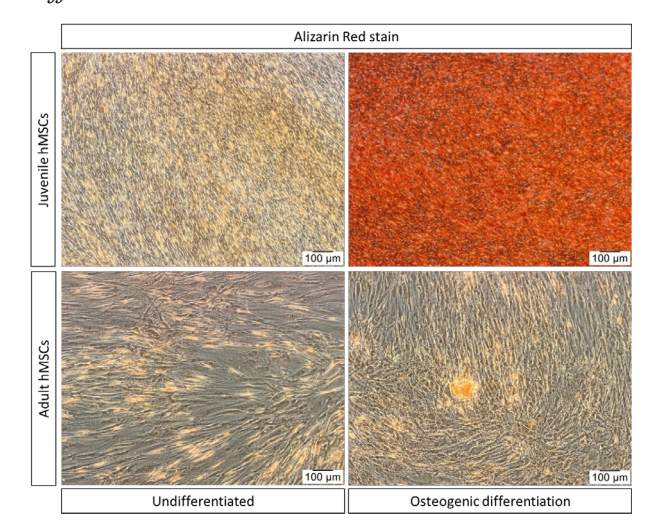


Fig. 2: Comparison of calcium deposits (stained red by Alizarin red dye) between hMSCs isolated from adult and juvenile patients after 21 days of osteogenic differentiation.

**REFERENCES:** <sup>1</sup> M. Dominici et al (2006). The *International Society for Cellular Therapy position statement. Cytotherapy.* **8**:315-317.

**ACKNOWLEDGEMENTS:** The authors wish to thank Heike Kaltenegger and Nicole Stuendl for technical support.

### Influence of fetal bovine serum on the initial degradation behavior of Zn and Zn alloys

P. Li<sup>1</sup>, C. Schille<sup>1</sup>, E. Schweizer<sup>1</sup>, F. Rupp<sup>1</sup>, A. Heiss<sup>2</sup>, C. Legner<sup>2</sup>, U.E. Klotz<sup>2</sup>, J. Geis-Gerstorfer<sup>1</sup>, L. Scheideler<sup>1</sup>

INTRODUCTION: Biodegradable Zn alloys are widely investigated as potential implant materials, mainly due to their moderate degradation rates. The degradation behavior depends on the specific physiological environment. Released metallic ions and corrosion products directly influence biocompatibility. The initial contact of orthopedic implants or vascular stents after implantation will be with blood [1]. In the present study, the influence of blood components on the initial degradation behavior of Zn and Zn alloys was investigated. Fetal bovine serum (FBS) was used as a model system.

**METHODS:** Pure Zn, Zn-4Ag and Zn-2Ag-1.8Au-0.2V (wt. %) alloy (Zn-Ag-Au-V) were melted, cast, cut, ground and sterilized. Five different solutions were used: FBS, Dulbecco's modified Eagle's medium (DMEM), DMEM + 10 % FBS, McCoy's 5A, McCoy's 5A + 15 % FBS. Samples with dimensions of  $30 \times 10 \times 0.5$  mm were immersed under cell culture condition (37 °C, 5 % CO<sub>2</sub>, 20 % O<sub>2</sub>, 95 % RH) for 24 h. According to ISO 10993-12, a surface/vol. ratio of 3 cm²/ml was used. ICP-OES was employed to detect released metallic ions in the solution, and pH value changes were measured. The corrosion rates were calculated. Corrosion products on the surfaces were observed by SEM-EDX.

#### **RESULTS:**

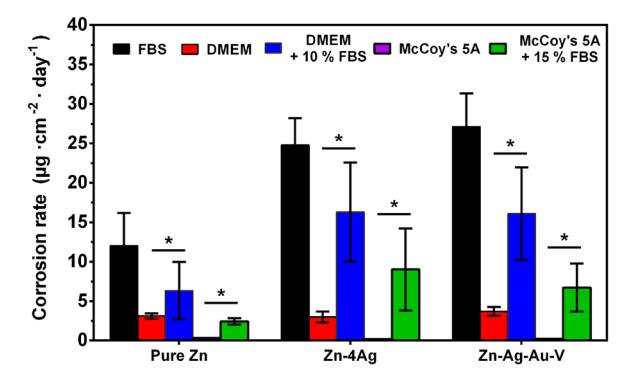


Fig. 1: Corrosion rate estimation of Zn and Zn alloys calculated from released Zn ion.

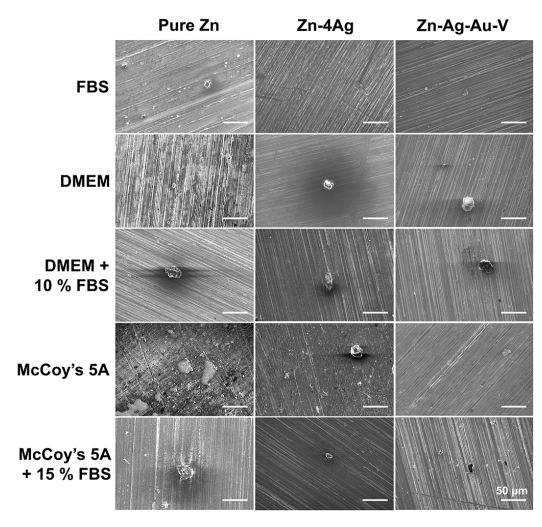


Fig. 2: SEM images of corrosion products on the surfaces after immersion (magnification 1000×).

As shown in Fig.1, the highest corrosion rates of Zn and Zn alloys were obtained in FBS, followed by DMEM + 10 % FBS, McCoy's 5A + 15 % FBS, DMEM and McCoy's 5A in that order. The corrosion rates in DMEM and McCoy's 5A were increased by supplementation with FBS. Also, the corrosion products on the surfaces after immersion in different media were detected by SEM (Fig.2). Only a small number of particles was detected on the surfaces at high magnification. The EDX analysis showed that most particles on the surfaces were mainly composed of Zn, P, O and C.

**DISCUSSION & CONCLUSIONS:** The initial degradation rate of Zn alloys after implantation might be accelerated by contact with serum. Besides tests with salt solutions, as used in standard corrosion tests, the influence of serum on the corrosion mechanism of Zn alloys should be further investigated.

**REFERENCES:** <sup>1</sup>L. Scheideler et al. (2013), Acta Biomater. **9**:8740-8745.

<sup>&</sup>lt;sup>1</sup> <u>Section Medical Materials Science and Technology</u>, University Hospital Tübingen, Germany.

<sup>2</sup> <u>Research Institute for Precious Metals and Metals Chemistry (fem)</u>, Germany

### Magnesium ions activates canonical Wnt signaling to induce osteogenesis in hBMSCs

C Hung<sup>1</sup>, K Liu<sup>1</sup>, C Sfeir<sup>1, 2</sup>

<sup>1</sup> <u>Department of Bioengineering, University of Pittsburgh</u>, Pittsburgh, PA, USA. <sup>2</sup> <u>School of Dental</u> <u>Medicine</u>, University of Pittsburgh, Pittsburgh, PA, USA.

**INTRODUCTION:** Magnesium (Mg) and its alloys have been widely explored to be used in the field of medical devices. Several studies reported new bone formation or osteoblastic response around the Mg implants<sup>1,2</sup>. However, the underlying intracellular mechanism of how the Mg<sup>2+</sup> induces osteogenic effects is still unclear. Previously, our group reported a RT-PCR gene screening using human bone marrow stromal cells (hBMSCs) with or without Mg<sup>2+</sup> treatment<sup>3</sup>. In the present study, we focused on analyzing the canonical Wnt signaling which is one of the pathways that were predicted to be activated by the results of the gene screening. Canonical Wnt signaling is known to regulate multiple mechanisms including bone regeneration. Hence, we hypothesize that Mg<sup>2+</sup> will activate canonical Wnt signaling and further induce osteogenesis.

METHODS: The data of osteogenic genes from qPCR arrays that we previously reported were further analyzed using Ingenuity Pathway Analysis (IPA;Qiagen). The upstream analysis indicated that the canonical Wnt signaling was involved in activation of osteogenic genes. hBMSCs were cultured in 6-well plates at an initial density of  $3x10^5$  cells per well with  $\alpha$ -MEM and 5% FBS. Cells were treated with or without adding extra MgSO<sub>4</sub> to the medium at a concentration of 10 mM of Mg<sup>2+</sup> as we previously found this concentration was able to trigger the osteogenic effects. Protein lysates and total RNA were extracted from cells for further experiments. Western blotting was used to detect the difference of protein expressions and qPCR was used to detect the difference of gene expressions. To demonstrate the activation of canonical Wnt signaling under Mg<sup>2+</sup> stimulation, we first investigated the accumulation of active βcatenin in cytoplasm.

**RESULTS:** Western blot analysis showed that the active  $\beta$ -catenin expression was significantly increased in the Mg<sup>2+</sup> group compared to the control. The Wnt3a group (positive control) showed a similar level of expression to the Mg<sup>2+</sup> group (Figure 1, left).  $\beta$ -actin demonstrated equal loading on each band. Quantitative data demonstrated

statistical significance between the Mg<sup>2+</sup> group and control as well as the Wnt3a group and control (Figure 1, right). Two of the direct downstream target genes of canonical Wnt signaling, LEF1 and Dkk1, both increased in fold change in the Mg<sup>2+</sup> group (data not shown). The summarized diagram of how Mg<sup>2+</sup> activates canonical Wnt signaling is shown in figure 2.

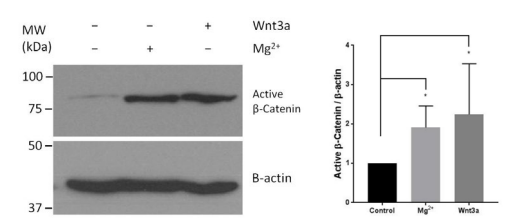


Fig. 1: Western blotting and quantification results of active  $\beta$ -catenin (M.W. 92kDa). n=5. \*p<0.05.



Fig. 2: Schematic of predicted activation of canonical Wnt signaling by stimulation of hBMSCs with  $Mg^{2+}$ .

**DISCUSSION & CONCLUSIONS:** The data in this study suggest that canonical Wnt/β-catenin signaling was activated by the stimulation of  $Mg^{2^+}$ . R Baron et al. suggested in a Nature medicine paper that positive modulation of canonical Wnt signaling was able to induce osteogenic effects, including, but not restricted to, bone regeneration and bone healing<sup>4</sup>. Taken together, these findings suggest that the activation of canonical Wnt signaling was involved in Mg-induced osteogenesis.

**REFERENCES:** <sup>1</sup>F. Witte et al. (2005) Biomaterials **26**:3557-3563, <sup>2</sup>A. Chaya et al. (2015) *Acta biomaterialia* **18**:262-269, <sup>3</sup>S. Yoshizawa et al. (2014) *Acta biomaterialia* **10**:2834-2842, <sup>4</sup> R. Baron et al. (2013) *Nature medicine* **19**:179.

**ACKNOWLEDGEMENTS:** This study is supported by NSF Revolutionizing Metallic Biomaterials Engineering Research Center under grant number 0812348.

#### Influence of glioblastoma cell lines on magnesium degradation

R Unbehau<sup>1, 2</sup>, BJC Luthringer-Feyerabend<sup>2</sup>, R Willumeit-Römer<sup>1, 2</sup>

<sup>1</sup> <u>Institute for Material Science</u>, Christian-Albrechts-Universität zu Kiel, Kiel, Germany. <sup>2</sup> <u>Institute</u> of <u>Materials Research</u>, Helmholtz-Zentrum Geesthacht, Geesthacht, Germany

INTRODUCTION: The treatment of severe brain related diseases, such as *glioblastoma multiforme* (GBM), requires innovative local therapeutic approaches. Magnesium-based neuro implants hold potential for local treatment, as they facilitate long-term, controlled drug and ion release due to their biodegradability. The present study characterizes cell-material interactions, focussing on the influence of GBM cell lines on magnesium (Mg) degradation.

METHODS: Cell influence on Mg degradation was analysed by semi static immersion test. Mg discs were ground, cleaned and sterilised. Preincubation was performed in DMEM + 10 % fetal bovine serum (FBS) for 24 h under cell culture conditions. Subsequently, two different human GBM cell lines (A172, LN229) and human astrocytes were seeded on the Mg discs. Mg discs immersed in DMEM + 10% FBS without cells were used as control. Immersion test was conducted for 6 days after pre-incubation. Removal of the degradation layer was carried out using chromic acid treatment. Supernatant analysis by osmolality and pH measurement at day 1, 3 and 6 was performed additionally. Atomic adsorption spectroscopy (AAS) was conducted to quantify the Mg content in the supernatant. Cell viability was determined by Live/Dead staining after 6 days.

**RESULTS:** The mean degradation depth (MDD) h values displayed in *Figure 1* were calculated as following:

$$h = \Delta m/A\rho \tag{1}$$

with  $\Delta m$  representing the mass loss, A representing the surface area and  $\rho$  representing the density of pure Mg.

Mg discs cultured with GBM cell lines, especially LN229, exhibited increased degradation, whereas discs cultured with astrocytes showed no significant difference in degradation compared to Mg immersed with no cells (material control). AAS measurement results coincide with these findings. Osmolality and pH values were slightly decreased

for discs seeded with cells compared to the material controls.

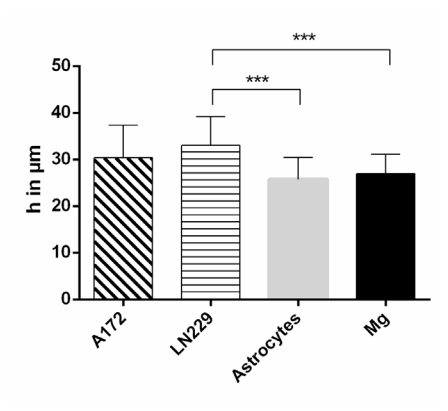


Fig. 1: MDD ( $\mu$ m) for Mg discs seeded with GBM cell lines, astrocytes and no cells after 6 days of immersion (\*\*\* significance level p<0.001).

Live/Dead staining revealed predominantly viable cells on Mg for all cell types. However, the cell density was visibly reduced compared to cell controls and morphological alterations occurred especially for A172 GBM cells and astrocytes.

**DISCUSSION & CONCLUSIONS:** GBM cells were shown to increase Mg degradation, whereas healthy cells slightly reduced degradation. The results suggest, that GBM cells influence Mg degradation through active degradation mechanisms. Cancer cells are known to excessively excrete lactate due to their altered cellular respiration<sup>1</sup>. Further, the expression of some matrix metalloproteinases (MMPs) was found to be upregulated in GBM cells<sup>2</sup>. The combination of locally lowered pH values, due to elevated lactate levels, and altered degradation layers, due to the digestion of extracellular matrix (ECM) compounds by MMPs, might lead to increased degradation. To verify this, lactate and MMP content analysis in the supernatant, as well as ECM analysis is essential.

**REFERENCES:** <sup>1</sup> S.K.N. Marie, S.M.O. Shinjo (2011) *Clinics* **66(S1)**:33-43. <sup>2</sup> G. Musumeci et al. (2015) *Cell Tissue Res* **362**:45–60.

**ACKNOWLEDGEMENTS:** This work was funded by the German Research Foundation (DFG) as part as of the Research Training Group "Materials4Brain" (GRK2154; P1b).

#### Fe-based bioresorbable alloy inhibits platelet activation

C Verhaegen, S Lepropre<sup>1</sup>, M Octave<sup>1</sup>, S Kautbally<sup>1</sup>, A Thomas<sup>1</sup>, S Reuter<sup>1</sup>, E Scarcello<sup>1</sup>, D Lison<sup>1</sup>, L Bertrand<sup>1</sup>, L Delannay<sup>1</sup>, P Jacques<sup>1</sup>, C Beauloye<sup>1</sup>, S Horman<sup>1</sup>, J Kefer<sup>1</sup>

<sup>1</sup>Université catholique de Louvain, Bruxelles, Belgique

INTRODUCTION: Bioresorbable polymer stents have been used to provide a transient scaffold after coronary angioplasty. However, an increase in stent thrombosis has been observed [l]. A current challenge is thus to develop new bioresorbable stents combining optimised mechanical and biodegradation properties together with limited thrombogenicity. In this context Fe-based alloys are amongst the good candidates for stent manufacture. In this work blood compatibility of a new Fe-based alloy was studied *in vitro* via assessment of haemolysis and platelet activation.

**METHODS:** Human whole blood was incubated for 60 minutes with either the Fe-based alloy or the cobalt-chromium (Co-Cr) alloy composing the bare metal stent used as a reference. After centrifugation optical density (OD) of the supernatant was measured at 540 nm and haemolysis was calculated as followed:

$$Haemolysis = (OD_{test} - OD_{negative control})/$$
  
 $(OD_{positive control} - OD_{negative control} \square x \square \square \square \%$ 

A value lower than 5% represents a judging criterion for excellent blood compatibility [2].

For platelet activation assays, human or rat washed platelets were incubated for 60 minutes with both alloys before measuring their reactivity to a platelet agonist by flow cytometry, using CD62P and activated  $\alpha 2b\beta 3$  antibodies. In addition, phosphorylation of PKC substrates was evaluated by western blot.

**RESULTS:** No significant red cells haemolysis was induced by both alloys (0,5 and 0,3 % respectively). In addition, Co-Cr alloy did not affect CD62P exposure and  $\alpha$ 2b $\beta$ 3 activation at platelet surface upon thrombin (0,03 to 0,3 U/ml) stimulation. In contrast, Fe-based alloy completely abolished their response to the agonist (Fig.1). A drastic inhibition of the phosphorylation state of

PKC substrates was also observed after activation with thrombin (0,03 to 0,3 U/ml). Since similar inhibitory effects were obtained when using a conditioned-reaction medium previously incubated with this Fe-based alloy, we postulate that its biocorrosion might release components counteracting platelet activation.

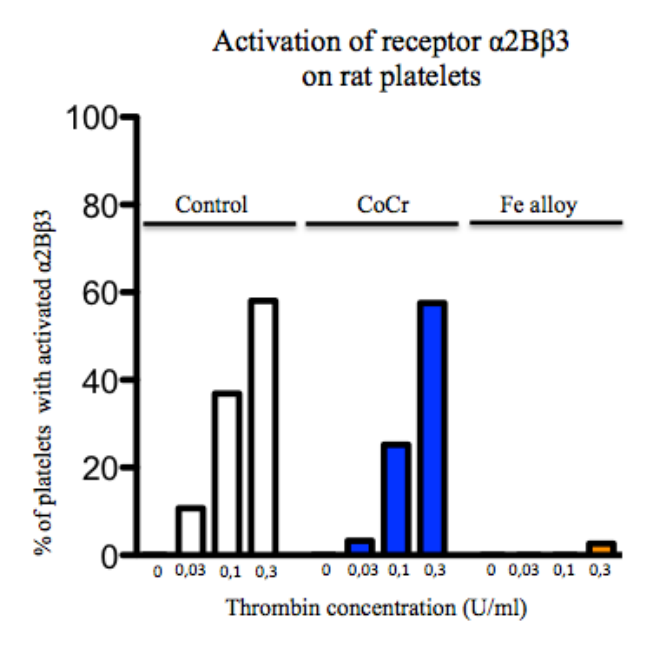


Fig. 1: Rat platelet activation quantified by activation of receptor  $\alpha 2b\beta 3$  following thrombin stimulation. Fe-based alloy inhibits platelet activation.

**DISCUSSION & CONCLUSIONS:** The Fe-based resorbable scaffold doesn't induce haemolysis and displays anti-thrombogenic properties. Because stent implantation is currently still associated with thrombosis our stent is a promising platform for next-generation stent technologies.

**REFERENCES:** <sup>1</sup>Cassesse *et al.* (2016). *The Lancet* **387**:537-544. <sup>2</sup> Cheng et al. (2013). *J. Mater. Sci. Technol.* **29**:619-627.

# The long term degradation and transport mechanism of a Mg-Nd-Zn-Zr stent in rabbit common carotid artery

Jian Zhang<sup>1</sup>, Jia Pei<sup>1</sup>, Guangyin Yuan<sup>1</sup>

<sup>1</sup> Shanghai Jiao Tong University, Shanghai, China</sup>

**INTRODUCTION:** Despite the success of the Mg alloy based stents in clinical trials, some important and fundamental questions still remain unanswered, e.g. whether the degradation products (usually composed of O/P/Ca/Mg) could be further safely degraded, whether the alloying elements would accumulate in the organs etc. In this study, a 20 month research was carried out after the bare Mg-2.1Nd-0.2Zn-0.5Zr (wt.%, abbr. JDBM) stent prototype was implanted into the common carotid artery of the New Zealand white rabbit in order to evaluate its safety, efficacy and especially the long term degradation behavior. In vitro time lapse observation of the macrophage (RAW 264.7) phagocytosis of JDBM degradation product particles were also conducted.

**METHODS:** The JDBM vascular stent prototype used was 3 mm in diameter, 16 mm in length, with a stent strut thickness of 150  $\mu$ m. The stent was delivered to the common carotid artery (CCA) of the New Zealand white rabbits via minimally invasive surgery from femoral artery. Then the degradation morphology and the element composition of the degradation products were studied by micro CT and SEM/EDS, respectively. The alloying element concentration of the main organs were analyzed by ICP-OES and ICP-MS.

**RESULTS:** Results showed that the bare JDBM stent had good safety and efficacy with a complete re-endothelialization within 28 days. The JDBM stent struts were mostly replaced in situ by degradation products in 4 month. The important finding was that the volume and Ca concentration of the degradation products decreased in the long term (Fig. 1), eliminating the clinicians' concern of possible vessel calcification. In addition, all the alloving elements showed no continuous enrichment in the main organs of the rabbits. [1]. In macrophage phagocytosis of vitro JDBM degradation product particles were directly observed, which could be the possible further degradation pathway [2].

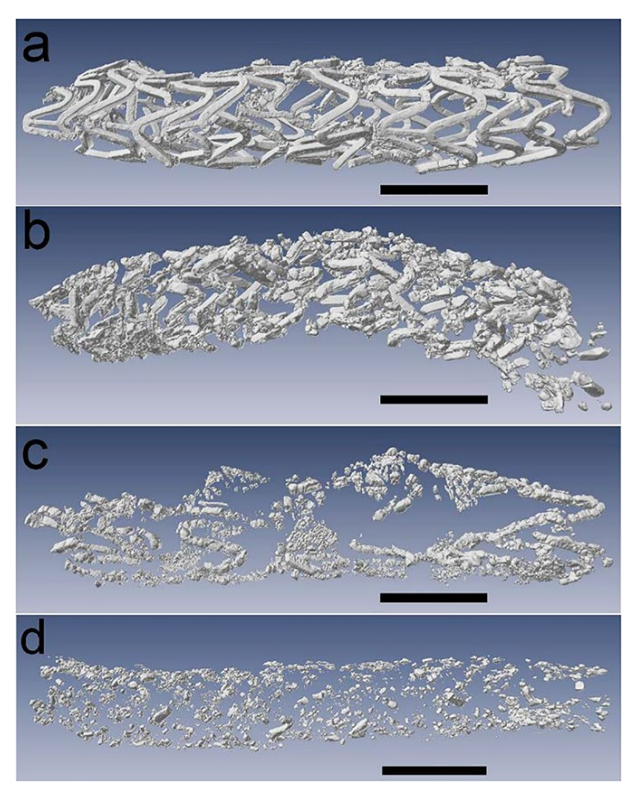


Fig. 1: Micro CT result of the JDBM stent after (a) 1, (b) 4, (c) 12 and (d) 20 month implantation. Scale bar = 2 mm.

**DISCUSSION & CONCLUSIONS:** The long term *in vivo* results showed the rapid reendothelialization of the JDBM stent and the long term safety of the degradation products, indicating its great potential as the backbone of the fully degradable vascular stent.

**REFERENCES:** <sup>1</sup> J Zhang, HY Li, W Wang et al (2018) *Acta Biomater* **69**:372-84. <sup>2</sup> J Zhang, S Hiromoto, T Yamazaki et al (2017) *Mat Sci Eng C-Mater* **75**:1178-83.

ACKNOWLEDGEMENTS: This work was supported by Natural Science Foundation of China (No. 31771024) and the National Key Research and Development Program of China (No. 2016YFC1102400).

#### Testing magnesium metal alloys for use as pediatric bone nails

K Little<sup>1,2</sup>, S Pixley<sup>3</sup>, D Glos<sup>1</sup>, V Shanov<sup>4</sup>, Z Xu<sup>5</sup>

<sup>1</sup><u>Department of Orthopaedics,</u> Cincinnati Children's Hospital Medical Center, Cincinnati, OH.

<sup>2</sup><u>Department of Orthopaedic Surgery</u> University of Cincinnati, OH. <sup>3</sup><u>Department of Pharmacology</u> & Systems Physiology, University of Cincinnati, OH. <sup>4</sup><u>Department of Chemical and Environmental Engineering,</u> University of Cincinnati, OH. <sup>5</sup><u>Department of Mechanical Engineering,</u> NC A&T State University, Greensboro, NC.

INTRODUCTION: Magnesium (Mg) metal has shown significant promise for medical implants in bone and Mg bone screws are currently being implanted in Europe<sup>1</sup>. Biodegradable Mg implants are especially of interest in pediatric applications. We proposed that Mg alloys would have sufficient strength and ductility for use as intramedullary bone nails (IMNs), particularly in upper extremity pediatric applications. Towards this goal, we investigated whether the mechanical properties of Mg alloy IMNs may suffice to withstand the loads due to surgical insertion and subsequent in vivo loading. The required stiffness for upper limb applications in pediatric populations, versus lower limb applications, was estimated at 25-50% that of titanium nails of the same diameter. This is based on the fact that the strength of current IMNs are greater than needed for upper arm pediatric applications.

METHODS: Cadaveric porcine femurs (obtained from other IACUC-approved studies that did not involve the limbs) were used as the model because they best simulated the size and biomechanical properties of pediatric forearms. Tests were performed before and after creating, then treating, a mid-shaft fracture with paired IMNs. The nails were inserted by a board-certified pediatric surgeon using clinically relevant procedures. For preliminary testing, Mg nails were obtained from commercial sources (Goodfellow, Inc.) and compared to titanium and stainless steel (SS) IMNs. Data are now being generated using nails of single crystal Mg and proprietary Mg alloys. Four-point bending tests were performed to apply a constant moment across the fracture site, as adapted from the standard for IMNs (ASTM F1264). Reduced spacing between supports was used to accommodate the shorter specimen length compared to adult femurs. Quasi-static loading of 10 cycles was applied, the 8th cycle was used to calculate construct stiffness, the slope of the loading curve.

**RESULTS:** No difficulties were encountered inserting Mg rods through pre-drilled holes into porcine femurs, across a break. The load-unload curves are shown in Fig. 1A, for an intact femur and femurs with two titanium or SS IMNs and, in this

initial study, IMNs of the Mg alloys AZ31 and AZ61 (all of diameter, 3.5mm). The stiffness of the Mg IMNs was 15% of intact, or 33% of titanium rods (Fig. 1B). A radiograph of a bone with the

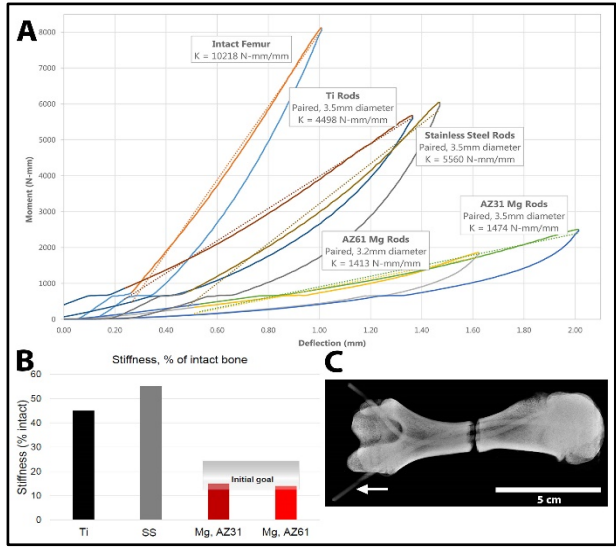


Fig. 3. A) Bending moment-deflection curves for 5 types of IMNs after fixing fractures with paired IMNs. B) Stiffness calculated from the curves. C) Radiograph of porcine femur with Mg IMNs. inserted IMNs is shown in Fig. 1C.

**DISCUSSION & CONCLUSIONS:** Certain Mg alloy IMNs have potential for clinical applications based on their stiffness, although further testing is needed. Our established test protocols and standards are being applied to study IMNs made of proprietary Mg alloys, including highly ductile single crystal Mg.

**REFERENCES:** <sup>1</sup> D. Zhao et al (2017) *Biomaterials* 112:287-302.

**ACKNOWLEDGEMENTS:** D Bylski-Austrow, PhD, J Avant, NSF ERC for Revolutionizing Biomaterials, EEC-EEC-0812348 and Centre to Centre Supplement, UC CEAS Research Internship Program.

### Biodegradable PLA/Mg films for tissues regeneration

A.Ferrandez-Montero<sup>1,2</sup>, M.Lieblich<sup>1</sup>, J.L.Gonzalez-Carrasco<sup>1,3</sup>, R. Detsch<sup>4</sup>, A.R. Boccaccini<sup>4</sup>, B.Ferrari<sup>2</sup>

<sup>1</sup> <u>CENIM-CSIC</u>, Spain, <sup>2</sup> <u>ICV-CSIC</u>, Spain <sup>3</sup> <u>CIBER-BBN</u>, Spain <sup>4</sup> <u>Institute of Biomaterials</u>, <u>University of Erlangen-Nuremberg</u>, Erlangen, Germany

**INTRODUCTION:** PLA/Mg composites have been proposed as new biodegradable and fully bioabsorbable materials that show good mechanical properties, cell development and in vitro degradation properties [1-5]. This work studies PLA films with Mg content as high as 50wt.% obtained by colloidal processing routes. To produce PLA anchorage, a metal surface modification was carried, without compromising the biodegradation and biocompatibility. The Mg protection was evaluated by zeta potential, Fourier-transform infrared spectroscopy (FTIR) and nanoindentation, and the biological response by in vitro immersion test and cell viability.

**METHODS:** The colloidal suspension of Mg particles in aqueous solution was achieved by adding polyethylenimine (PEI) or cetyltrimethylammonium bromide (CTAB) as stabilizers and a proper optimization of the pH. Stabilizers adsorption was evaluated by zetapotential experiments. The Mg suspension was mixed with the PLA solution. This mixed solution was shaped by tape casting to obtain PLA/Mg films. In vitro immersion test was carried out in PBS to monitor  $H_2$  and  $Mg^{2+}$  ions release. Mouse embryo fibroblast cells (MEF) were used to examine the cytocompatibility of films.

**RESULTS:** Zeta potential curves vs dispersant content % showed evidence of CTAB/PEI adsorption on Mg surface. Specific changes between FTIR spectra of neat PLA and composites indicate a PLA interaction with the stabilizer.

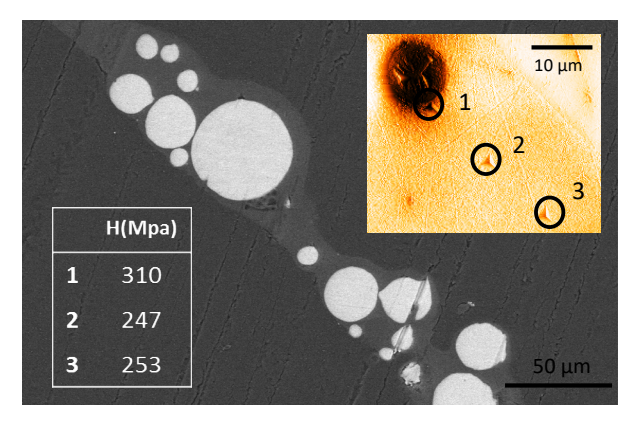


Fig. 1: Cross section of 50%Mg film, footprints of the nanoindentation test and hardness.

The PLA nanoindentation hardness test shows differences between areas far and near Mg particles.

During immersion test, H<sub>2</sub> release depends on stabilizer type, being lower for PEI than CTAB, indicating a better protection of the former. Finally, cytocompatibility tests evidenced cell proliferation on films (Fig. 2).

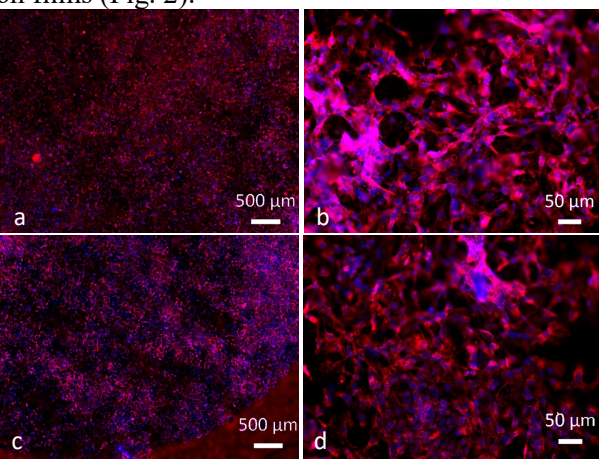


Fig. 2: MEF cells (blue = nucleus, red = cytoskeleton) grown on (a,b) 30%Mg-PEI film and (c,d) 30%Mg.CTAB film surface.

**DISCUSSION & CONCLUSIONS:** PLA/Mg films exhibit good properties due to metal surface modification with two different stabilizers. The high magnesium reactivity has been controlled obtaining materials with a biological response that confirms their potential for biomedical application.

**REFERENCES:** <sup>1</sup>SC Cifuentes et al (2012) *Mater Lett* **74**:239-42. <sup>2</sup>SC Cifuentes et al (2016) *J Mech Beh Biomed* Mater **65**:781-90. <sup>3</sup>SC Cifuentes et al (2016) *J Biomed Mater Res A* **104**:866–78. <sup>4</sup>MC Fernández-Calderón et al. (2017) *Biomed Mater* **12**: 015025. <sup>5</sup>SC Cifuentes et al (2016) *Acta Biomater* **32**:348–57.

ACKNOWLEDGEMENTS: MAT2015-63974-C4-1,MAT2016-79869-C2-1-P, POLYMAGIC: PCIN-2017-036 (MINECO, Spain), MULTIMAT Challenge: S2013/MIT-2862 (CM, Spain).

#### Effect of biodegradable magnesium on the immune response in vitro

Qian Wang<sup>1</sup>, Regine Willumeit-Römer<sup>1</sup>, Bérengère Luthringer<sup>1</sup>

<sup>1</sup><u>Helmholtz-Zentrum Geesthacht Centre for Materials and Coastal Research Institute of Materials Research</u>, Division of Metallic Biomaterials, Max-Planck-Street 1, 21502 Geesthacht, Germany

INTRODUCTION: Human mesenchymal stem cells (MSC) have been shown to interact with immune cells and possess broad immunoregulatory properties. One of the mechanisms through which MSC modulate immune response is by the monocytes polarization. Biomaterials have been indicated to affect such interactions during fracture healing [1]. Besides, Human umbilical cord perivascular cells (HUCPV) has been reported as a prolific source of MSC. We hypothesised that the cross-talk between HUCPV and the immune system (human peripheral blood mononuclear cells -PBMC) may be specifically influenced by biodegradable magnesium (Mg) during fracture repair. In order to elucidate the mechanisms, we developed and applied two in vitro systems: (i) a conditioned medium system (CM) to study effect of HUCPV or/and Mg on PBMC and (ii) a more elaborated transwell coculture system (TW) which further allow to evaluate the HUCPV / PBMC crosstalk.

**METHODS:** HUCPV were isolated from human umbilical cords, and PBMC were obtained by density gradients. For CM, conditioned media were obtained after 1 day of HUCPV alone or cultured on preincubated Mg-discs and Mg-discs alone. PBMC were then cultured for 1, 4, and 7 days with these different conditioned media. In TW, HUCPV and PBMC cells were seeded on preincubated Mg disc in the plate wells and in upper chambers of transwell, respectively. The viability proliferation were monitored by live/dead staining (Invitrogen - Fisher Scientific GmbH, Schwerte, Germany) and DNA content. PBMC cells were sorted by CD68 and CD163 (Human, Miltenyi Biotec GmbH, Bergisch Gladbach, Germany) using flow cytometry. Proportion of M2-macrophage within the monocyte population was calculated as followed: (CD68+ CD163+) / CD68+ cells (%) [2].

**RESULTS:** Live/dead staining and DNA content of PBMC in CM as well as HUCPV and PBMC in TW revealed that Mg disc have no significant effect on the viability, except for HUCPV at day 7 in TW,

where less cells were found. Flow cytometry (Fig. 1) revealed that, in CM, M2/CD68<sup>+</sup> cells population increased in presence of Mg and HUCPV+Mg, after 4 and 7 days, respectively. Similar results obtained from TW experiments: M2/CD68<sup>+</sup> cells population increased from day 4 on, in the HUCPV+PBMC+Mg treatment.

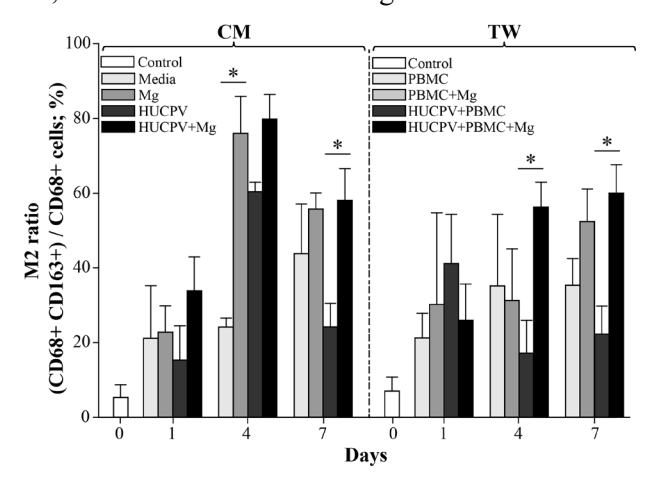


Fig. 1: M2 ratio in the CM and TW systems. Bars represent the mean $\pm$ SD of three independent experiments (3 donors), each with n=6. Stars indicate significant differences between treatments with and without Mg (ANOVA on Ranks; \*  $p \le 0.05$ ).

**DISCUSSION & CONCLUSIONS:** CM and TW systems are 2 methods to mimic the immune response after biodegradable Mg implantation. With these system, direct effect of Mg on PBMC could be measured. Furthermore, in general, a synergistic effect of HUCPV and Mg could be observed, which is associated with monocytes polarization, accompanying with a higher appearance of M2- macrophages.

Specific gene expressions and cytokines production of HUCPV and PBMC cells in the immune response to Mg disc will be further studied to clarify the underlying mechanisms.

**REFERENCES:** <sup>1</sup> J. Kim, et al (2009) *Cell.* **137**:459-71 <sup>2</sup> D. YS Vogel, et al (2013) **10**: 35.

## Silk coating on fluoride-treated MgZnYNd alloy: Improved corrosion resistance, hemocompatibility and biocompatibility

P Wang<sup>1</sup>, TF Xi<sup>1</sup>

<sup>1</sup>Academy for Advanced Interdisciplinary Studies, Peking University, Beijing, China

**INTRODUCTION:** Magnesium alloys have been intensively investigated as potential absorbable coronary stent materials. However, the over-rapid corrosion rate of magnesium alloys, thrombosis formation and delayed endothelium after operation are the main challenges hindering their applications. In this study, silk coating were immobilized on hydrofluoric acid (HF) treated MgZnYNd alloy surface via dopamine layer to improve corrosion resistance, hemocompatibility and biocompatibility.

**METHODS:** The MgZnYNd samples were immersed in HF solution and then the silk coating were immobilized on sample surface by spin coating. The in vitro corrosion behavior were assessed by standard electrochemical measurements along with the long-term immersion. Hemolysis rate was executed to evaluate the hemocompatibility. Human umbilical vein endothelial cells were used for the in vitro biocompatibility measurements.

**RESULTS:** The SEM results confirmed the uniform film was coated on the substrate successfully. (Fig.1a) The electrochemistry tests showed the coating improve the corrosion resistance significantly.(Fig.1c-d)Hemolysis rate test exhibited the excellent hemocompatibility for the coating. (Fig.1b) Cells direct culture experiment showed the excellent biocompatibility of the coating.(Fig.2)

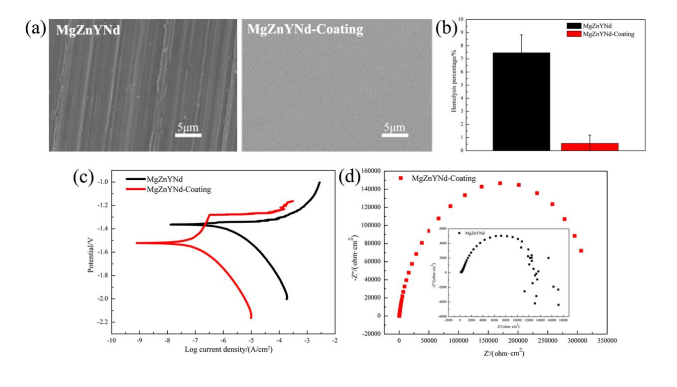


Fig. 1: (a) Surface morphologies of bare MgZnYNd alloy and modified sample; (b) Hemolysis rate (c) potentiodynamic polarization curves; (d) Nyquist plots

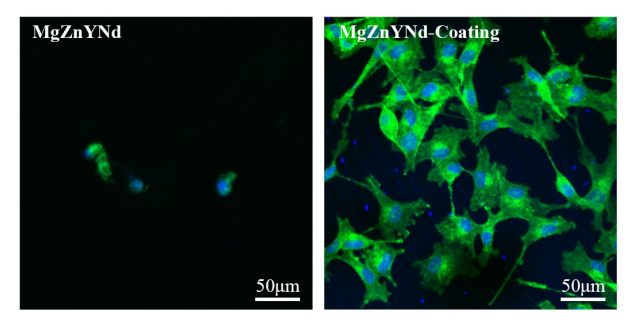


Fig.2: Actin-nucleus costained HUVECs imaged by a confocal microscope 24 h post seeding (nucleus was dyed blue, while actin was dyed green)

**DISCUSSION & CONCLUSIONS:** The larger capacitive loops as well as the higher Zre value, and lower  $I_{corr}$  values, indicating the effectiveness and solidness of the  $MgF_2$  layer and silk coating in improving the corrosion resistance of magnesium alloys. Moreover,the cells were fully stretched out with intense actin filaments stretching into various orientations, and the cells showed reorganization of the cytoskeleton equipped with strong actin fibers indicating the favorable biocompatibility of the surface coating.

With this multifunctional coating, we significantly improved in vitro anticorrosion ability, hemocompatibility as well as biocompatibility of the surface modified MgZnYNd materials.

**REFERENCES:** <sup>1</sup> Michael Haude, Hüseyin Ince,et al. (2016) *Lancet* **387**:31-39.

**ACKNOWLEDGEMENTS:** This work was supported by grants of the National Key Research and Development Plan (2017YFB0702504),

### In vitro corrosion behavior, cytotoxicity and antibacterial properties of Zn-2Ag-1.8Au-0.2V alloy

P. Li<sup>1</sup>, C. Schille<sup>1</sup>, E. Schweizer<sup>1</sup>, E. Kimmerle-Müller<sup>1</sup>, F. Rupp<sup>1</sup>, A. Heiss<sup>2</sup>, C. Legner<sup>2</sup>, U.E. Klotz<sup>2</sup>, J. Geis-Gerstorfer<sup>1</sup>, L. Scheideler<sup>1</sup>

<sup>1</sup> <u>Section Medical Materials Science and Technology</u>, University Hospital Tübingen, Germany.

Research Institute for Precious Metals and Metals Chemistry (fem), Germany

**INTRODUCTION:** Biodegradable Zn-based alloys with superior strength have been achieved by adding alloying elements or/and appropriate thermomechanical treatments. Alloys including mainly Mg, Cu, Ag, Ca, Sr, Al, Li and Mn have been investigated. Au is a highly biocompatible material, and it has often been used in biomaterials because of its radiopacity and flexibility. Recently, we developed a Zn-2Ag-1.8Au-0.2V (wt. %) alloy (Zn-Ag-Au-V) with improved mechanical properties [1]. In this study, in vitro corrosion behavior, cytotoxicity and antibacterial properties of the Zn-Ag-Au-V alloy were investigated.

METHODS: Specimens were prepared from casting rods by rolling and cutting, followed by mechanical grinding, ultrasonic cleaning and sterilization. A corrosion test was performed by immersion in DPBS solution according to ISO 10271: 2011. Released metallic ions were detected by ICP-OES, and pH value changes were measured. Corrosion products were analyzed by SEM-EDX. Corrosion rates were calculated by weight loss according to ASTM-G31-72. Cytotoxicity was evaluated by extract testing according to ISO 10993-5: 2009 (3 cm<sup>2</sup>/ml cell culture medium with FBS for 24 h at 37°C). Mouse fibroblast cells (L929) and human primary osteosarcoma cells (Saos-2) were used to evaluate inhibition of cell metabolic activity (XTT) and cell proliferation (BrdU). Potential antibacterial effects were evaluated with S. gordonii by Live/Dead staining.

**RESULTS:** The corrosion rate of Zn-Ag-Au-V alloy in DPBS was  $7.34 \pm 0.64$  µm/year, which is slightly lower than that of pure Zn,  $8.66 \pm 0.35$  µm/year. Fig. 1a shows that the cumulative released Zn<sup>2+</sup> concentration of the Zn-Ag-Au-V alloy from the  $28^{th}$  day on was lower than that of pure Zn. The pH values stayed in the range of  $7.2\sim7.4$ . SEM-EDX analysis showed that the corrosion products on the Zn-Ag-Au-V surface were mainly composed of Zn, P, O and C.

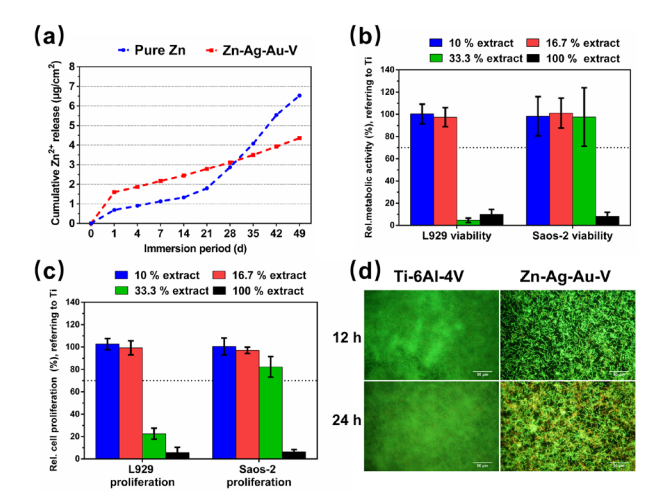


Fig. 1: Cumulative Zn<sup>2+</sup> release (a), cell viability (b) and proliferation (c) of L929 and Saos-2, (d) S. gordonii adhesion.

Fig. 1b and Fig. 1c compare cell viability and proliferation of L929 and Saos-2 cultured in 10 %, 16.7 %, 33.3 % and 100 % extracts of Zn-Ag-Au-V for 24 h. Undiluted extracts decreased cell viability and proliferation of both cell types, indicating obvious cytotoxic effects. Cytotoxicity was more pronounced in L929 cells, showing inhibition in the 33% extracts as well. Fig.1d demonstrates a thinner layer of green fluorescent, living bacteria on the Zn-Ag-Au-V surfaces, indicating inhibition of initial *S. gordonii* colonization compared to the Ti-6Al-4V reference.

**DISCUSSION** & **CONCLUSIONS:** The investigated Zn-Ag-Au-V alloy exhibits predictable degradation behavior, acceptable cytotoxicity and effective antibacterial properties *in vitro*, making it a promising biodegradable implant material.

**REFERENCES:** <sup>1</sup> C. Legner, et al. (2014), Pforzheimer Werkstofftag Conference: 85-94.

**ACKNOWLEDGEMENTS:** Research supported by AiF-ZIM (KF2342806CK2) and China Scholarship Council (Grant 201608440274).

## Constrained distribution of bacteria on biodegradable AZ31 Mg alloy. Protective effect of a polymerized phytocompound

M Bertuola<sup>1</sup>, A Miñan<sup>1</sup>, CA Grillo<sup>1</sup>, MC Cortizo<sup>1,2</sup>, MA Fernández Lorenzo de Mele<sup>1,3</sup>

<sup>1</sup> INIFTA, Facultad de Ciencias Exactas, UNLP, Argentina <sup>2</sup> Facultad de Odontología, UNLP, Argentina <sup>3</sup> Facultad de Ingeniería, UNLP, Argentina

INTRODUCTION: The prevention of microbial biofilm formation on the biomaterial surface is crucial in avoiding implants failures and the development of antibiotic resistant bacteria [1,2]. The objective of this work was to analyze bacterial distribution over corroding AZ31 surface and examine possible preferential sites for attachment according the surface composition. In order to achieve an effective constriction of bacterial attachment a polymer coating (polythymol) was developed to investigate possible antibiofilm and corrosion inhibition effects.

**METHODS:** Cylindrical AZ31 alloy samples were mechanically polished, cleaned and dried with nitrogen. The polymerization of thymol (polyTOH) was performed by cyclic voltametry in an electrochemical cell using 0.1 M water/ethanol (70:30) with 0.5 M sodium salicilate as electrolyte. The samples were exposed to S. aureus culture for 2h. Adherent bacteria were detached by sonication and then were enumerated after serial dilutions. The samples with bacteria attached were also observed by epifluorescence microscopy after acridine orange staining, by SEM microscopy and finally, EDS element mapping was performed. Corrosion test were additionally conducted in nutrient broth at 33°C using anodic polarization and measurements of Mg ions released in the solution for 1, 2 and 3 days by colorimetric test were made.

#### **RESULTS:**

Epifluorescence microscopy image showed the non uniform distribution of bacteria on AZ31 surface (Fig. 1A). Bacteria were found preferentially on the corrosion products where, apart from Mg, Al, the presence of P, C, O, and Ca was detected by EDS. Corrosion active centre with hydrogen bubbles evolution, associated with localized changes of pH, were not selected as suitable places for bacterial attachment.

The polyTOH layer increased the corrosion resistance of AZ31 (ions release was reduced to almost the half, and the corrosion current decreased

from 96.90±7.65 mAcm<sup>2</sup> to 6.74±2.61 mAcm<sup>2</sup>) and created an anti-biofilm surface (bacterial attachment was 50-fold lower on polyTOH-AZ31 than on non-coated Mg alloy). Corrosion of polyTOH-AZ31 was weaker than on bare AZ31 and was restricted to smaller regions. High P, Al and O percentages were found in the pit surroundings probably due to the change of pH in this region. P was absent on the rest of the metal surface (Fig. 2B).

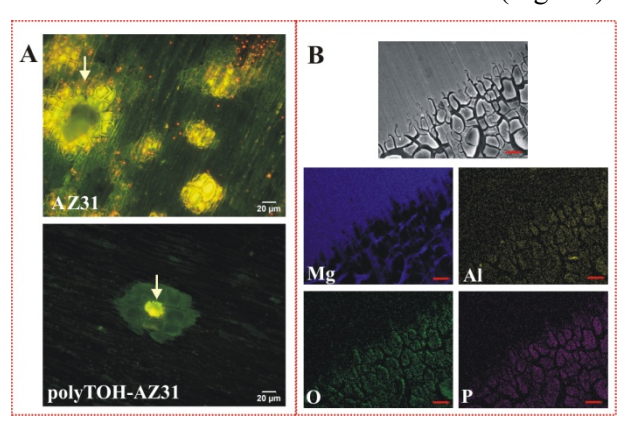


Fig. 1: A) Epifluorescence microscopy of pit corrosion in treated surfaces where bacteria are attached (white arrow) without (top) and with (bottom) polythymol. B) SEM image of polyTOH-AZ31 and mapping of the elements (scale bars: 20µm).

**DISCUSSION & CONCLUSIONS:** Results shown here demonstrated that bacterial adhesion on AZ31 shows some preferential sites (P- and C-containing precipitates) and others that are particularly avoided (active corrosion sites). Polythymol layer was able to constrain even more bacterial attachment by reducing the formation of corrosion products.

**REFERENCES:** <sup>1</sup> P. Tian, D. Xu, X. Liu, (2016) *Colloids Surfaces B Biointerfaces* **141**:327–337. <sup>2</sup> J. Sun, Y. Zhu, L. Meng, et al (2016) *Acta Biomater* **45**:387–398.

**ACKNOWLEDGEMENTS:** CONICET (PIP 2016-2018 GI 0601, P-UE 22920170100100CO), UNLP (11/I221), ANPCyT (PICT 2016-1424).

## Interaction of novel polylactic (PLA)/Mg particles and their degradation products with osteoblastic cells

C.A. Grillo<sup>1</sup>, A. Ferrández-Montero<sup>2,3</sup>, B. Ferrari<sup>3</sup>, M. Lieblich<sup>2</sup>, M. Fernández Lorenzo de Mele<sup>1,4</sup>, J.L. González-Carrasco<sup>2</sup>

<sup>1</sup><u>INIFTA</u>, Argentina <sup>2</sup><u>CENIM-CSIC</u>, Spain, <sup>3</sup><u>ICV-CSIC</u>, Spain, <sup>4</sup> <u>Facultad de Ingenieria, UNLP</u>, Argentina

**INTRODUCTION:** PLA/Mg composites have been suggested as a suitable bioabsorbable biomaterial [1]. With regards to the neat polymer, Mg enhances its creep strength and biocompatibility.[2] With regards to Mg, the polymer modulates its degradation rate and balances pH within physiological values. The aim of this work is to assess the *in vitro* interaction between different powdered PLA/Mg composites (p(PLA/xMg)) and their degradation products (DP), with mouse osteoblastic cells.

METHODS: Micrometric granular particles of pure Mg (pMg) and of p(PLA/Mg) (~100 µm diameter), with Mg/PLA ratio in the x=10, 30, 50 %(mass) range, were prepared through a colloidal dispersion technique.[3] Three sets of experiments were performed: (E1) Acridine Orange staining (AO) was used to evaluate the effect of p(PLA/xMg) and their DP on MC3T3-E1 cell viability after exposure for 24 h (37 °C, 5% CO<sub>2</sub>) in complete culture medium (CCM). Surface densities of cells were obtained from digital images. Additionally, the cells were exposed to CCM extracts (Exs) obtained after the 24h of exposure to 2000 μg/mL of p(PLA/xMg) (**E2**) and to the proper (PLA/xMg) amount associated to 2000 µg/mL of Mg (E3). In both cases Exs were subsequently filtrated. The effect of the Mg release was followed by Neutral Red (NR) endpoint. Each assay was repeated three times in independent experiments.

**RESULTS:** Average data of viability corresponding to **E1** assay showed a significant decrease in the living cells for p(PLA/xMg) x=30, 50 and for pMg (p<0.001) (Fig.1A). In Fig. 1B a non uniform distribution of cells with a strong decrease of cell number in the zone around particles (high concentration of corrosion products) can be seen.

NR assay (E2) made with Exs containing Mg ions released from 2000 µg/mL p(PLA/xMg) or pMg showed a significant decrease in lisosomal activity only for Exs of pMg (p<0.001).

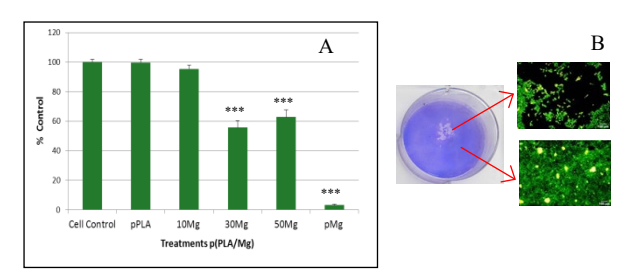


Fig. 1:A. Viability of MC3T3-E1 cells by AO staining after 24 h exposure to p(PLA/xMg, pPLA and pMg; B. Petri dish with a cell culture stained with Giemsa, containing p(PLA/xMg)(x=30, white area). Details of two regions show lower number of cells in the vicinity of the particles.

E3 results show the effect of Exs obtained with identical total Mg content (Mg=2000  $\mu$ g/mL) but from various sources (p(PLA/xMg) and pMg) i.e. of different total weight, volume and density showed a similar decrease in lisosomal activity (p<0.001), respect to the control p(PLA). This highlights the important deleterious effect of a high and uniform concentration of Mg ions in these Exs that is present since the beginning of E3 assay.

**DISCUSSION & CONCLUSIONS:** Results showed that granules of PLA/xMg (x=10) are not cytotoxic in the present experimental conditions. Local effects around the p(PLA/xMg) exists and cytotoxic effects are dependent on the amount of the degradation products release. Thus, the study of the biomaterial-cells interfaces where different local changes occur is relevant.

**REFERENCES:** <sup>1</sup>S.C. Cifuentes, et al., (2012) Mater. Lett. **74**:239-42. <sup>2</sup>S.C. Cifuentes et al., (2016) J. Biomed. Mater. Res. A **104**: 866–78. <sup>3</sup>A. Ferrandez et al., (2018) Mat Sci Eng C, submitted 2018.

**ACKNOWLEDGEMENTS:** ANPCyT (PICT 2016-1424) UNLP (I221), MINECO (MAT2015-63974-C4-1-R), CM (MULTIMAT Challenge: S2013/MIT-2862.

### Magnesium metal electrospun with polycaprolactone into nanofibrous fabrics has tissue reparative effects in vivo

S. Pixley<sup>1</sup>, U Adhikari<sup>2</sup>, X An<sup>3</sup>, S Khanal<sup>4</sup>, T Hopkins<sup>1</sup>, N Bhattarai<sup>5</sup>, W Heineman<sup>6</sup>

<sup>1</sup> <u>Department of Pharmacology & Systems Physiology, College of Medicine,</u> University of Cincinnati, Cincinnati, OH. <sup>2</sup> <u>Departments of Mechanical Engineering,</u> <sup>4</sup> <u>Department of Energy and Environmental Systems and <sup>5</sup> Chemical, Biological and Bioengineering,</u> North Carolina A&T State University, Greensboro, NC. <sup>3</sup> <u>College of Pharmacy,</u> University of Cincinnati, OH. <sup>6</sup> <u>Department of Chemistry, College of Arts & Sciences,</u> University of Cincinnati, OH.

INTRODUCTION: Magnesium metal has promise for use as medical implants in bone and as a vascular stent material<sup>1</sup>. We previously showed that nerve repair was improved by placing a magnesium (Mg) metal wire inside a hollow nerve guide and that tissue inflammation was also reduced<sup>2</sup>. To further explore in vivo effects of Mg metal degradation and to deliver metal degradation products during acute phases of nerve recovery after injury, Mg metal particles were embedded within nerve guide fabrics by electrospinning. Prior to use in nerve injury, we characterized fabric physical properties, release of degradation products, cytotoxicity in culture and tissue responses in vivo.

METHODS: Poly(caprolactone) (PCL) and sieved Mg metal particles (<44µm diameter, Sigma-Aldrich) were dissolved/suspended in organic solvents at several PCL:Mg w/w ratios (100:0 (PM-0), 100:10 (PM-10), etc.) and electrospun to form nanofiber fabric meshes. Physical properties were analysed and free Mg2+ release was determined by a Xylidyl blue assay, over 2 weeks of immersion in culture medium, under cell culture conditions. Hydrogen release was determined after a 24 hr incubation, using an electrochemical electrode. Cytotoxicity was tested by direct and indirect methods using 3T3 fibroblasts and PC12 cells. Pieces of nanofiber fabric were inserted under the flank skin of adult female C57/B6 mice, using UC IACUC approved protocols. Animals were sacrificed and skin was removed at 3, 8 and 28 days, fixed, paraffin embedded, sectioned and stained (with Masson's trichrome.

RESULTS: Mg metal particles were coated by PCL and embedded in fabric nanofibers (Fig. 1A). Mg particle presence within electrospun nanofibers was confirmed by energy dispersive X-ray spectroscopy (EDS) analysis (Fig. 1B). Hydrogen release was significant and fabrics were not cytotoxic in vitro (not shown). After subcutaneous implantation, initial inflammation (3 days in vivo (DIV)) was reduced (not shown). At 8DIV, Mg fabrics (PM-10), compared to PCL only (PM-0), had significantly greater infiltration of waves of macrophages into the loose mesh of fabrics from

adjacent connective tissues. Fig. 1C & 1D compare lower edges of PM-0 and PM-10 fabrics. Arrows show macrophages (cytoplasm is red in this stain) above connective tissue (has more collagen, blue in this stain). By 28 DIV, fabrics were filled with macrophages and foreign body giant cells.

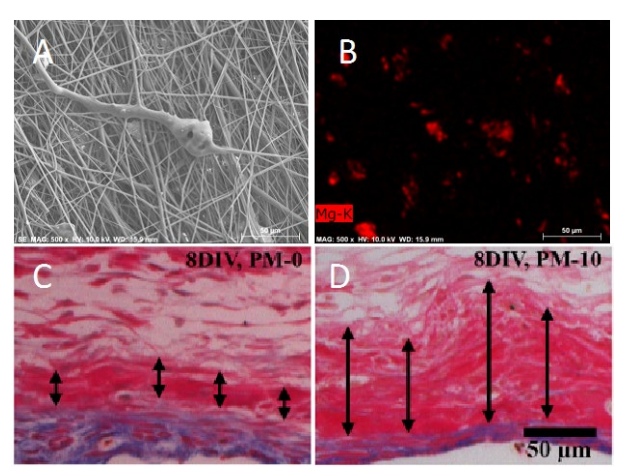


Fig.4. SEM image of PM-10 nanofiber mesh (A) with EDS mapping of Mg (B). In vivo fabric implants (C and D) show greater macrophage infiltration (arrows) into fabrics from the lower edge of the fabric, with Mg (PM-10).

**DISCUSSION & CONCLUSIONS:** Nanofiber PCL fabrics containing embedded Mg metal particles, prepared by electrospinning, released both Mg ions and hydrogen gas in physiological solutions, were not cytotoxic in vitro and were well tolerated in vivo. Mg metal reduced inflammation and improved ingrowth of macrophages, both important in mitigating the tissue responses to a biodegradable, implanted material like PCL.

**REFERENCES:** <sup>1</sup>Zhao D, Witte F, Lu F, Wang J, Li J, Qin L. *Biomaterials*. 2017;112:287-302. <sup>2</sup>Hopkins TM, Little KJ, Vennemeyer JJ, et al. *J Biomed Mater Res Part A*. 2017;105(11):3148-3158.

**ACKNOWLEDGEMENTS:** NSF ERC for Revolutionizing Biomaterials, EEC-EEC-0812348.

### Mg-Zn-Sr alloy based interference screw developed for ACL reconstruction

Huafang Li<sup>1\*</sup>, Yuanhao Wu<sup>2</sup>, Jiali Wang<sup>3</sup>, Yufeng Zheng<sup>4</sup>, Ling Qin<sup>3</sup>

<sup>1</sup>State Key Laboratory for Advanced Metals and Materials, School of Materials Science and Engineering, University of Science and Technology Beijing, Beijing, China

<sup>2</sup> Center for Biomedical Materials and Tissue Engineering, Academy for Advanced Interdisciplinary Studies, Peking University, Beijing, China.

<sup>3</sup>Department of Orthopaedics & Traumatology, The Chinese University of Hong Kong, Hong Kong, China

<sup>4</sup>State Key Laboratory for Turbulence and Complex System and Department of Materials Science and Engineering, College of Engineering, Peking University, Beijing, China

INTRODUCTION: Peri-tunnel bone loss after anterior cruciate ligament (ACL) reconstruction is often observed clinically, which may detrimentally affect tendon graft integration with surrounding bone tissue. Biodegradable magnesium (Mg) based fixators in terms of interference screws may be suitable for fixation of the tendon graft due to their favorable effects on promotion of new bone formation. The biodegradable Mg-6Zn-0.5Sr interference screw was designed for fixation of the tendon graft to the femoral tunnel in a rabbit model of ACL reconstruction, with a commercially available poly-lactide (PLA) screw for comparison.

METHODS: In vivo high resolution peripheral quantitative computed tomography (HR-pQCT) scanning was performed to measure the degradation behavior of Mg-6Zn-0.5Sr interference screws and peri-tunnel bone quality at 0, 6, 12 and 16 weeks post-surgically. Stevenel blue-Van Gieson-Alizarin Red S (SVA) staining was performed in MMA sections at a thickness of approximate 100μm. Paraffin sections with 5μm in thickness were stained with hematoxylin and eosin (H&E). The tensile tests were performed in femur-tendon graft-tibia complexes (FTGTC) with the knee flexed to 90degree with a preload of 1 N and a rate of 50 mm/min to record the maximal load to failure.

**RESULTS:** As shown in Fig.1, more bone was observed in the peri-tunnel region in the Mg-6Zn-0.5Sr group when compared to the PLA group at both 6 and 16 weeks post-operation according to histological sections stained with H&E and SVA, which were also supported by those with fluorescent labelling. The degradation products of the Mg-6Zn-0.5Sr screws induced the formation of the fibroustissue around the screws at week 6 post

operation, which was not observable in the PLA control group.

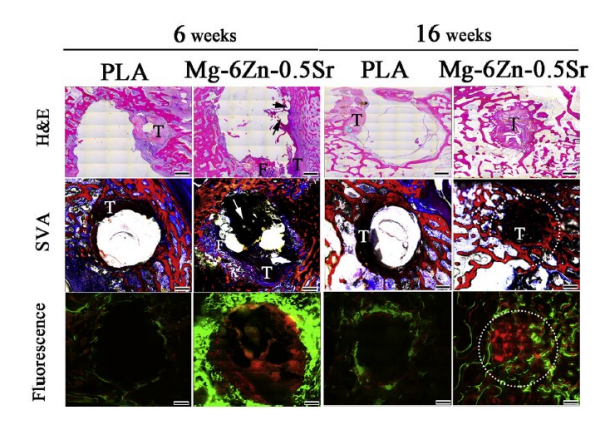


Fig. 1: Representative histology of the peri-tunnel tissue in the PLA and Mg-6Zn-0.5Sr groups at 6 and 16 weeks after surgery. F: fibrous tissue; T: tendon graft. Scar bar: 200µm.

DISCUSSION & CONCLUSIONS: The released ions from Mg-6Zn-0.5Sr screw resulted in larger fluorescent positive area in surrounding bone tissue around tunnels, indicating promoted new bone formation. More trabecular bone around bone tunnels can minimize bone fracture in tunnel surface and maintain the fixation strength of the tendon graft into tunnels for better healing. Therefore, we observed a significant increase in the maximal load to failure of FTGTC in the Mg-6Zn-0.5Sr group when compared to the PLA group at week 16 postoperation, indicating the beneficial effects of Mg-6Zn-0.5Sr metals on the graft healing.

**ACKNOWLEDGEMENT:** This work was supported by the National Natural Science Foundation of China (Grant No. 31700819) and the Fundamental Research Funds for the Central Universities.

### Effects of magnesium on bone-implant interfaces with and without polyetherether-ketone particle interference: a rabbit model based on porous Ti6Al4V implants

Zhe Du, Xiaoming Yu, Muhammad Ibrahim, Ke Yang, Lili Tan\*, You Wang

<sup>1</sup> Department of Bone and Joint Surgery, Renji Hospital, School of Medicine, Shanghai Jiaotong University, Shanghai, China. <sup>2</sup> Institute of Metal Research, Chinese Academy of Science, Shenyang, China

**INTRODUCTION:** Wear particles are inevitably produced at the bearing surface, and a previous study demonstrated that the immunological responses induced by polyether-ether-ketone (PEEK) particles were comparable with those induced by highly cross-linked polyethylene, a common wear particle in failed prostheses. A recent study also reported that PEEK wear particles induce a comparable degree of osteolysis to CoCrMo particles. A 3D-printedporous Ti6Al4Vimplant coated with Mg was introduced, and polyetherether-ketone wear particles were added to generate an animal model of implant loosening. We hypothesized that Mg-coating of the porous structures would enhance osteoblastogenesis while decreasing bone resorption.

**METHODS:** The deposition of Mg coating ontoTi6Al4Valloy was performed using an arc ion plating method. Ti6Al4Vsamples with dimensions of  $\Phi$  10 × 2 mm and 3D printed porous cylinders with dimensions of  $\Phi$  4.2  $\times$  8 mm were used as substrates. Forty female rabbits weighing 2.5–3.0 kg were obtained from the animal experimental center of Renji Hospital (Shanghai Jiaotong University, Shanghai, China). They were randomly assigned to one of 4 treatment groups: the porous group, the Mg group, the porous with PEEK particles group, and the Mg with PEEK particles group (all n = 10). The early stage of osteoclast differentiation and inhibited bone resorption were studied. The effects of Mg leach liquor on osteoblast/osteoclast gene expression, alkaline phosphatase activity, collagen secretion, tartrateresistant acid phosphatase activity, and bone resorption in vitro were examined.

**RESULTS:** We reconstructed 2D images of the distal femurs and 3D images of the peripheral area (VOI 2; Fig. 1). The BD and BV/TV of the porous structures (VOI 1) did not change in either particle group compared with the controls (p > 0.05, Fig. 5B), while the BD of the peripheral regions (VOI 2) in the porous group with particles decreased

markedly compared to the control group (p = 0.03, Fig. 1B). The BV/TV of the peripheral regions (VOI 2) did not show significant differences between the 205 control and Mg groups. However, the BV/TV in VOI 2 decreased significantly in the particle groups (p = 0.02, Fig. 1B), and the VOI 2 BV/TV in the Mg group was higher than in the porous with particles group.

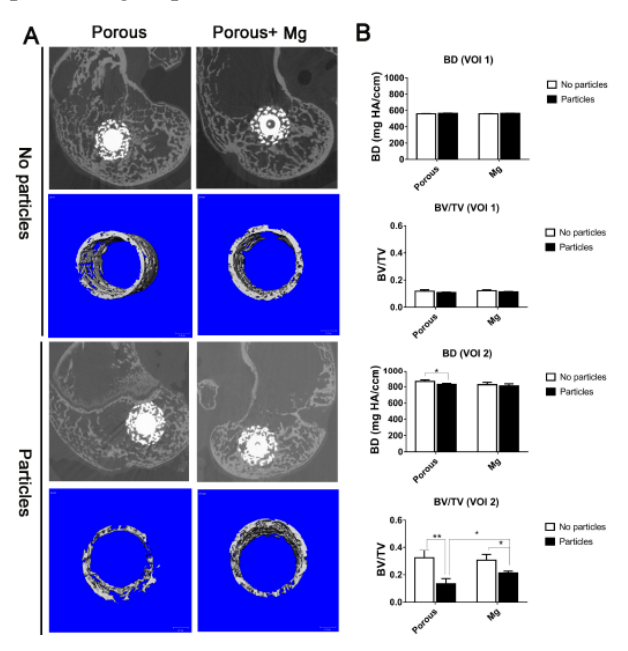


Fig. 1: Micro-CT analyses of distal femurs containing implants. A. Radiological reconstruction images of peripheral bone regions. Distal femur 2D reconstructions and peripheral bone 3D reconstructions are shown in 4 groups. B. Micro-CT analysis of bone-related parameters in the VOIs. \*P < 0.05, \*\*P < 0.001.

**DISCUSSION & CONCLUSIONS:** When coated onto implants with porous structure, Mg coating inhibited peri-implant osteolysis, making it potentially favorable for patients with osteoporosis.

**ACKNOWLEDGEMENTS:** This study was supported by the National Key R&D Program of China (No. 2016YFC1101804).

### Comparison of MgZnCa degradation between juvenile and old rats

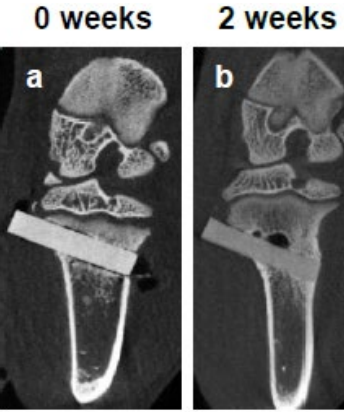
Grün NG<sup>1</sup>, Donohue N<sup>1</sup>, Holweg P<sup>1</sup>, Berger L<sup>2</sup>, Hahn D<sup>1</sup>, Löffler JF<sup>2</sup>, Weinberg AM<sup>1</sup> <sup>1</sup>Department of Orthopaedics and Traumatology, Medical University of Graz, Graz, Austria <sup>2</sup>Laboratory of Metal Physics and Technology, Department of Materials, ETH Zurich, 8093, Zurich, Switzerland.

INTRODUCTION: Conventional rigid and titanium (Ti) and stainless steel implants are currently used for stabilization of bone fractures. In many cases permanent rigid implants must be removed otherwise impeding longitudinal bone growth in children. In elderly, permanent implants can induce stress-shielding leading to bone loss and increased risk of peri-implant fractures. Especially osteoporotic patients with weak trabecular and cortical bone might have an increased risk for fractures with rigid Ti implants. However, biodegradable magnesium (Mg) implants would constitute a promising alternative for both, children and elderly patients: on the one hand rendering a second removal surgery unnecessary, and on the other hand functionally supporting bone formation. Previous studies have focused on decreasing the degradation rate of Mg alloys by adding rare earth elements (REEs) including yttrium or gadolinium. However, there is rising evidence that REEs are mildly toxic<sup>1,2</sup>. Whether REEs might be harmful, especially in children, in a long term view is still unclear. Previous studies have already shown that the lean Mg-0.45%wt Zn- 0.45%wt Ca (ZX00) implant material can be successfully implanted into femoral bone of juvenile rats and tibial bone of juvenile sheep, thereby supporting bone formation with adequate gas evolution. In this study we compared, therefore, the degradation and osseointegration of ZX00 after bicortical implantation into the metaphyseal tibia of juvenile, growing and old, osteoporotic rats.

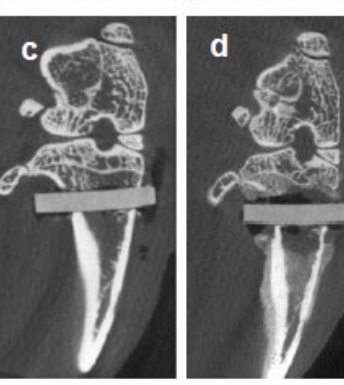
METHODS: Female 4 weeks-old Sprague Dawley® (SD) rats were purchased from Janvier Labs and kept on normal chow. At 6 weeks of age, seven SD rats underwent bilateral, bicortical and diaphyseal implantation of MgZnCa pins into metaphyseal tibiae. For osteoporotic animals, 12 months old rats underwent ovariectomy to induce osteoporosis. After 12 weeks, implantation was performed according to juvenile rats. In vivo microcomputed tomography scans were performed 2, 6, 12 and 24 weeks after surgical intervention at a resolution of 56 µm per voxel. After 24 weeks, animals were euthanized and explanted bones were embedded in Technovit 9100 New according to the protocol established by<sup>3</sup>. Ex vivo µCT

imaging of embedded hard tissue samples was performed.

RESULTS: In vivo µCT imaging demonstrated homogenous degradation of ZX00 over the entire







study period of 24 weeks (Fig. 1). However, juvenile rats (Fig. la and b), gas evolution was markedly decreased 2 weeks **ZX00** after implantation compared osteoporotic animals (Fig. 1c and d). Additionally, adequate osseointegration and bone ingrowth was greatly pronounced in juvenile compared osteoporotic

**DISCUSSION & CONCLUSIONS:** Here we compared ZX00 in tibiae of juvenile and osteoporotic rats. ZX00 markedly differed between both groups and demonstrated faster degradation and higher gas evolution in osteoporotic compared to juvenile rats. Whether weakened bone structure or differences in bone metabolism might influence implant degradation needs to be evaluated.

REFERENCES: <sup>1</sup>Pichler K, Kraus T, Martinelli E, et al. (2014) Int Orthop. 38(4):881. <sup>2</sup>Drynda A, Deinet N, Braun N, Peuster M. (2008) J Biomed Mater Res A. 91A(2):360–9. Willbold E, Witte F. (2010) Acta Biomater. 6(11):4447–55

**ACKNOWLEDGEMENTS:** We want acknowledge Anastasia Myrissa and Daniela Hirzberger for Technical Support.

## A biodegradable magnesium-based implant combined with codelivery of chemotherapeutic drug to improve tumor-induced bone defect healing

Lei Zhang<sup>1</sup>, Tu Hu<sup>2</sup>, Chenxin Chen<sup>1</sup>, Hongwei Miao, Guangyin Yuan<sup>\*, 1</sup>, Zhiquan An<sup>\*, 2</sup>, Jia Pei <sup>\*, 1</sup>

**INTRODUCTION:** Primary bone tumor, as one of the major bone disease, has a highly deleterious influence on both the quality of life for patients and health expenditure worldwide<sup>1</sup>. Generally, surgical intervention is the most typical treatment for primary bone tumor in clinic, consisting of the resection of bone-localized tumors and curing of surrounding tissues by chemo/radiotherapy<sup>2</sup>. To deal with the large bone defects resulting from bone tumor resection, bone substitute biomaterials with good bone-forming ability should be implanted to repair bone defects. Furthermore, in order to reduce the risk of local bone tumor recurrence, it is essential to completely kill the residual tumor cells around bone defects. However, as far as we know, there are few biomaterials with the ability of both bone tumor therapy and bone regeneration. Here, we prepared a biodegradable magnesium-based implant integrated with a typical chemotherapeutic drug paclitaxel (PTX), with the capability of both localized tumor therapy and bone regeneration.

METHODS: JDBM implants were prepared and pretreated according to our previous protocol<sup>3</sup>. The long-term corrosion behavior was studied by immersing the implants in cell culture medium (DMEM) for 60 days. Osteosarcoma cells (U2 OS & MNNG) and osteoblast cells (MC3T3-E1) were used to evaluate the inhibitory effect on tumor cells and the cytotoxicity on osteoblast cells. After that, the implants were implanted next to the osteosarcoma of nude mice for 7 days to assess the *in vivo* tumor inhibitory efficiency. Meanwhile, the *in vivo* bone-forming ability was evaluated by imbedding the implants in femur bones of SD rats for up to 16 weeks.

**RESULTS:** The designed implant exhibits a slow and controllable degradation *in vitro*. The systematic investigation of cellular response confirmed the implant induces no toxicity to osteoblastic cells but rather promotes the osteoinductivity of osteoblastic cells, besides that, it could kill osteosarcoma cells, revealing excellent biosafety and antineoplastic activity *in vitro*. The *in* 

vivo results showed the implant inhibits tumor growth most efficiently, mainly due to the released drug, in addition to the released magnesium ions secondarily; meanwhile, presents significant advantages in osteogenesis of femur bone of the rats compared to conventional titanium, mainly due to the released calcium and magnesium ions.

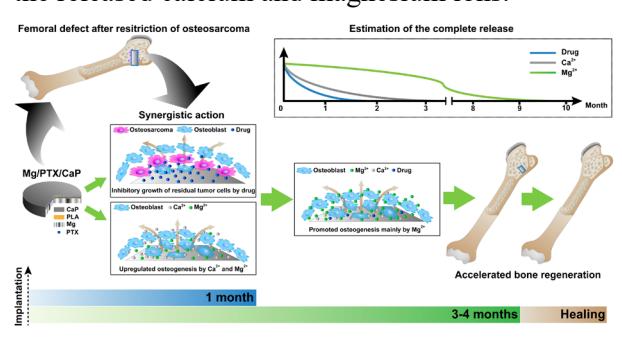


Fig. 1. Schematic diagram depicting the possible mechanism of the anti-tumor and osteogenic efficacy of Mg/PTX/CaP.

**DISCUSSION & CONCLUSIONS:** In this study, the sustain released drug plays the key role to kill bone tumor cells and inhibit in vivo tumors. Osteointegration between the implant surface and remodeled bone was essential for implant success and internal fixation stability. It is reasonable to speculate the improved osteogenic differentiation of osteoblasts may be directly related to the specific bioactive groups and protein absorbance of Mg substrate and CaP coating, and the improved osteogenic differentiation for osteoblasts further contributes to the enhancement of in vivo formation of new bone. The potential mechanism of the antitumor and osteogenic efficacy is illustrated in Fig. 1. Mg/PTX/CaP have potential application in killing the residual bone tumor cells by localized chemotherapeutic treatment, and taking advantage of the bioactivity of magnesium and calcium ions for promoting the healing of bone defect after surgical resection of bone tumor.

**REFERENCES:** <sup>1</sup> E. Segal, et al (2011) *Biomaterials.* **32**: 4450-63. <sup>2</sup> A. Luetke, et al (2014) *Cancer Treat Rev.* **40**: 523-32. <sup>3</sup> L. Zhang, et al (2017) *ACS Appl. Mater. & Interfaces.* **9**: 9437-48.

<sup>&</sup>lt;sup>1</sup> National Engineering Research Center of Light Alloys Net Forming and State Key Laboratory of Metal Matrix Composite, Shanghai Jiao Tong University, Shanghai 200240, China

<sup>&</sup>lt;sup>2</sup> Department of Orthopedics, Shanghai Sixth People's Hospital, Shanghai Jiao Tong University, Shanghai, 200233, China

### An insight into the *in vivo* degradation of magnesium alloys with the help of nondestructive synchrotron radiation microcomputer tomography

D. Krüger<sup>1</sup>, D.C.F. Wieland<sup>1</sup>, J. Moosmann<sup>1</sup>, B. Zeller-Plummhoff, J. U. Hammel<sup>3</sup>, Silvia Galli<sup>2</sup>
R. Willumeit-Römer<sup>1</sup>

<sup>1</sup>Institut für metallische Biomaterialien, Helmholtz-Zentrum Geesthacht, Hamburg, Germany <sup>2</sup>Malmö University, Malmö, Sweden

INTRODUCTION: The in vivo degradation of Magnesium (Mg) is still not well understood. However, with high resolution synchrotron radiation tomography (SRµCT) experiments it is possible to analyse the degradation behaviour of Mg implants ex vivo, by terms of degradation rate (DR), mean degradation depth (MDD), degradation homogeneity described with surface to volume ratios (S/V), pitting factor (PF), distribution of precipitates of alloying elements, morphology of the corrosion layer, bone porosity on the different volumes of interests (VOI) from the implant, hence bone volume density (BV/TV) and bone implant contact area (BIC). Here we make a comparison between SRµCT and histology to estimate the errors and comparability of both techniques.

**METHODS:** Screws (dimensions 2 mm diameter x 4 mm height, 0.2 mm thread) of two Mg-gadolinium (Gd) alloys (5, 10 wt% Gd), Ti and PEEK were implanted into rat femur and analyzed after 4, 8 and 12 weeks of implantation. The explants (ca. 5 x 5 mm / diameter x height) were critical point dried and examined with synchrotron tomography at the beamline P05 (voxel size: 1-3µm) at PETRAIII Elektronen-Synchrotron Deutsche Hamburg. Same samples were afterwards analyzed histologically. The data was analyzed by Ilastik for segmentation; Avizo® 9, ImageJ(Fiji) visualization/registration/resampling; ImageJ(Fiji), Matlab2015a and R2016a for the computations.

**RESULTS:** Exemplary calculations on *ex vivo* data of a Mg-10Gd screw after 12 weeks healing can be found in table 1.

Table 1. BIC of Mg-10Gd screw after 12 weeks in vivo measured on a histology section from [1] and on a 3D reconstructed  $SR\mu CT$  (\*measurements from the current experiment)

	BIC [%]	DR [mm/y]
SRμCT *	57.6	0.4
SRµCT [1]	45.2	$0.39 \pm 0.04$
Histology [1]	71.3	

& CONCLUSIONS: Every DISCUSSION measuring technique has its advantages, disadvantages and data errors. By taking the values of the BIC in [1] of a Mg-10Gd screw after 12 weeks of in vivo corrosion measured by SRµCT and histological anylsis a difference of 36.6% between both values can be seen. A reason for this variance between the 3D and 2D BICs is the possibility that the 2D histological section is simply not representative for the whole sample. This is one disadvantage of the histological investigation technique in comparison to the SRµCT, in addition to the complex histological sample preparation procedure. The fact being able to gain information on a sample in 3D without destroying it with high spatial resolution in a short period of time is the benefit of the SRµCT measurement technique.

All in all, by means of analysing two *in vivo* degraded Mg-Gd implants, the impact of the degradation homogeneity on the representativeness of a 2D slice is going to be discussed. Hence the significance and efficiency of SRµCT for being able to judge the interaction between the living organism and the biodegradable implant will be clarified.

**REFERENCES:** <sup>1</sup> S. Galli, et al. *Degradation behavior and bone response of 3 magnesium alloys in comparison with titanium: an in vivo investigation*, in preparation

**ACKNOWLEDGEMENTS:** We acknowledge our project partners at Malmö University in Sweden for carrying out the animal experiments and Röntgen-Ångström Cluster for funding of the project SynchroLoad 05K16CGA. We also wish to thank all colleagues for experimental support especially during the beamtimes.

<sup>&</sup>lt;sup>3</sup>Institut für Werkstoffphysik, Helmholtz-Zentrum Geesthacht, Hamburg, Germany

### Algorithms for the multidimensional microscopy images analysis. Application to study of macrophages-Fe based degradable biomaterials interactions

NS Fagali<sup>1</sup>, MA Madrid<sup>2</sup>, BT Pérez Maceda<sup>3</sup>, RM Lozano Puerto<sup>3</sup>, M Fernández Lorenzo <sup>1,4</sup>
(1) Instituto de Investigaciones Fisicoquímicas Teóricas y Aplicadas (<u>INIFTA</u>), CCT La Plata, CONICET - Facultad de Ciencias Exactas, UNLP. La Plata, Argentina. (2) Dpto. Ingeniería Mecánica, Facultad Regional La Plata, Universidad Tecnológica Nacional (<u>FRLP-UTN</u>) - CONICET. (3) Grupo Reconocimiento Célula-Biomaterial. Departamento de Biología Celular y Molecular, Centro de Investigaciones Biológicas (<u>CIB-CSIC</u>), Madrid, España. (4) Facultad de Ingeniería, UNLP. La Plata, Argentina.

**INTRODUCTION:** Advantages and disadvantages of the use of pure iron (Fe) and some of its alloys for the manufacture of biodegradable temporary stents have been discussed in the last decades. The evaluation of biocompatibility "in vivo" (in the area of the implant), is complex and the use of cell cultures is a valuable model for preliminary studies [1]. The analysis of the interactions between cells and materials at real time is helpful to provide information related to possible toxic effects of Fe and its degradation products formed after exposure to the biological media.

**RESULTS:** Multidimensional microscopy (MDM) at real time was employed in this work to obtain images and videos of live non-stained macrophages in contact with bulk Fe. The acquired images were later analyzed using different algorithms. The MDM allows the study of the cell behavior in conditions where non-staining is required, avoiding a possible effect on cell metabolism.

In order to study these interactions, murine macrophages (J774A.1) were exposed to rings of pure Fe<sup>o</sup> (99.9% SpecPure) and their response was analyzed by MDM at real time. Images were taken every 15 minutes for 24 and 48 hours, and then the frames were mounted as a video film.

Several algorithms were designed for the analysis of the sequences of images using free software FIJI and different parameters were obtained such as number of live/dead cells, displacement, average speed, number of divisions (splitting) and others morphological parameters. It could be noticed that the speed, displacement and cell division were altered with respect to control cells (in absence of Fe). As metal degrades, the macrophages capture and accumulate the degradation products as a dark deposit of insoluble material and cells die.

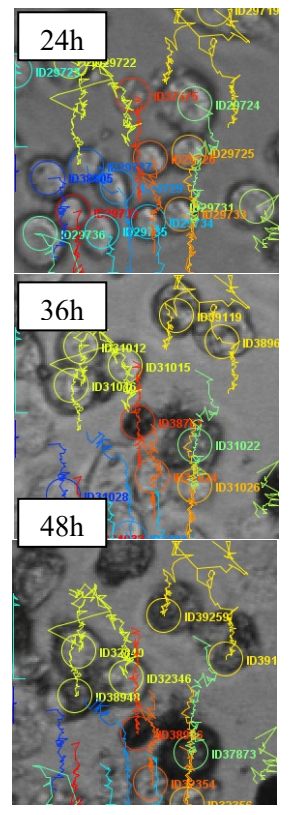


**Fig1.** Tracking of macrophages in the vicinity of Fe<sup>0</sup> rings for 24, 36 and 48 h. The colored lines represent the displacement of the center of each cell. The accumulation of insoluble products of Fe<sup>0</sup> degradation can be observed as dark deposits.

**CONCLUSIONS:** The use of different algorithms enables to collect useful information from images of non-stained live cells using MDM. Particularly, ofapplication these algorithms in the study of the effect of degradation of Fe on macrophages, allowed to identify and select the most relevant parameters describe the effects

produced by the degradation of Fe on these cells.

#### **REFERENCES:**

<sup>1</sup>Fagali NS, Grillo CA, Puntarulo S, Fernández Lorenzo MA (2017). Is there any difference in the biological impact of soluble and insoluble degradation products of iron-containing biomaterials? *Colloids and Surfaces B: Biointerfaces* 160: 238–246

**ACKNOWLEDGMENTS:** CONICET (PIP 2016-2018 GI 0601, P-UE 22920170100100CO), UNLP (11/I221), ANPCYT (PICT 2015-0232, PICT 2016-1424), MICINN (MAT2011-29152-C02-02)

#### Quantification of implant components in biological matrix

J Bode<sup>1</sup>, M Rinne<sup>2</sup>, J Thieleke<sup>2</sup>, C Vogt<sup>1</sup>

<sup>1</sup> TU Bergakademie Freiberg, Faculty f. Chemistry and Physics, Institute f. Analytical Chemistry, Leipziger Str. 29, 09599 Freiberg, Germany

<sup>2</sup> University of Hannover, Institute for Inorganic Chemistry, Callinstr. 9, 30167 Hannover, Germany

Components of implants or surface coatings - even those of permanent implants - can migrate out of the implant and can possibly get enriched in different organs.

In this study, implant components were quantified in two rat brain samples of a pre-clinical animal model. The rats had a subcutaneous implant of a TiAl6V4-alloy with a surface coating of TiO<sub>2</sub> with included silver nanoparticles. Silver is known for its antimicrobial activity since the ancient times and gets utilized as coating material in endoprosthesis recently. It is used to get released slowly into the surrounding area of the implant to inhibit bacterial activity. The object of this study was to determine the potential (unwanted) enrichment of silver, especially in form of nanoparticles, in the brains of the rats and its local distribution. Therefore, cryomicrotome-sections with a thickness of 10 µm were generated from the brains and mappings (elemental distribution with spatial resolution) were generated via LA-ICP-MS. The method was tested with the frequent trace elements magnesium and zinc.

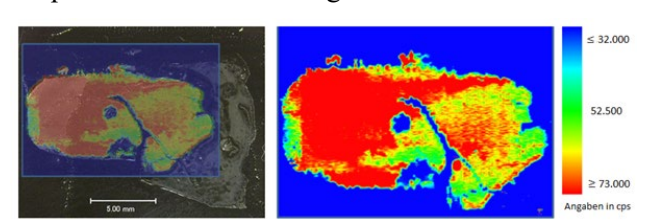


Fig. 1: Mapping of <sup>25</sup>Mg

A new method for the quantification of silver by means of solid body-isotope dilution analysis with LA-ICP-MS (laser-ablation mass spectrometry with inductively coupled plasma) was established.

Beyond that, the main components of the alloy (titanium, vanadium, aluminium) were also quantified in the brain tissue sections, however with external calibration in form of in-house polymer-based reference materials (UV-radiation hardening acrylic resin polymers).

Besides the brain samples, also a sheep bone section sample with an included implanted screw of the titanium alloy mentioned above was analyzed in the same way. Mappings of the implant components, but also of other significant elements such as calcium and phosphorus near the screw in the bone tissue were generated.

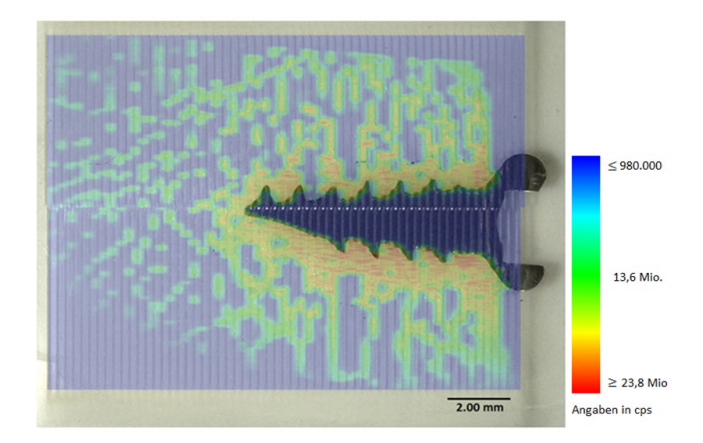


Fig. 2: Mapping of  $^{42}$ Ca; LA-ICP-MS parameters: 60 lines á 6600  $\mu$ m (top) und 59 lines at 6840  $\mu$ m (bottom), distance 300  $\mu$ m, fluence 3,7  $J/cm^2$ , frequency 20 Hz, spot diameter 90  $\mu$ m; presented on top of the optical microscope image of the sample after ablation

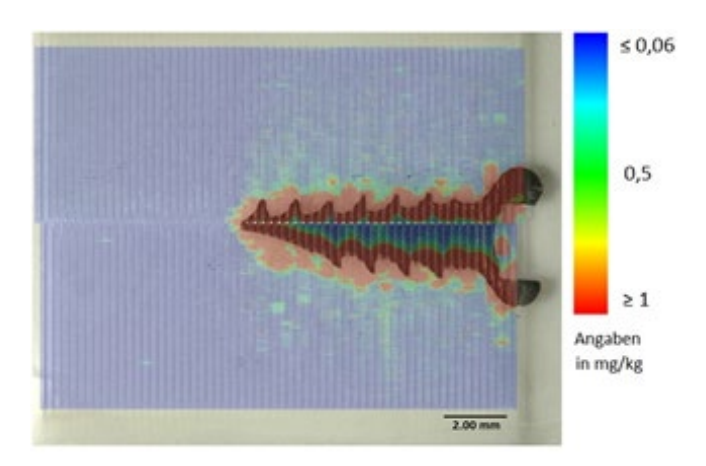


Fig. 3: Mapping of <sup>107</sup>Ag; LA-ICP-MS parameters: 60 lines á 6600 μm (top) und 59 lines at 6840 μm (bottom), distance 300 μm, fluence 3,7 J/cm², frequency 20 Hz, spot diameter 90 μm; presented on top of the optical microscope image of the sample after ablation